MAGNETO-OPTICAL STUDIES IN $In_{1-x}Ga_xAs_yP_{1-y}$
SEMICONDUCTING ALLOYS

BY

KAMBIZ ALAVI

S.B., Massachusetts Institute of Technology
(1972)

S.M., Massachusetts Institute of Technology
(1977)

SUBMITTED IN PARTIAL FULFILLMENT
OF THE REQUIREMENTS FOR THE
DEGREE OF
DOCTOR OF PHILOSOPHY

at the

MASSACHUSETTS INSTITUTE OF TECHNOLOGY

June, 1981

© Massachusetts Institute of Technology

Signature of Author _____Signature redacted_____
Department of Physics, April 29, 1981

Certified by _____Signature redacted_____
Thesis Supervisor

Accepted by _____Signature redacted_____
Chairman, Department Committee

MAGNETO-OPTICAL STUDIES IN In$_{1-x}$Ga$_x$As$_y$P$_{1-y}$ SEMICONDUCTING ALLOYS

BY

KAMBIZ ALAVI

Submitted to the Department of Physics on
April 29, 1981 in partial fulfillment of the
requirements for the Degree of Doctor of Philosophy
in Physics.

ABSTRACT

Interband magneto-optical absorption in the Voigt and the Faraday configuration has been studied near liquid-helium temperature in samples of In$_{1-x}$Ga$_x$As$_y$P$_{1-y}$ grown by liquid-phase epitaxy on InP substrates and are reported here in two samples with (x=0.25, y=0.52) and (x=0.47, y=1). The magnetotransmission spectra were analyzed using the quasi-Ge model with exciton corrections. It is found that such measurements determine E_g, $1/\mu_+ \equiv (1/m_c + 1/m_{\ell h})$, and $1/\mu_- \equiv (1/m_c + 1/m_{hh})$, and therefore m_c and $m_{\ell h}$, within a narrow range ($m_{hh} >> m_c$ and $m_{\ell h}$). The anisotropy factor $\gamma_3 - \gamma_2$ is also determined within a narrow range when measurements are performed with H oriented along two different crystal axes. Using a minimization routine the following quasi-Ge parameters were obtained. For (x=0.25, y=0.52): E_g=1065±1 meV, m/μ_-=18.8±0.5, m/μ_+=29.5±0.5. Assuming $(m_{hh}/m)_{100}$=0.45±0.05, Δ=0.24±0.01 eV, and E_p between 17.5 and 25.8 eV (F=0 to -3.5) we obtain m_c/m=0.0602±0.001 $m_{\ell h}/m$=0.078±0.001, g_c=-0.06 to -1.25. $\gamma_3 - \gamma_2$=0.35 or 0.7 gave the same values, within the error bars, for the above parameters. (Only $\vec{H}||[100]$ data were taken). With $\gamma_3 - \gamma_2$=0.7, γ_1^L=7.5±0.3, γ_2^L=2.4±0.1, γ_3^L=3.1±0.1, κ^L=1.5±0.1. For (x=0.47, y=1): E_g=813±1 meV, m/μ_-=26.1±0.5, m/μ_+=43.4±1.0. $\gamma_3 - \gamma_2$=0.8±0.2. With $(m_{hh}/m)_{100}$=0.45±0.05, Δ=0.35±0.01 eV, and E_p between 21 and 27 eV (F=0 to -3.5) we obtained m_c/m=0.0415±0.0015, $m_{\ell h}/m$=0.0515±0.0015, g_c=-3 to -5, $\gamma_3 - \gamma_2$=0.8±0.05, γ_1^L=10.6±0.2, γ_2^L=4.0±0.1, γ_3^L=4.8±0.1, κ^L=3.3±0.1.

E_p could not be precisely determined even when the nonparabolicity of the conduction band was examined. A precise measurement of E_p requires precise measurements of g_c.

THESIS SUPERVISOR: Dr. Roshan L. Aggarwal, Senior Research Scientist,
Department of Physics and
Associate Director, Francis Bitter National Magnet
Laboratory

THESIS READERS: Dr. Benjamin Lax, Professor, Department of Physics, and
Director, Francis Bitter National Magnet Laboratory

Dr. Steven H. Groves, Research Staff Member,
M.I.T. Lincoln Laboratory

To My Parents

ACKNOWLEDGEMENTS

I wish to express my deepest gratitude and appreciation to all three members of my thesis committee for indeed making the completion of this thesis a reality:

To my thesis supervisor Dr. Roshan Aggarwal for his continual interest, guidance, helpful suggestions, understanding, and his confidence in me time and again. Also much credit goes to his patience, clarity, insight, and decisiveness.

To Professor Benjamin Lax for opening the doors of the Magnet Laboratory to me and keeping them open, for his continual encouragement and positiveness, and for supervising me in the earlier stages of my graduate studies.

To Dr. Steven Groves, for his active interest in this project, for his always being available and helpful, for his refreshing clarity and insight, and for his personable manner.

I gratefully acknowledge the availability of samples grown by Dr. Groves and Mrs. Muriel Plonko at the Lincoln Laboratory.

It is apleasure to express my thanks to Professor Margaret Weiler for her help with aspects of the theory and for generously making her computer programs available, and to Dr. David Larsen for making some of his unpublished numerical results available,as well as for helpful discussions.

Many thanks to Don Nelson and Dorette Sarachik for helping me with the computer, and to Larry Rubin and the staff of the I&O group.

I gratefully acknowledge the helpful suggestions made by Dr. Hernan Praddaude regarding the organization of this thesis.

To the many good people of the Magnet Laboratory who have extended their friendship and technical expertise goes my deepest gratitude. In particular I would like to mention the names of Larry Sousa and Frank Ricchio, whom I have known the longest and whose technical help and friendship has been invaluable.

I gratefully acknowledge the financial support which was made available to me through Professor Lax and Dr. Aggarwal in the form of

several research assistantship grants, as well as the Physics Department for three years of teaching assistantship support.

I am grateful to Dr. T. P. Pearsall for making available to me results of optical pumping measurements prior to publication, and for his encouragement.

Over the years, it has always been a pleasure to see Mrs. Terry Crossley with her graceful manners at the Physics Graduate Office and I would like to pay tribute to her kindness extended to all graduate stundents.

To all my friends,thank you for your affection, encouragement, advice, patience, and sense of humor, and for sometimes telling it like it is.

To Dr. and Mrs. Hossein A. Shushtari and family, thank you for your hospitality and your interest.

And finally to my parents, sisters Kamelia and Katayoon, brother-in-law Kambiz, and nephew Amir-Nasser Pourrezaei, thank you for always being there and for your unqualified love.

Thank God this thesis is over.

TABLE OF CONTENTS

LIST OF FIGURES

LIST OF TABLES

CHAPTER I

INTRODUCTION

In this thesis we report on the interband magnetoabsorption measurements carried out in two members of the family of semiconducting III-V alloys $In_{1-x}Ga_xAs_yP_{1-y}$ which are grown by liquid phase epitaxy lattice matched to InP substrates.

One of the motivating factors for this investigation is that the $In_{1-x}Ga_xAs_yP_{1-y}$ quaternary alloys have recently become technologically important semiconductor materials for optoelectronic devices because of (1) wide variation of the bandgap between 0.36 and 2.2 eV by varying the composition parameters x and y, and (2) lattice-matched epitaxial growth on GaAs or InP substrates. These materials have been used successfully for the fabrication of a number of important devices such as light emitting diodes,[1,2] photocathodes,[3] photodiodes,[4] Gunn oscillators,[5] and double heterojunction lasers.[6,7]

An important application of the $In_{1-x}Ga_xAs_yP_{1-y}$ quaternary expitaxial films is in the field of fiber-optics communications, since using these materials it is possible to fabricate lasers and detectors which operate in the wavelength region corresponding to the region of minimum loss and minimun dispersion of optical fibers. Until recently, this has been the 1.2 μm region,[8,9] corresponding to 1.0 eV. More recently, however, fibers have been developed whose optimal operation region lies in the longer wavelength region

corresponding to alloy compositions closer to the $In_{0.53}Ga_{0.47}As$ end of the family.[10]

Another aspect of these quaternary materials which is interesting from the point of view of device application as well as physics of III-V semiconductors is the fact that in addition to the band gap, other electronic band parameters for these materials can be varied by varying the alloy composition.

A potentially interesting application of these materials from both device and physics point of view is to the fabrication of super-lattices. The evidence for the growth of interest in these materials comes from the increase in the number of contributions in the literature in recent years dealing with this alloy family.[11] The first systematic measurements of the relationship between x and y and the laser emission photon energies at temperatures of 300K and 80 K for the quaternaries lattice matched to InP were obtained by Hsieh.[12] Nahory et al[13] used photoluminescence spectra to measure energy gaps, as well as the lattice matching condition. The lattice matching condition is generally taken to be $y \approx 2.2x$ or $x \approx 0.47y$.

The first measurement of the effective mass in a member of this alloy family was reported by Restorff et al[14] who deduced a value of $m_c = 0.060 \, m$ (where m is the free electron mass) from the temperature dependence of the amplitude of weakly resolved Shubnikov-de Haas measurements in a quaternary sample with composition parameters x=0.10, y=0.22.

At very nearly the same time that we reported our first interband magnetoabsorption measurements of these materials (x=0.25, y=0.52),[15] Portal et al[16] reported measurements of the effective masses of four members of the alloy family using magnetophonon resonance, Shubnikov-de Haas oscillations, and cyclotron resonance. Our effective mass value of m_c=0.061 m and those of Ref. 16. suggested very strongly a linear variation of m_c with y for $In_{1-x}Ga_xAs_yP_{1-y}$ alloys lattice matched to InP. In fact, Nicholas et al[17] suggested the empirical relationship $m_c(y)$=(0.080 - 0.039y) m. It was noted [16,17] that the value of m_c for samples with x=0.12 and y=0.23 reported in Ref. 16 was 0.072, 20% higher than the value reported earlier in Ref. 14 for x=0.10, y=0.22. Furthermore, the value of m_c=0.038 m estimated by Nishino et al[18] from electro-reflectance studies of an alloy with x=0.21, y=0.54 fell well below our value of 0.061m for x=0.25, y=0.52. In a more recent publication by Brendecke et al[19] cyclotron resonance results were reported and effective masses were deduced giving values between 20% and 30% below the linear interpolation. Shubnikov-de Haas measurements reported by Perea et al[20] were closer to the linear interpolation with a small downward bowing which was about 9% at the most. The more recent Shubnikov-de Haas measurements of Restorff et al[21] were also in better agreement with the linear interpolation compared to the previously reported results of Ref. 14. In a very recent article, Nicholas et al[22] have reported cyclotron resonance and magnetrophonon resonance measurements of the effective mass m_c for several members of the alloy family over the whole range y=0.23 to y=1 for lattice matched samples. These results agree very well with

the linear interpolation for m_c mentioned above and as pointed out in Ref.22, our result[15] is in agreement with theirs. Furthermore, in Ref. 22, the authors show evidence that the low masses deduced by Ref. 19 result from an observation of an impurity transition which is dominant for lattice temperatures below 30K. In summary, our results and those of Refs. 16, 17 and 22, are in excellent agreement with the linear interpolation for m_c.

Interband magneto-optics has played an important role in providing a quantitative understanding of important energy bands in semiconductors. The interband magneto-optical effects have been the subject of extensive experimental and theoretical investigations. Extensive references to these important contributions can be found in the review articles by Lax and Mavroides,[23] and Aggarwal.[24] One feature of magneto-optics is the richness of the spectra as a result of optical transitons between the $a^{\pm}(n')$, $b^{\pm}(n')$, $a^{SO}(n')$, and $b^{SO}(n')$ series of the heavy (-), light (+), and the spin-orbit split-off (so) valence band magnetic sublevels to the conduction band $a^c(n)$ and $b^c(n)$ magnetic sublevels. This enables one to extract a lot of information about these bands by examining interband magneto-optical spectra as a function of light polarization and crystal axis orientation with respect to the magnetic field, provided the sampes are of high enough quality to allow some of these features to be resolved. Therefore, one aspect of our intial objective was to determine whether these alloy semiconductors can indeed be amenable to magneto-optical studies and whether they could provide

magneto-optical spectra with enough structure to enable us to obtain
some of the band parameters. This thesis reports on such studies
and indicates that there is a great potential for applying the rich
method of interband magneto-optics to this alloy family. We bring to
attention the results for one of our quaternary samples[15] and those
for a ternary $In_{0.53}Ga_{0.47}As$ sample,[25,26] which are described in
this thesis. We have also obtained room temperature electro-
reflectance spectra for a number of quaternary samples using the
electrolyte method of Cardona et al[27] which we present in Appendix A.
The signal to noise ratio and the presence of the onset of Franz-
Keldysh oscillations[28] point to the high quality of samples avail-
able to us (for example compare spectra in Appendix A with those
reported in the literature). These studies of electroreflectance,
although preliminary, are encouraging and suggest that magneto-
electroreflectance measurements[29,30] for both the fundamental edge
and the split-off edge would be possible in these alloys. Stress
modulated magnetoreflection measurements may also turn out to be
possible.[31]

Interband magneto-optical measurements, as mentioned before,
have been extensively used to determine band parameters of semi-
conductors. The model which is most applicable for the analysis
of these spectra is the "Quasi-Ge" coupled band model of Pidgeon
and Brown,[32] with the improvements incorporated by Weiler.[33]
The band parameters we shall refer to are those which appear in Ref.33
for example. In Chapter II of this thesis a review of the "quasi-Ge"

model, based on Ref. 33, will be given. In Chapter III, we present

our magnetoabsorption experiments in two members of the alloy family.

In Chapter IV, we present analysis of our magnetoabsorption experi-

ments based on the quasi-Ge model. The presentation in this thesis

would be similar to those in Refs. 31 and 33. In addition, we

include a discussion of the effect of higher bands on our measurements.

In Chapter V, we give a summary of the results and suggestions for

future work. In Appendix A, electroreflectance spectra for a few

quaternary samples will be presented. The remaining Appendices,

will be dealing with some of the details of Chapter IV and the

nonparabolicity of the conduction band.

Briefly, the band parameters which are readily obtained

(within a few per cent or less) from interband magneto-optical

measurements (in the absence of well resolved spectra from the

spin-orbit split-off band to the conduction band transitions) are

the following: the energy gap E_g, the reduced effective masses

$(1/\mu_\pm)=(1/m_c)+(1/m_\pm)$ for the conduction and heavy (-) or light (+)

hole bands, and the anisotropy factor γ_3-γ_2. Since m_- is quite

large compared to m_c (by a factor of ~ 10) $1/\mu_-$ determines m_c

within a marrow range, thus the value of m_+ is also determined

within a narrow range.

Another important parameter is E_p, the interband transition

energy, which is proportional to the square of momentum matrix

element between valence and conduction bands. Since the effect of

higher bands is quite small on g_c, the conduction band g-factor,[33,34]
the measured value of g_c can be used to obtain E_p provided the
g-factor values are measured to a good degree of precision and the
spin-orbit splitting energy Δ and the energy gap E_g measurements are
available. On the other hand, since the effect of high bands on
the curvature (effective mass) of the conduction band could be as
large as 20% of that due to the valence bands, m_c cannot precisely
determine E_p. However, magneto-optical measurements can determine
E_p to within about 20%. We have found that a linear interpolation
of the values of E_p from the binaries InAs, GaAs, and InP can give
good fits to our data. Ignoring the effect of higher bands, which
would predict a smaller E_p, can also give good fits.

Recently, Hermann et al[35,36] have applied the technique
of optical pumping for the measurements of valence band spin-
orbit splitting in several samples of $In_{1-x}Ga_xAs_yP_{1-y}$ over the range
$y=0$ to 1 and their values for m_c, m_+(lighthole effective mass), and

$$\bar{\beta} \equiv \frac{1}{3} \frac{(3/\mu_+) + (1/\mu_-)}{(1/\mu_+) - (1/\mu_-)}$$

are in excellent agreement with the values we have obtained for our
quaternary and ternary samples. For g_c a preliminary value of
$(-4.2\pm25\%)$ has been obtained[36] for the ternary $In_{0.53}Ga_{0.47}As$, again
in very good agreement based on interpolated value of E_g which we
had used for the ternary, however, work is being done to reduce
the error-bars on g_c.[36]

REFERENCES

1. L. M. Dolginov, N. Ibakhimov, M. G. Milk'vidskii, V. Yu. Rogulin, and E. G. Shevchenko: Soviet Physics-Semicond. 9, 871 (1976).

2. T. P. Pearsall, B. L. Miller, R. J. Capik, and K. J. Bachmann, Appl. Phys. Letters 28, 499 (1976).

3. L. W. James, G. A. Antypas, R. L. Moon, J. Edgecumbe, and R. L. Bell, Appl. Phys. Letters 22, 270 (1973).

4. G. A. Antypas, R. L. Moon, L. W. James, J. Edgecumbe, and R. L. Bell, Proceedings of the 4th International Symposium on GaAs and Related Compounds (Institute of Physics, London, 1973), p. 48.

5. R. E. Hayes and R. M. Raymond, Appl. Phys. Letters 31, 300 (1977).

6. W. R. Hitchens, N. Holonyak, Jr., P. D. Wright, and J. J. Coleman, Appl. Phys. Letters 27, 245 (1975).

7. C. C. Shen, J. J. Hsieh and T. A. Lind, Appl. Phys. Letters 30, 353 (1977).

8. W. G. French et al, Bell Systems Tech. J. 53, 951 (1974).

9. D. Gloge, IEEE Trans. Microwave Theory and Techniques MTT-23, 106 (1975).

10. T. Miya, Y. Terunuma, T. Hosaka, and T. Miyashita, Electron. Lett. 15, 106 (1979).

11. For a partial list of contributions, see for example the Materials Index to Applied Physics Letters, Vols. 24-36, Nos.12 (1974-80). See also the Subject Index to IEEE Journal of Quantum Electronics.

12. J. J. Hsieh, J. Electron. Mater. 7, 31 (1978).

13. R. E. Nahory, M. A. Pollack, W. D. Johnston, Jr. and R. L. Barns, Appl. Phy. Lett. 33, 659 (1978).

14. J. B. Restorff, B. Houston, J. R. Burke, and R. Hayes, Appl. Phys. Lett. 32, 189 (1978).

15. K. Alavi, R. L. Aggarwal, and S. H. Groves, in Proceedings of the International Conference on Solids and Plasmas in High Magnetic Field, Cambridge, Massachusetts, 18-20 September 1978, edited by R. L. Aggarwal et al (North-Holland Publishing Co., Amsterdam 1979), p.136; also published in J.Magn. Magn. Mater. 11, 136 (1979).

16. J. C. Portal, P. Perrier, M. A. Renucci, S. Askenazy, R. J. Nicholas, and T. P. Pearsall, in Proceedings of the 14th International Conference on the Physics of Semiconductors, Edinburgh, 4-8 September 1978, p. 829. (Institute of Physics. London, 1979).

17. R. J. Nicholas, J. C. Portal, C. Houlbert, P. Perrier, and T. P. Pearsall, Appl. Phys. Lett. 34, 492 (1979).

18. T. Nishino, Y. Yamazoe, and Y. Hamakawa, Appl. Phys. Lett. 33, 861 (1978).

19. H. Brendecke, H. L. Störmer, and R. J. Nelson, Appl. Phys. Lett. 35, 772 (1979).

20. E. H. Perea, E. Mendez, and C. G. Fonstad, J. Electron. Mater. 9, 459 (1980).

21. J. B. Restorff, B. Houston, R. S. Allgaier, M. A. Littlejohn, and S. B. Phatak, J. Appl. Phys. 51, 2277 (1980).

22. R. J. Nicholas, S. J. Sessions and J. C. Portal, Appl. Phys. Lett. 37, 178 (1980).

23. B. Lax and J. G. Mavroides, "Interband Magnetooptical Effects" in Semiconductors and Semimetals (R. K. Willardson and A. C. Beer, eds.) Vol. 3, p.321 (Academic Press, New York, 1967).

24. R. L. Aggarwal, "Modulated Interband Magnetooptics" in Semiconductors and Semimetals (R. K. Willardson and A. C. Beer, eds.) Vol. 9, p.151 (Academic Press, New York, 1972).

25. K. Alavi, R. L. Aggarwal, and S. H. Groves, Bull. Am. Phys. Soc. 24, 336 (1979).

26. K. Alavi, R. L. Aggarwal, and S. H. Groves, Phys. Rev. B21, 1311 (1980).

27. M. Cardona, K. L. Shaklee, and F. H. Pollak, Phys. Rev. 154, 696 (1967).

28. See for example, D. E. Aspnes, Surface Science, 37, 418 (1973).

29. S. H. Groves, C. R. Pidgeon, and J. Feinleib, Phys. Rev. Lett. 17, 643 (1966).

30. C. R. Pidgeon, S. H. Groves and J. Feinleib, Solid State Commun. 5, 677 (1967).

31. M. Reine, Ph.D. Thesis, Massachusetts Institute of Technology (1970); M. Reine, R. L. Aggarwal, and B. Lax, Phys. Rev. B5, 3033 (1972).

32. C. R. Pidgeon and R. N. Brown, Phys. Rev. 146, 575 (1966).

33. M. H. Weiler, Ph.D. Thesis, Massachusetts Institute of Technology (1977); M. H. Weiler, R. L. Aggarwal, and B. Lax, Phys. Rev. B17, 3269 (1978).

34. C. Hermann and C. Weisbuch, Phys. Rev. B15, 823 (1977).

35. C. Hermann, G. Lampel, and T. P. Pearsall, in Proceedings of the 15th International Conference on the Physics of Semiconductors, Kyoto, Japan, 1-5 September 1980.

36. T. P. Pearsall, Private Communications.

CHAPTER II

THEORETICAL BACKGROUND

A. Introduction

The effect of a magnetic field on the energy bands of a semiconductor particularly as it affects the interaction of electromagnetic radiation with these materials has been the subject of a great deal of theoretical and experimental studies. The impetus for the vast amount of research in this area was the early intraband cyclotron resonance experiment first carried out at micro-wave frequencies,[1,2] and later at infrared wavelengths.[3,4] In this thesis we are interested in optical transitions (in the infrared region) from the valence bands' magnetic sublevels to the conduction band's magnetic sublevels, corresponding to the fundamental gap of a semiconductor in the presence of an external magnetic field. This is in general referred to as interband magneto-optics. The interband magneto-optical effects have been the subject of extensive experimental and theoretical investigations. Extensive references to these important contributions can be found in the review articles by Lax and Mavroides[5] and Aggarwal.[6]

Specifically, we are interested in a theory which enables us to calculate the energies of the above mentioned magnetic sublevels for a direct gap III-V semiconductor of the zinc-blende type (point group symmetry T_d) with the fundamental gap occurring

at the Brillouin zone center ($\vec{k}=0$)

The theory we shall use to interpret our magnetoabsorption experiments is the coupled-band quasi-Ge model based on the $\vec{k}\cdot\vec{p}$ perturbation theory carried out by Pidgeon and Brown[7] and later modified by Weiler[8] and coworkers.[9]

In Section B we give a brief review of $\vec{k}\cdot\vec{p}$ theory for zinc-blende semiconductors leading to the quasi-Ge model Hamiltonian of P.B. modified by Weiler. In Section C we give some of the results of the quasi-Ge model. In Section D the selection rules for optical transitions will be given.

B. Effective-Mass Theory and the Magnetic Field -- $\vec{k}\cdot\vec{p}$ Theory For Zinc-Blende Semiconductors

A principal approach to describing the motion of charged carriers in a perturbed periodic potential is the effective-mass theory. In this method, the effect of the periodic potential on the dynamics of the charged carrier is replaced by terms which appear in the equation of motion much in the same way that mass appears in the case of free electron. In the simplest case these constants take the form of a mass tensor. In the case of degenerate or nearly degenerate bands, the effective-mass constants appear in a more complicated form. In the effective-mass method of Luttinger and Kohn (L.K.)[10] the motion of an electron in a perturbed periodic potential (e.g., electron in a semiconductor in the presence of an external magnetic field) was considered

and effective-mass Hamiltonian was obtained, including the $\vec{k} \cdot \vec{p}$
and spin-orbit terms.

B. 1. <u>A Brief Review</u>

Before we give the formalism of the coupled band
quasi-Ge model we review some of the work which led to that of
P.B. and Weiler for the case of zinc-blende type semiconductors.
In the case of InSb, with band extrema at the fundamental gap
at the Brillouin zone center, in the absence of an external magnetic
field, Kane[11] did the following. He considered the Schrödinger
equations for the cell periodic functions, including the $\vec{k} \cdot \vec{p}$ and
the spin-orbit interaction terms. For $\vec{k}=0$ he used the single-group
basis functions of the T_d group. He explicitly considered basis
states Γ_1 (S for conduction band) and Γ_4 (X,Y,Z for valence bands)
for $\vec{k}=0$ at the fundamental edge. Including up and down spin
wave functions he obtained two degenerate sets of four basis
functions and for the $\vec{k} \cdot \vec{p}$ Hamiltonian obtained two 4x4 matrices.
In these matrices he considered all possible matrix elements of
the $\vec{k} \cdot \vec{p}$ as well as the spin-orbit term between these Γ_1 and Γ_4
functions (S,X,Y,Z) of the fundamental edge up to second order
in $\vec{k}$. The first-order matrix elements coupled different
members of the (S,X,Y,Z) set. The second-order terms included
not only these four functions, but also the higher bands as
intermediate states. For the case of these higher bands spin-
orbit splitting was ignored and single-group basis functions Γ_1',

Γ_3', Γ_4', and Γ_5' appeared in Kane's treatment (prime indicates higher bands). The effect of these higher bands appeared as band parameters in the 4x4 Hamiltonians of Kane and the effect of spin-orbit splitting was included only in the conduction and valence bands of the fundamental gap. The effect of higher bands appeared only as coefficients multiplying k^2 terms in the 4x4 Hamiltonian matrices. (For Kane band parameters see Appendix B.) The Hamiltonian was then expressed in terms of linear combinations of X,Y,Z and the spin-functions ↑ and ↓, which diagonalized the spin-orbit interaction.

A second approach was chosen by Luttinger,[12] who used group theory with the double-group representation of T_d to obtain all of the allowed matrix elements of $\vec{k}$ and $\vec{k}x\vec{k}$ among the four-fold degenerate valence band states transforming as the Γ_8 double-group representation of T_d. The intermediate states (which included the Γ_6 conduction band) were also taken in the double-group representation. His results involved band parameters which were linear combinations of those of Kane, but in addition included a parameter q, which is nonzero only in the presence of spin-orbit splitting of the intermediate states. Since he considered coupling only among Γ_8 valance band state, Luttinger obtained a 4x4 matrix. Roth, Lax, and Zwerdling (R.L.Z)[13] improved the treatment by including also the spin orbit split-off band Γ_7, but still leaving the Γ_6 conduction band as an intermediate state

(getting a 6x6 Hamiltonian). Pidgeon and Brown[7] included the Γ_6 conduction band in their analysis (8x8 Hamiltonian). However, they ignored the spin-orbit splitting of the intermediate states. Thus, P.B. combined Kane's method of calculating bands for H=0 with R.L.Z.'s method of treating the magnetic field in the coupled-band scheme. Thus, P.B. included the coupling between the conduction and valence bands exactly, and the effect of higher bands to order k^2. In this manner the effects of nonparabolic conduction and light-hole bands, warping of the conduction and valence bands, and the quantum effects of light- and heavy-hole valence bands were included. Their 8x8 Hamiltonian does not include q and higher term corrections to the conduction band g-factor, i.e., N_1. The 8x8 Hamiltonian can, under certain approximation, be broken into two 4x4 block diagonal Hamiltonians; the so-called quasi-Ge model Hamiltonians.

In Weiler's[8,9] treatment (unlike in P.B.) the spin-orbit intereation as regards to its effect on the symmetrics of the intermediate states was __not__ ignored. In this treatment, the double-group basis states Γ_6 (for the conduction band), Γ_8 (for the heavy and light hole valence bands) and Γ_7 (for the spin-orbit split-off valence band) were used, both for the fundamental edge bands and the intermediate bands. Thus an 8x8 matrix was obtained with Γ_6^c, Γ_8^v, and Γ_7^v as its basis (c refers to conduction band and v to valence band, see Figure II-1). These basis

functions are given in Table II-1.

To obtain the 8x8 Hamiltonian group theoretical analysis
was used utilizing tables of Koster, Dimmok, Wheeler, and Statz,
(K.D.W.S.)[14] to find all of the allowed matrix elements of $\vec{k}$ and
$\vec{k}x\vec{k}$ among the Γ_6. Γ_7, and Γ_8 basis states of the double-group
representation of T_d and a complete set of independent parameters
were obtained (see Table II-2). These include, in addition to
the P.B. parameters and q, three additional small parameters
N_1, N_2, and N_3 where N_1 is the contribution of the higher bands
to the conduction band g-factor g_c and is nonzero only in the
presence of spin-orbit splitting of the higher bands, and N_2 and
N_3 are two inversion assymmetry parameters. In the rest of
Section B we give a brief account of the formalism of the $\vec{k}\cdot\vec{p}$
theory in a zinc-blende type semiconductor (point group
symmetry T_d) in the vicinity of the zone center ($\vec{k}=0$) near the
fundamental gap, in the presence of an external magnetic field
H, up to second order in k and first order in H, as presented
in Weiler's thesis. We also compare the two 4x4 quasi-Ge
Hamiltonians for the a- and b- sets obtained from the 8x8 Hamil-
tonian under certain approximations with those given by P.B. who
neglect terms involving N_1 and q. For the purpose of analyzing
our experiments we have used Weiler's quasi-Ge model Hamiltonians
which include N_1 and q, although it turns out that for the
physically reasonable range of N_1 and q, our experimental data

are insensitive to these two parameters. This will be discussed further in Chapter IV and Appendix B.

B. 2. The Effective-Mass Hamiltonian

The envelope functions $f_j(r)$ are the solutions of the effective-mass Hamiltonian. This is given below up to second-order in k and first-order in H, according to the L.K.[10] method as given in P.B.[7]

$$\sum_{j'} \{\hbar^2 D_{jj'}^{\alpha\beta} k_\alpha k_\beta + \frac{\hbar}{m} \pi_{jj'}^\alpha k_\alpha + \mu_B(\vec{H}\cdot\vec{\sigma})_{jj'} +$$

$$+\frac{\hbar}{4m^2c^2} [(\vec{\sigma}\times\vec{\nabla}V)\cdot\vec{p}]_{jj'} + E_{j'}\delta_{jj'}\}f_{j'}(\vec{r}) = E_j f_j(\vec{r}) \qquad (2\text{-}1)$$

where

$$D_{jj'}^{\alpha\beta} \equiv \frac{1}{2m}\delta_{jj'} + \frac{1}{m^2} \sum_{\substack{i \\ i\neq j,j'}} \frac{\pi_{ji}^\alpha \pi_{ij'}^\beta}{E_{j'}-E_i} \qquad (2\text{-}2)$$

and

$$\pi_{\ell\ell'} \equiv \int_{\text{unit cell}} u_{\ell 0}^*(\vec{r}) [\vec{p} - \frac{\hbar}{4mc^2}(\vec{\nabla}V\times\vec{\sigma})] u_{\ell'0}(\vec{r}) \, d^3r \qquad (2\text{-}3)$$

The functions $f_j(\vec{r})$ are envelope functions and the total zeroth order wave function is

$$\psi(\vec{r}) = \sum_j f_j(\vec{r}) u_{j0}(\vec{r}) \qquad (2\text{-}4)$$

The functions $u_{jo}(\vec{r})$ are the Bloch functions at $\vec{k}=0$ and include both space and spin variables. The symbols used above are:

α, β = x,y,z are the indices in a right-handed coordinate system (x,y,z) along the principal cubic axes.

$\vec{r}$ $\equiv (r_x, r_y, r_z)$ is the position vector in the (x,y,z) system.

$\vec{H}$ $\equiv$ The external static magnetic field $= \vec{\nabla} \times \vec{A}$.

$\vec{A}$ $\equiv$ The vector potential, will be taken in the Landau gage.

$\vec{\sigma}$ $\equiv$ Pauli spin matrices, e.g., $\sigma_z = \begin{pmatrix} 1 & 0 \\ 0 & -1 \end{pmatrix}$.

μ_B $\equiv \dfrac{e\hbar}{2mc}$ = Bohr magneton.

m $\equiv$ Free electron mass.

e $\equiv$ Absolute value of electron charge.

c $\equiv$ Speed of light in vacuum.

$\hbar$ $\equiv h/2\pi$, where h is Planck's constant.

V $\equiv V(\vec{r})$ is the periodic crystal potential.

$\vec{p}$ $\equiv -i\hbar\vec{\nabla} \equiv -ih\left(\dfrac{\partial}{\partial r_x}, \dfrac{\partial}{\partial r_y}, \dfrac{\partial}{\partial r_z}\right)$ is the momentum matrix element.

$\vec{\pi}_{\ell\ell'}$ $\equiv$ Modified momentum matrix element between bands ℓ and ℓ' at $\vec{k}=0$, including spin-orbit interaction.

$u_{\ell o}(\vec{r})$ $\equiv$ The Bloch function at $\vec{k}=0$ for the ℓ'th band. It has the periodicity of $V(\vec{r})$. These functions include the electron spin variable as well.

j and j' ≡ Indices which run over the two conduction bands (Γ_6^C) the four valence bands (Γ_8^V) and the two split-off bands (Γ_7^V) of the fundamental gap.

E_j ≡ The energy of state j at $\vec{k}=0$.

i ≡ The index which runs over all higher bands, clearly $i \neq j, j'$.

E_i ≡ The energy of the ith state at $\vec{k}=0$, including spin-orbit interaction.

The terms involving subscript jj' are understood to be matrix elements between $u_{jo}(\vec{r})$ and $u_{j'o}(\vec{r})$. Equation (2-1) is actually a set of eight equations since j refers to eight different bands. The sum over j' in Eq.(2-1) extends over the eight bands represented by j and j'. In the presence of a magnetic field, the operators $\vec{k}(k_\alpha; \alpha=x,y,z)$ which appear in Eq.(2-1) are defined as

$$\vec{k} \equiv \frac{1}{\hbar} \left[\vec{p} + \left(\frac{e}{c}\right) \vec{A}\right] \tag{2-5}$$

Equation (2-2) defines the effective-mass tensor, the summation here is over i, all the intermediated (so-called higher) bands outside of the eight bands Γ_6^C, Γ_8^V, and Γ_7^V, corresponding to the fundamental gap. The energy $E_{j'}$ in the denomenator is usually replaced by an average energy E_0. Equation (2-3) defines the modified momentum matrix element $\vec{\pi}_{\ell\ell'}$. The Γ_6, Γ_7, and Γ_8 are double-group representations of T_d.

FIGURE II-1 Schematic diagram of the band structure near $\vec{k}=0$
in a direct gap zinc-blende type semiconductor at the
fundamental gap E_g, at zero magnetic field. The bands
which are explicitly treated by the 8x8 $\vec{k}\cdot\vec{p}$ Hamiltonian
are Γ_6^c conduction band (2-fold spin degenerate) the
Γ_6^c valence band (4-fold degenerate at $\vec{k}=0$) and the
Γ_7^v split-off band (2 fold spin degenerate). The Γ_7^c and
Γ_8^c bands shown above are the closest higher bands.

For $\vec{k}\neq 0$ the $\vec{k}\cdot\vec{p}$ interaction reduces the 4-fold degenerate
of Γ_8^v into two 2-fold spin degenerate heavy (-) and ligth
(+) hole valence bands. In the presence of a magnetic
field, the spin degeneracies are removed. In the single-
group representation the valence bands belong to Γ_4 (in the
notation of Ref. 14, this is called Γ_5).
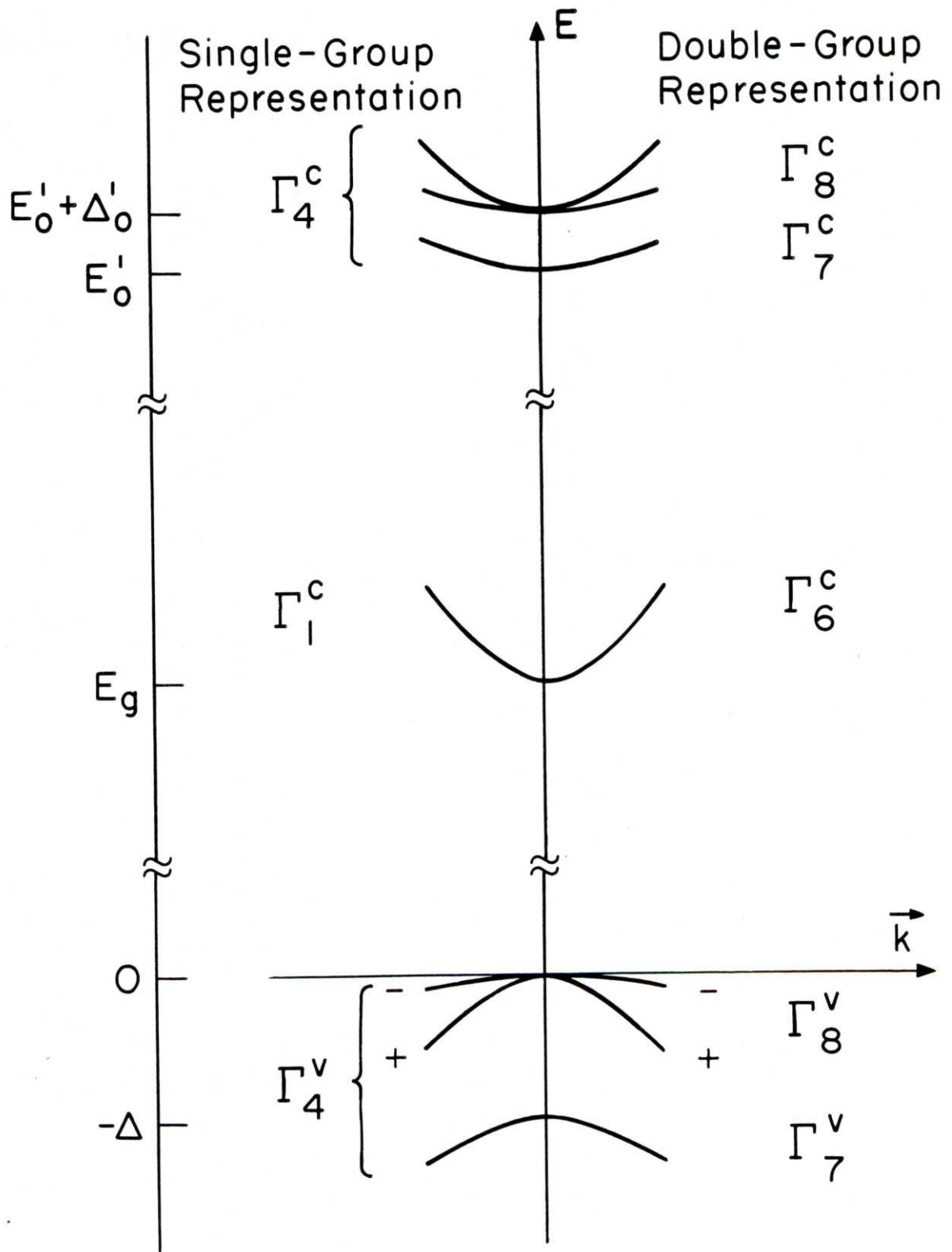
In P.B. treatment, the second term in $\pi_{\ell\ell'}$ is ignored. Also the intermediate states $u_{\ell_0}(\vec{r})$, where $\ell \neq j$ are those corresponding to the unperturbed Hamiltonian without spin-orbit interaction, that is, they have the symmetry of the single-group representations of the T_d group. Weiler[8,9] on the other hand considers $u_{\ell_0}(\vec{r})$ belonging to the double-group representation of the T_d group and as a result she obtains additional parameters N_1, N_2, N_3 and q, where q is the parameter found earlier by Luttinger.[12] For $\vec{\pi}_{\ell\ell'}$ she also disregards the second term for ℓ, ℓ' outside the 8 bands under consideration. However, note that $\vec{p}_{\ell\ell'}$ and $\vec{\pi}_{\ell\ell'}$ have the same symmetry properties. From here on we give a brief account of her method and follow her results.

In Section B.3 the (effective-mass or so-called $\vec{k}\cdot\vec{p}$) Hamiltonian of Eq.(2-1) is retained to second order in k and first order in H and obtained as an 8x8 matrix coupling the Γ_6^C(J=1/2) conduction band, the Γ_8^V(J=3/2) light and heavy hole bands, and the Γ_7^V(J=1/2) spin-orbit split-off valance band (see Figure II-1 for band diagram). The effect of other bands appears as coefficients in the 8x8 Hamiltonian matrix. In Section B.4, we give the simplified version of the Hamiltonian which is decoupled in two block-diagonal 4x4 matrices for the so-called a-set and b-set This is the so-called quasi-Ge model Hamiltonian which affords us the ability to calculate numberically the energies of the valance and conduction bands in a magnetic field. The quasi-Ge model is

obtained from the full 8x8 Hamiltonian by neglecting a number of small terms which are proportional to the warping and asymmetry parameters. Weiler[8,8] has shown that when those terms are included they are responsible for cyclotron harmonic transitions which have been observed in InSb.

B. 3. The 8x8 Hamiltonian Matrix Using Double-Group Representation of T_d

The basis functions $u_{jo}(\vec{r})$ used by Weiler[8,9] in the effective-mass Hamiltonian of Eq.(2-1) is given below in Table II-1.

TABLE II-1

a-set

$$|1\rangle = \psi^6_{1/2,1/2} = S\uparrow$$

$$|3\rangle = \psi^8_{3/2,3/2} = -\frac{i}{\sqrt{2}}(X + iY)\uparrow$$

$$|5\rangle = \psi^8_{3/2,-1/2} = \frac{i}{\sqrt{6}}[(X - iY)\uparrow + 2Z\downarrow]$$

$$|7\rangle = \psi^7_{1/2,-1/2} = -\frac{i}{\sqrt{3}}[(X - iY)\uparrow - Z\downarrow]$$

b-set

$$|2\rangle = \psi^6_{1/2,-1/2} = S\downarrow$$

$$|6\rangle = \psi^8_{3/2, 1/2} = -\frac{i}{\sqrt{6}}[(X + iY)\downarrow - 2Z\uparrow]$$

$$|4\rangle = \psi^8_{3/2,-3/2} = \frac{i}{\sqrt{2}}(X - iY)\downarrow$$

$$|8\rangle = \psi^7_{1/2,1/2} = -\frac{i}{\sqrt{3}}[(X + iY)\downarrow + Z\uparrow]$$

In Table II-1 spatial functions X, Y, Z and the spin functions ↑ and ↓ are those used by Kane,[11] for the zero magnetic field case. The superscript on ψ indicates which double-group representation of T_d ψ belongs to, and the subscripts give J and M_J, the quantum numbers for the total angular momentum and its z component, respectively.

As mentioned in B.1 of this Chapter Weiler[8,9] considers all of the matrix elements of $\vec{k}$ and $\vec{k}x\vec{k}$ among Γ_6^c, Γ_8^v, and Γ_7^v (Figure II-1). Some of these couplings involve only these subset of bands, and some involve higher bands with Γ_6, Γ_8, and Γ_7^- symmetry as intermediate states. Table II-2 summarizes all of the real independent parameters in this manner (same as Table II-2 of Ref. 8 and Table I of Ref. 9). The $\Gamma_8x\Gamma_8$ parameters γ_1, γ_2, γ_3, κ and q are defined in Ref. 12. The $\Gamma_7x\Gamma_8$ parameters are independent of the $\Gamma_8x\Gamma_8$ parameters, but are expected to be very close to them. Explicit expressions for these band parameters will be given in Appendix B. Table II-3 of Ref. 8, (same as Table II of Ref. 9) gives the 8x8 $\vec{k}\cdot\vec{p}$ Hamiltonian to second order in k and first order in H and will not be reproduced here.

B. 4. Quasi-Ge Model in a Magnetic Field

For a magnetic field H in the direction defined by the spherical polar angles θ and ϕ, with respect to the principal symmetry axes (x,y,z), a coordinate transformation is performed

TABLE II-2 Parameters of the $\vec{k}\cdot\vec{p}$ Hamiltonian among the Γ_8, Γ_7 and Γ_8 band-edge states. (After Ref. 8).

$f(\vec{k})$	$\begin{array}{c}k_x\\k_y\\k_z\end{array}$	$\vec{k}^2$	$\begin{array}{c}2k_z^2-k_x^2-k_y^2\\\sqrt{3}(k_x^2-k_y^2)\end{array}$	$\begin{array}{c}\{k_y,k_z\}\\\{k_z,k_x\}\\\{k_x,k_y\}\end{array}$	$\begin{array}{c}i[k_y,k_z]\\i[k_z,k_x]\\i[k_x,k_y]\end{array}$
$\langle\Gamma_6^C|f(\vec{k})|\Gamma_6^C\rangle$		F			N_1
$\langle\Gamma_8^V|f(\vec{k})|\Gamma_8^V\rangle$	C	γ_1	γ_2	γ_3	κ,q
$\langle\Gamma_7^V|f(\vec{k})|\Gamma_7^V\rangle$		γ_1'			κ'
$\langle\Gamma_6^C|f(\vec{k})|\Gamma_8^V\rangle$	P		N_2	G	N_3
$\langle\Gamma_6^C|f(\vec{k})|\Gamma_7^V\rangle$	P'			G'	
$\langle\Gamma_7^V|f(\vec{k})|\Gamma_8^V\rangle$	C'		γ_2'	γ_3'	κ''

so that in the new-coordinate system (1,2,3), the magnetic field would be along the 3-axis. The corresponding rotation of the basis states results in a transformation of the $\vec{k}\cdot\vec{p}$ Hamiltonian according to $\mathcal{H}(\theta,\phi)=U^{+}\mathcal{H}U$ with U given in Table II-4 of Ref. 8.

Note that with H along the 3-axis, i.e., $\vec{H}=H(0,0,1)$, $\vec{A}$ can be chosen such that $\vec{A}=\frac{1}{2}H(-\vec{r}_2,\vec{r}_1,0)$ (Landau gauge). Then, since $\hbar\vec{k}=[\vec{p}+(e/c)\vec{A}]$, we have $k_1=(1/\hbar)[p_1-(\frac{eH}{2c})r_2]$, and $k_2=(1/\hbar)[p_2-(\frac{eH}{2c})r_1]$. Since $[r_\alpha,p_\beta]=i\hbar\delta_{\alpha\beta}$ it is recognized that if one defines $a\equiv\frac{\lambda}{\sqrt{2}}(k_1-ik_2)$ and $a^{+}\equiv\frac{\lambda}{\sqrt{2}}(k_1+ik_2)$ with $\lambda\equiv(\hbar c/eH)^{1/2}$ then one obtains

$$[a,a^{+}] = 1 \tag{2-6}$$

a^{+} and a are thus recognized as the raising and lowering operators for the harmonic oscillator wave functions with $a^{+}\phi_n=\sqrt{n+1}\ \phi_{n+1}$, $a\phi_n=\sqrt{n}\ \phi_{n-1}$, and $a^{+}a\phi_n=n\phi_n$. The operators k_1 and k_2 can then be expressed as

$$k_1 = \frac{1}{\lambda\sqrt{2}}(a+a^{+}), \tag{2-7a}$$

$$k_2 = \frac{i}{\lambda\sqrt{2}}(a-a^{+}) \tag{2-7b}$$

$$k_3\equiv k_H \tag{2-7c}$$

in the 8x8 Hamiltonian of Refs. 8 and 9.

Next in the transformed Hamiltonian $\mathcal{H}(\theta,\phi)$ if one neglects terms proportional to k_H, q,C,G,N_2 and N_3 and most terms proportional to the warping parameter $\mu \equiv \frac{1}{2}(\gamma_3-\gamma_2)$ one gets the 8x8 Hamiltonian separated into two block diagonal 4x4 Hamiltonians corresponding to the a-set and the b-set, i.e.,

$$\mathcal{H}(\theta,\phi) \simeq \begin{bmatrix} \mathcal{H}_a & 0 \\ & \\ 0 & \mathcal{H}_b \end{bmatrix}_{(8\times8)} \tag{2-8}$$

where $\mathcal{H}_a$ and $\mathcal{H}_b$ are called the quasi-Ge model Hamiltonians given here in Table II-3 where

$$\gamma' = \gamma_3 + (\gamma_2-\gamma_3)f(\theta,\phi) \tag{2-9a}$$

$$\gamma'' = \frac{1}{3}\gamma_2 + \frac{2}{3}\gamma_3 + \frac{1}{6}(\gamma_2-\gamma_3)f(\theta,\phi) \tag{2-9b}$$

with

$$f(\theta,\phi) = \left(\frac{3\cos^2\theta-1}{2}\right)^2 + \frac{3}{4}\cos^2 2\phi \sin^4\theta \tag{2-9c}$$

For $\phi=45°$, i.e., H in the $(1\bar{1}0)$ plane $\bar{q}_1$ ans $\bar{q}_2$ are given as:

TABLE II-3 The Quasi-Ge Model Hamiltonian

$$\mathcal{H}_a = \begin{array}{cccc} |1\rangle & |3\rangle & |5\rangle & |7\rangle \\ \left[\begin{array}{cccc} E_g + 2\beta H[F(2a^+a+1) \\ \qquad + N_1 + (a^+a+1)] & (\beta H E_p)^{1/2}\, a^+ & -(\tfrac{1}{3}\beta H E_p)^{1/2}\, a & (\tfrac{2}{3}\beta H E_p)^{1/2}\, a \\\\ (\beta H E_p)^{1/2}\, a & -\beta H[(\gamma_1+\gamma')(2a^+a+1) \\ \qquad +3\kappa+\bar{q}_1] & 2\sqrt{3}\,\gamma''\beta H\, a^2 & -2\sqrt{6}\,\gamma''\beta H\, a^2 \\\\ -(\tfrac{1}{3}\beta H E_p)^{1/2}\, a^+ & 2\sqrt{3}\,\gamma''\,\beta H\, a^{+2} & -\beta H[(\gamma_1-\gamma')(2a^+a+1) \\ \qquad -\kappa+\bar{q}_5] & \sqrt{2}\beta H[\gamma'(2a^+a+1) \\ \qquad -\kappa-1] \\\\ (\tfrac{2}{3}\beta H E_p)^{1/2}\, a^+ & -2\sqrt{6}\,\gamma''\beta H\, a^{+2} & \sqrt{2}\beta H[\gamma'(2a^+a+1) \\ \qquad -\kappa-1] & -\Delta-\beta H[\gamma_1(2a^+a+1) \\ \qquad -2\kappa-1] \end{array}\right] \begin{array}{c} |1\rangle \\\\ |3\rangle \\\\ |5\rangle \\\\ |7\rangle \end{array} \end{array}$$

$$\mathcal{H}_b = \begin{array}{cccc} |2\rangle & |6\rangle & |4\rangle & |8\rangle \\ \left[\begin{array}{cccc} E_g + 2\beta H[F(2a^+a+1) \\ \qquad -N_1 + a^+a] & (\tfrac{1}{3}\beta H E_p)^{1/2}\, a^+ & -(\beta H E_p)^{1/2}\, a & (\tfrac{2}{3}\beta H E_p)^{1/2}\, a^+ \\\\ (\tfrac{1}{3}\beta H E_p)^{1/2}\, a & -\beta H[(\gamma_1-\gamma')(2a^+a+1) \\ \qquad +\kappa-\bar{q}_5] & 2\sqrt{3}\,\gamma''\,\beta H\, a^2 & -\sqrt{2}\,\beta H[\gamma'(2a^+a+1) \\ \qquad +\kappa+1] \\\\ -(\beta H E_p)^{1/2}\, a^+ & 2\sqrt{3}\,\gamma''\,\beta H\, a^{+2} & -\beta H[(\gamma_1+\gamma')(2a^+a+1) \\ \qquad -3\kappa-\bar{q}_1] & 2\sqrt{6}\gamma''\,\beta H\, a^{+2} \\\\ (\tfrac{2}{3}\beta H E_p)^{1/2}\, a & -\sqrt{2}\,\beta H[\gamma'(2a^+a+1) \\ \qquad +\kappa+1] & 2\sqrt{6}\,\gamma''\,\beta H\, a^2 & -\Delta-\beta H[\gamma_1(2a^+a+1) \\ \qquad +2\kappa+1] \end{array}\right] \begin{array}{c} |2\rangle \\\\ |6\rangle \\\\ |4\rangle \\\\ |8\rangle \end{array} \end{array}$$

$$\bar{q}_1 = \frac{3}{4} q(3 \cos^4\theta - 2\cos^2\theta + 8) \qquad (2\text{-}10a)$$

$$\bar{q}_5 = \frac{1}{4} q(27\cos^4\theta - 18\cos^2\theta - 10). \qquad (2\text{-}10b)$$

The operators a and a^+ are given by

$$a = \left(\frac{2eH}{\hbar c}\right)^{-1/2}(k_1 + ik_2) , \qquad (2\text{-}11a)$$

$$a^+ = \left(\frac{2eH}{\hbar c}\right)^{-1/2}(k_1 + ik_2) \qquad (2\text{-}11b)$$

and $\qquad \beta \equiv \mu_B \equiv (e\hbar/2mc) \equiv$ Bohr magneton $\qquad (2\text{-}11c)$

$$E_p \equiv 2mP^2/\hbar^2 \qquad (2\text{-}12)$$

The Hamiltonians in Table II-3 are equivalent to those of P.B.[7] with the following corrections:

1) The parameter N_1, which gives the effect of intermediate states on the g-factor of the conduction band, as well as diagonal terms proportional to q, are included here.

2) In Eq.(10) of Ref. 7, for the (3,7) and (7,3) matrix elements, γ' should be replaced by $-\gamma''$.

3) In Eq.(11) of Ref. 7, for the (4,8) and (8,4) matrix elements, γ' should be replaced by γ''.

In the quasi-Ge model one then has to solve these two Schrödinger equations for the a-set and the b-set.

$$\mathcal{H}_a |a\rangle = E_a|a\rangle \qquad (2\text{-}13a)$$
$$\mathcal{H}_b |b\rangle = E_b|b\rangle \qquad (2\text{-}13b)$$

The solutions are of the following form.

$$
|a\rangle = \begin{bmatrix} a_1^n \, \phi_n \\ a_3^n \, \phi_{n-1} \\ a_5^n \, \phi_{n+1} \\ a_7^n \, \phi_{n+1} \end{bmatrix}, \qquad
|b\rangle = \begin{bmatrix} b_2^n \, \phi_n \\ b_6^n \, \phi_{n-1} \\ b_4^n \, \phi_{n+1} \\ b_8^n \, \phi_{n-1} \end{bmatrix}
$$

(2-14a)

(2-14b)

where n is an interger and $n \geq -1$.

Here ϕ_n is the harmonic oscillator wave function so that $a^+\phi_n = \sqrt{n+1} \, \phi_{n+1}$ and $a\phi_n = \sqrt{n} \, \phi_{n-1}$. The coefficients a_j^n and b_j^n are zero for those values of n which make the subscript of ϕ negative: i.e.,

$$a_1^{-1} = a_3^{-1} = a_3^0 = b_2^{-1} = b_6^0 = b_6^{-1} = b_8^{-1} = b_8^0 = 0$$

For each integer $n \geq 1$ the two 4x4 Hamiltonians give eight independent solutions: $|a^c(n)\rangle$, $|b^c(n)\rangle$, $|a^-(n)\rangle$, $|b^-(n)\rangle$, $|a^+(n)\rangle$, $|b^+(n)\rangle$, $|a^{so}(n)\rangle$, $|b^{so}(n)\rangle$, where "c" refers to the conduction band, "-" and "+" to the heavy and light hole valence bands respectively, and "so" to the spin-orbit split-off band. In fact with eigen-vectors of the form in Eqs.(2-14) the a, a^+, a^2, and a^{+2} operators in matrices of Table II-3 can be replaced by

expressions involving n, more explicitly: a^2 and a^{+2} are replaced by $[n(n+1)]^{1/2}$, and

$$a^+a \rightarrow \begin{cases} (n) & \text{in } (1,1), (2,2) \\ (n-1) & \text{in } (3,3), (6,6), (8,8), (6,8), (8,6) \\ (n+1) & \text{in } (5,5), (7,7), (5,7), (7,5), (4,4) \end{cases}$$

$$a \rightarrow \begin{cases} (n+1)^{1/2} & \text{in } (1,5), (1,7), (2,4) \\ (n)^{1/2} & \text{in } (3,1), (6,2), (8,2) \end{cases}$$

$$a^+ \rightarrow \begin{cases} (n+1)^{1/2} & \text{in } (5,1), (7,1), (4,2) \\ (n)^{1/2} & \text{in } (1,3), (2,6), (2,8) \end{cases}$$

giving the two 4x4 quasi-Ge model Hamiltonian matrices in terms of n. One can then use a computer to determine eigenvalues for Eqs.(2-13) as well as eigen-vectors (i.e., values for a_n and b_n's), for a given set of band parameters and aribtrary n.

C. Some Results of the Quasi-Ge Model

Reference 6 gives explicit expressions for the deter-minantal equations for the eigenvalue problem of Eqs.(2-13); this is given in Eq.(83), where the terms involved are defined in Eqs.(81) and (82) for the a-set and the b-set respectively. In Eq.(81) one should read $F=-[6n(n+1)]^{1/2}\gamma''$. In this treatment N_1 and q are ignored. The eigenvalues (E_a and E_b in our

notation) are expanded in a power series in $s(s \equiv 2\beta H)$ and expressions are obtained for the eigen-energies up to second-order in H.

C. 1. Energies Up to First Order in H

The conduction band energies to first order in H are

$$\left.\begin{array}{c} E[a^c(n)] \\[2ex] E[b^c(n)] \end{array}\right\} = E_g + (n+\tfrac{1}{2})\hbar\omega_c \pm \tfrac{1}{2}g_c\beta H \qquad (2\text{-}15)$$

where ω_c, the cyclotron frequency, m_c the effective mass, and g_c the g-factor, are for the conduction band and they are given as follows:

$$\omega_c = eH/m_c c \qquad (2\text{-}16)$$

$$\frac{m}{m_c} \equiv 1 + \frac{1}{3} E_p\left(\frac{2}{E_g} + \frac{1}{E_g + \Delta}\right) + 2F \qquad (2\text{-}17)$$

$$g_c \equiv 2 - \frac{2}{3} E_p\left(\frac{1}{E_g} - \frac{1}{E_g + \Delta}\right) + 4N_1 \qquad (2\text{-}18)$$

$$= 2[1 - \frac{E_p}{3E_g} \cdot \frac{\Delta}{E_g + \Delta}] + 4N_1 \qquad (2\text{-}18a)$$

which include the higher band contributions F and N_1. These contribution have been considered earlier by Groves[15] and more recently by Hermann and Weisbuch[16] (see Appendix B). The valence band energies to first order are[8] (+ for light hole, - for heavy hole; $n \geq 1$ for heavy holes and $n \geq -1$ for light holes).

$$E[a^{\pm}(n)] = -2\beta H\{(n+\tfrac{1}{2})\gamma_1^L - \gamma'^L + \tfrac{1}{2}\kappa^L + (\tfrac{5}{8}+f)q \tag{2-19}$$

$$\pm\sqrt{[\gamma_1^L - (n+\tfrac{1}{2})\gamma'^L - \kappa^L - \tfrac{1}{2}(\tfrac{9}{2}-f)q]^2 + 3n(n+1)(\gamma''^L)^2}\}$$

$$E[b^{\pm}(n)] = -2\beta H\{(n+\tfrac{1}{2})\gamma_1^L + \gamma'^L - \tfrac{1}{2}\kappa^L - (\tfrac{5}{8}+f)q \tag{2-20}$$

$$\pm\sqrt{[\gamma_1^L + (n+\tfrac{1}{2})\gamma'^L - \kappa^L - \tfrac{1}{2}(\tfrac{9}{2}-f)q]^2 + 3n(n+1)(\gamma''^L)^2}\}$$

where $f \equiv f(\theta,\phi)$ and γ_1^L, γ'^L, etc. are the Luttinger[12] parameters:

$$\gamma_1^L \equiv \tfrac{1}{3}(E_p/E_g) + \gamma_1 \tag{2-21a}$$

$$\gamma'^L \equiv \tfrac{1}{6}(E_p/E_g) + \gamma' \tag{2-21b}$$

$$\gamma''^L \equiv \tfrac{1}{6}(E_p/E_g) + \gamma'' \tag{2-21c}$$

$$\kappa^L \equiv \tfrac{1}{6}(E_p/E_g) + \kappa \tag{2-21d}$$

For n=-1 and 0, and assuming q=0

$$E[a^+(-1)] = -\beta H[\gamma_1^L - \gamma'^L - \kappa^L] \tag{2-22a}$$

$$E[a^+(0)] = -\beta H[3\gamma_1^L - 3\gamma'^L - \kappa^L] \tag{2-22b}$$

$$E[b^+(-1)] = -\beta H[\gamma_1^L + \gamma'^L - 3\kappa^L] \tag{2-22c}$$

$$E[b^+(0)] = -\beta H[3\gamma_1^L + 3\gamma'^L - 3\kappa^L] \tag{2-22d}$$

For large n, Eqs. (2-19) and (2-20) give

$$E[a^{\pm}(n)] - E[a^{\pm}(n+1)] \simeq \left(\frac{m}{m_{\pm}}\right) \cdot 2\beta H > 0 \qquad (2\text{-}23)$$

and similarly for the b-set. Here the effective masses for the heavy (-) and the light (+) hole bands are given by

$$\frac{m}{m_{\pm}} = \gamma_1^L \pm [(\gamma'^L)^2 + 3(\gamma''^L)^2]^{1/2} \qquad (2\text{-}24)$$

For $E_p/E_g \gg \gamma', \gamma''$ this gives

$$\frac{m}{m_+} \simeq \frac{2}{3}\frac{E_p}{E_g} + \gamma_1 + \frac{1}{2}(\gamma'+3\gamma'') \qquad (2\text{-}25a)$$

$$\frac{m}{m_-} \simeq \gamma_1 - \frac{1}{2}(\gamma'+3\gamma'') \qquad (2\text{-}25b)$$

which shows that the light hole band is nearly the mirror image of the conduction band, and the heavy hole mass has a large effective mass $\sim \gamma_1^{-1}$

For the spin-orbit split-off band, to first order in H

$$E[a^{so}(n)] = -\Delta - (n+\tfrac{3}{2})\frac{m}{m_{so}} + \tfrac{1}{4}g_{so}]2\beta H, \text{ with } n=-1,0,1,\ldots \qquad (2\text{-}26a)$$

$$E[b^{so}(n)] = -\Delta - (n-\tfrac{1}{2})\frac{m}{m_{so}} - \tfrac{1}{4}g_{so}]2\beta H, \text{ with } n=1,2,3\ldots \qquad (2\text{-}26b)$$

$$\frac{m}{m_{so}} = \gamma_1^L - \frac{E_p}{3}[\frac{1}{E_g} - \frac{1}{E_g+\Delta}] \qquad (2\text{-}27a)$$

$$= \gamma_1 + \frac{E_p}{3(E_g+\Delta)} \qquad (2\text{-}27b)$$

and

$$g_{so} = -2[2\kappa^L + 1 - \frac{E_p}{3E_g} \cdot \frac{\Delta}{E_g + \Delta}] \tag{2-28}$$

which gives

$$g_c + g_{so} = -4(\kappa^L - N_1) \tag{2-29}$$

It turns out that N_1 is very small (Appendix B, and Ch.IV), therefore,

$$g_c + g_{so} \simeq -4\kappa^L \tag{2-30}$$

C. 2. Energies Up to Second Order in H

We now consider the corrections to the energies, second-order in H. For this purpose, we could follow the procedure of Ref.6 and use Eq.(102). From this equation one can find correction to the conduction band energy. For simplicity one can ignore the effect of higher bands and obtain Kane's formula,[11] namely set F=0, $\gamma_1 = -1$, $\gamma_2 = \gamma_3 = 0$, $\kappa = -\frac{1}{3}$. Then for the average conduction band a and b series energies in the units of $(2\beta H)^2$ Ref.6 finds the following second-order correction.

$$\mathcal{E}_2^c = (n + \frac{1}{2})^{1/2} (\frac{m}{m_c} - 1)^2 \left[\frac{3E_g + 4\Delta + 2\Delta^2/E_g}{(E_g + \Delta)(3E_g + 2\Delta)} \right] \tag{2-31}$$

[See Eq.(110) of Ref. 6 for example]. Note that in this formula

$\frac{m}{m_c}$ is given by Eq.(2-17) but with F=0. This result is in agreement with Vrehen.[17] He started with Kane's determinantal equation, i.e.,

$$E'[(E'-E_g)(E')(E'+\Delta) - k^2 P^2(E'+\tfrac{2}{3}\Delta)] = 0 \qquad (2-32)$$

where

$$E' = E(k) - \frac{\hbar^2 k^2}{2m} \qquad (2-33)$$

and from Eq.(2-12)

$$P^2 = \frac{\hbar^2}{2m} E_p \qquad (2-34)$$

For the conduction band, keeping only terms up to k^4, Vrehen obtained, again with F=0,

$$E_c = E_g + (\frac{m}{m_c}) \frac{\hbar^2 k^2}{2m} - (\frac{m}{m_c} -1)^2 (\frac{\hbar^2 k^2}{2m})^2 \left[\frac{3E_g + 4\Delta + 2\Delta^2/E_g}{(E_g+\Delta)(3E_g+2\Delta)} \right] \qquad (2-35)$$

One can then make the following substitution

$$\frac{\hbar^2 k^2}{2m} \rightarrow (n+\tfrac{1}{2})(2\beta H) \qquad (2-36)$$

to obtain the expression for the average energy of the conduction band a and b series in agreement with Eq.(2-31).

Johnson,[18] starts with Eq.(2-32) and rearranges terms to obtain

$$E'(E'-E_g) = k^2 P^2 (\frac{E'+\tfrac{2}{3}\Delta}{E'+\Delta}) \qquad (2-37)$$

This yields

$$E_c = \frac{1}{2}E_g + \frac{\hbar^2 k^2}{2m} + \frac{1}{2}E_g[1+4\frac{\hbar^2 k^2}{2m_c} \cdot \frac{f_1(E')}{E_g}]^{1/2} \qquad (2\text{-}38)$$

where

$$f_1(E') = \frac{E_g+\Delta}{E_g+\frac{2}{3}\Delta} \cdot \frac{E'+\frac{2}{3}\Delta}{E'+\Delta} \qquad (2\text{-}39)$$

Comparing this with Eqs.(41) and (51) of Ref. 18, one see that in Ref. 18, $f_1(E_c)$ is used instead of $f_1(E')$. Again when one keeps terms up to k^4, one can recover (2-35). In all of the above treatments the higher band contributions including F is ignored. We would like to keep F nonzero. We start from Kane's determinantal Equation,[11] this time including F, the higher-bands contribution to the conduction band effective mass. Kane's determinantal equation becomes:

$$E'[(E''-E_g)(E'')(E'+\Delta) - \frac{\hbar^2 k^2}{2m}E_p(E'+\frac{2}{3}\Delta)] = 0 \qquad (2\text{-}40)$$

Here

$$E'' = E' - \left(\frac{\hbar^2 k^2}{2m}\right)2F \qquad (2\text{-}41a)$$

$$E' = E - \frac{\hbar^2 k^2}{2m} \qquad (2\text{-}41b)$$

For the conduction band let us expand E up to k^4, i.e.,

$$E = E_g + (X+1)\frac{\hbar^2 k^2}{2m} + Y(\frac{\hbar^2 k^2}{2m})^2 \qquad (2\text{-}42)$$

we then have to find X and Y. Let us define

$$\lambda \equiv \frac{\hbar^2 k^2}{2m} \tag{2-43}$$

We now substitute (2-42) in (2-40) using (2-41). This gives the following equation, correct to λ^2:

$$\lambda[(X-2F)+Y\lambda][E_g+X\lambda + Y\lambda^2][(E_g+\Delta)+X\lambda + Y\lambda^2]$$

$$-\lambda E_p[(E_g+\tfrac{2}{3}\Delta) + X\lambda +Y\lambda^2] = 0$$

For this to hold for arbitrary k (and for terms up to k^4) we require the coefficients of k^2 and k^4, i.e., coefficients of λ and λ^2 to be identically zero: this gives

$$(X-2F)E_g(E_g+\Delta) - E_p(E_g+\tfrac{2}{3}\Delta) = 0 \tag{2-44}$$

$$(X-2F)[E_g X+X(E_g+\Delta)] + Y E_g(E_g+\Delta) - E_pX = 0 \tag{2-45}$$

Equation (2-44) gives:

$$X-2F = \frac{E_p(E_g+\tfrac{2}{3}\Delta)}{E_g(E_g+\Delta)} \tag{2-46}$$

or

$$X = \frac{E_p}{3}(\frac{2}{E_g} + \frac{1}{E_g+\Delta}) + 2F \tag{2-47}$$

We immediately recognize that the coefficient multiplying k^2 in Eq.(2-42) is

$$(X+1) \equiv \frac{m}{m_c} \tag{2-48}$$

Where $\frac{m}{m_c}$ is given by Eq.(2-17), and this is not surprizing. As for Y, Eq.(2-45) gives

$$Y = -X\left[\frac{(X-2F)(2E_g+\Delta)-E_p}{E_g(E_g+\Delta)}\right] \tag{2-49}$$

Using Eq.(2-46) this yields:

$$Y=-X \frac{E_p(3E_g+2\Delta)}{3E_g(E_g+\Delta)} \cdot \left(\frac{3E_g+4\Delta+2\Delta^2/E_g}{(E_g+\Delta)(3E_g+2\Delta)}\right) \tag{2-50}$$

Using Eqs. (2-48) and (2-17) and this gives

$$Y = -\left(\frac{m}{m_c}-1\right)\left(\frac{m}{m_c}-1-2F\right)\left(\frac{3E_g+4\Delta+2\Delta^2/E_g}{(E_g+\Delta)(3E_g+2\Delta)}\right) \tag{2-51}$$

Thus

$$E_c = E_g+\left(\frac{m}{m_c}\right)\frac{\hbar^2k^2}{2m} - \left(\frac{m}{m_c}-1\right)\left(\frac{m}{m_c}-1-2F\right)\left(\frac{\hbar^2k^2}{2m}\right)^2$$

$$\times \left(\frac{3E_g+4\Delta+2\Delta^2/E_g}{(E_g+\Delta)(3E_g+2\Delta)}\right) \tag{2-52}$$

In a magnetic field, the average energy of a and b series is obtained

below, using the substitution (2-36) in Eq.(2-52)

$$E_c = E_g + (n+\frac{1}{2})(\frac{m}{m_c})(2\beta H)$$

$$-(n+\frac{1}{2})^2 (\frac{m}{m_c} - 1)(\frac{m}{m_c} - 1 - 2F)\left[\frac{3E_g+4\Delta+2\Delta^2/E_g}{(E_g+\Delta)(3E_g+2\Delta)}\right](2\beta H)^2 \quad (2-53)$$

In Eqs.(2-52) and (2-53), $\frac{m}{m_c}$ is given by Eq.(2-17) which includes F.
Here m_c is the effective mass at the bottom of the conduction band.
For F=0, our result is in agreement with that of Refs. 6, 17 and
18. However, Eqs.(2-52) and (2-53) bring out a feature hidden
in the above references where F=0 is assumed. Note that in the
nonparabolic term, proportional to k^4 or H^2, $(\frac{m}{m_c} - 1 - 2F)$ is proportional
to E_p. Therefore presumably although different values of E_p and F
can be adjusted to give the same value for m_c for the parabolic
term (proportional to k^2 or H), the nonparabolic term is different
for different values of F. Would this help narrow down the range
of acceptable values for F? To answer this, the effect of $\gamma_1, \gamma_2, \gamma_3$, and
κ should also be included (see Appendix C). In Chaper IV this question
will be considered in some detail.

D. Magneto-optical Transitions: Selection Rules

Magneto-optical transitons come about from the coupling among
the eigenstates of Eqs.(2-13) which have the form given in Eqs.(2-14),
via the optical field Hamiltonian $\mathcal{H}'_0(\omega)$, at circular frequency ω.

The strongest allowed one photon optical transitions among
these eigenstates are those transitions which are proportional to the

interband matrix element P. For these transitions, the matrix elements containing terms of the type $\vec{k}P$ in the full 8x8 $\vec{k} \cdot \vec{p}$ Hamiltonian of Refs. 8 and 9 are replaced as follows:

$$\vec{k} \, P, \; \vec{k} \, P' \rightarrow [\vec{k} + (e/\hbar c)\vec{A}']P \tag{2-54}$$

where P is given by Eq.(2-34) in terms of E_p, and $\vec{A}'$ is the vector potential of the radiation field in the radiation gauge. In the 8x8 $\vec{k} \cdot \vec{p}$ Hamiltonian (Table II of Ref. 9) there are two types of terms proportional to P (and P' with P'~P). The first type couples the states of the a-set to those in the a-set; or the states in the b-set to those in the b-set. The second type couples the states of the a-set to those of the b-set. The latter type of terms appear in the following matrix elements: (1,6), (1,8), (2,5), (2,7), (6,1), (8,1), (5,2) and (7,2). These terms are proportional to PK_3 (or $P'K_3$; $P' \simeq P$). For the quasi-Ge model, we recall that C, G, N_2, N_3, and most terms proportional to $(\gamma_3 - \gamma_2)$ as well as $k_3 \equiv k_H$ were set equal to zero. However, in the presence of the radiation field according to Eq.(2-54) $k_3 \rightarrow k_3 + (e/\hbar c)A'_3$, and hence even with $k_3 = 0$, $(e/\hbar c)A'_3$ survives. As a result, the presence of radiation field can cause coupling between the a-set and the b-set states as well.

The matrix elements for the optical transitions are[8]

$$\langle a(n')| \mathcal{H} (\omega)| a(n)\rangle = \tag{2-55a}$$

$$\frac{eE}{\omega} \left(\frac{E_p}{6m}\right)^{1/2} \left\{[\sqrt{3} \; a_3^{n'} a_1^n - a_1^{n'} (a_5^n - \sqrt{2} \; a_7^n)]\hat{\epsilon}_- \; \delta_{n',n+1} + [n \leftrightarrow n']\hat{\epsilon}_+ \delta_{n',n-1}\right\}$$

$$\langle b(n')|\mathcal{H}'(\omega)\,b(n)\rangle =$$

$$\text{(2-55b)}$$

$$\frac{eE}{\omega}\left(\frac{E_p}{6m}\right)^{1/2}\left\{[(b_6^{n'}+\sqrt{2}\,b_8^{n'})b_2^n - \sqrt{3}\,b_2^{n'}\,b_4^n]\hat{\varepsilon}_-\delta_{n',n+1} + [n\leftrightarrow n']\hat{\varepsilon}_+\delta_{n',n-1}\right.$$

$$\langle b(n')|\mathcal{H}'(\omega)|a(n)\rangle =$$

$$-\frac{eE}{\omega}\left(\frac{E_p}{6m}\right)^{1/2}[b_2^{n'}(\sqrt{2}\,a_5^n + a_7^n) + (\sqrt{2}\,b_6^{n'} - b_8^{n'})a_1^n]\hat{\varepsilon}_3\delta_{n',n+1} \qquad \text{(2-55c)}$$

Here E is the optical electric field, and $\hat{\varepsilon}_{\pm}\equiv(\hat{\varepsilon}_1\pm i\hat{\varepsilon}_2)/\sqrt{2}$. The unit polarization vectors $\hat{\varepsilon}_+$ and $\hat{\varepsilon}_-$ correspond respectively to right and left circular polarization (RCP, LCP) transverse to $\vec{H}$ and $\hat{\varepsilon}_3$ is the unit polization vector parallel to $\vec{H}(\vec{E}||\vec{H}$, or $\hat{\varepsilon}$ polarization). The one photon optical selection rules are then

$$\vec{k}||\vec{H}\left\{\begin{array}{ll}\sigma_L(LCP) & a(n)\to a(n+1)\text{ and }b(n)\to b(n+1)\\[2mm]\sigma_R(RCP) & a(n)\to a(n-1)\text{ and }b(n)\to b(n-1)\end{array}\right.$$

$$\text{(2-56)}$$

$$\vec{k}\perp\vec{H}\left\{\begin{array}{ll}\pi(E||H) & a(n)\to b(n+1)\text{ and }b(n)\to a(n-1)\\[2mm]\vec{E}\perp\vec{H} & \begin{array}{l}a(n)\to a(n+1),\ a(a-1)\\b(n)\to b(n+1),\ b(n-1)\end{array}\end{array}\right.$$

Intuitively, if one recalls that generally speaking "a" is associated with spin up and "b" with spin down electron, and n with the orbital angular momentum of the electron, then the selection rules above could be considered as a statement of conservation of angular momentum for the "light and electron" system.

Figure II-2 shows schematically the Landau levels for the

conduction band a-set and b-set as well as the light-hole (+) and the heavy hole (-) a-set and b-set. The lowest-energy allowed interband magneto-optical transitions for the Voigt $\vec{E}||\vec{H}$ and for the Faraday (RCP and LCP) configurations are shown by arrows. It is seen from the selection rules that the first two transitions in the LCP originate from the light-hole bands.

FIGURE II-2   The Landau levels for the conduction band and the
             light-hole and heavy-hole valence bands. The value of
             the Landau quantum number for each level is shown.
             The lowest-energy allowed interband transitions for
             the Faraday configuration (RCP and LCP) and for the
             Voigt configuration are indicated by the arrows.
             ε_g is the same as E_g in our notation. (After
             Reine et al.[19])
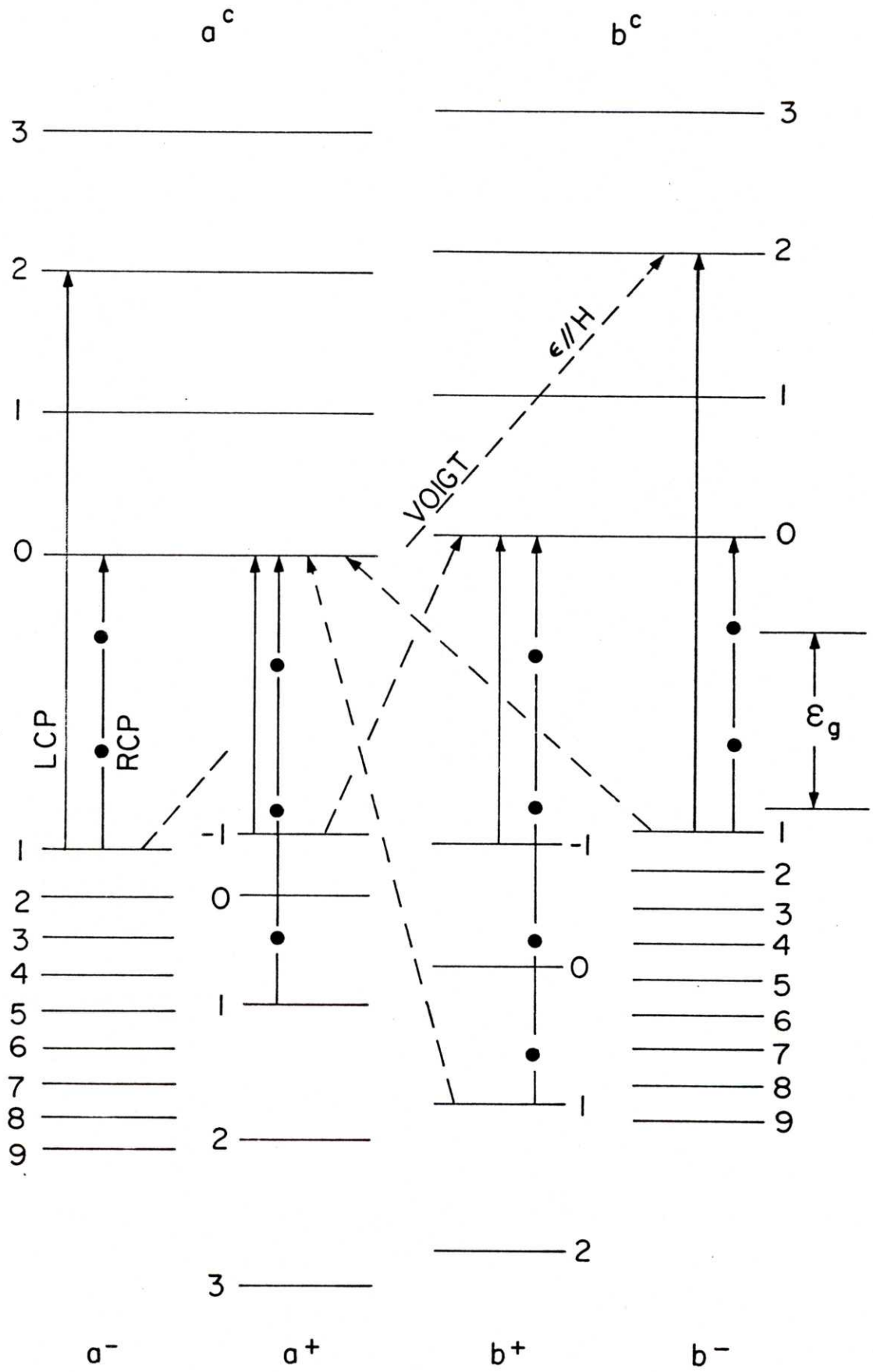
REFERENCES

1. G. Dresselhaus, A. F. Kip, and C. Kittel, Phys. Rev. 92, 827 (1953).

2. B. Lax, H. J. Zeiger, R. N. Dexter, and E. S. Rosenblum, Phys. Rev. 93, 1418 (1954).

3. E. Burstein, G. S. Picus, and H. A. Gebbie, Phys. Rev. 103, 825 (1956).

4. R. J. Keyes, S. Zwerdling, S. Foner, H. H. Kolm, and B. Lax, Phys. Rev. 105, 1804 (1956).

5. B. Lax and J. G. Mavroides, "Interband Magnetooptical Effects" in Semiconductors and Semimetals (R. K. Willardson and A. C. Beer, eds.) Vol. 3, p.321 (Academic Press, New York, 1967).

6. R. L. Aggarwal, "Modulated Interband Magnetooptics" in Semiconductors and Semimetals (R. K. Willardson and A. C. Beer, eds.) Vol. 9, p.151 (Academic Press, New York, 1972).

7. C. R. Pidgeon and R. N. Brown, Phys. Rev. 146, 575 (1966).

8. M. H. Weiler, Ph.D. Thesis, Massachusetts Institute of Technology (1977).

9. M. H. Weiler, R. L. Aggarwal, and B. Lax, Phys. Rev. B17, 3269 (1978); this paper is based on Ref. 8.

10. J. M. Luttinger and W. Kohn, Phys. Rev. 97, 869 (1955).

11. E. O. Kane, J. Phys. Chem. Solids 1, 249 (1957); ibid, "The $\vec{k} \cdot \vec{p}$ Method" in Semiconductors and Semimetals (R. K. Willardson and A. C. Beer, eds.) Vol. 1, p.75 (Academic Press, New York, 1966).

12. J. M. Luttinger, Phys. Rev. 102, 1030 (1956).

13. L. M. Roth, B. Lax, and S. Zwerdling, Phys. Rev. 114, 90 (1959).

14. G. F. Koster, J. O. Dimmock, R. G. Wheeler, and H. Statz, "Properties of the Thirty-Two Point Groups", (M.I.T. Press, Cambridge, 1966).

15. S. H. Groves, in M.I.T. Lincoln Laboratory Solid State Research, quarterly report, 16 Oct. 1970 (3rd quarter), p.33.

16. C. Hermann and C. Weisbuch, Phys. Rev. B15, 823 (1977).

17. Q. H. F. Vrehen, J. Phys. Chem. Solids <u>29</u>, 129 (1968).

18. E. J. Johnson, "Absorption near the Fundamental Edge" in <u>Semiconductors and Semimetals</u> (R. K. Willardson and A. C. Beer, eds.) Vol. <u>3</u>, p.153, (Academic Press, New York, 1967).

19. M. Reine, Ph.D. Thesis, Massachusetts Institute of Technology (1970); M. Reine, R. L. Aggarwal, and B. Lax, Phys. Rev. B<u>5</u>, 3033 (1972).

CHAPTER III

MAGNETOABSORPTION EXPERIMENTS

In this chapter, we describe the details of our experiments on $In_{1-x}Ga_xAs_yP_{1-y}$, describing the samples in Section A and the experimental setup and data acquisition system in Section B. In Section C we present some magnetotransmission spectra $T(H)/T(0)$ vs. photon energy, where $T(H)$ is the signal from transmitted light in the presence of the magnetic field and $T(0)$ is that in the absence of the magnetic field. In this section, we also describe how the spectra were obtained.

In Chapter IV, we give plots indicating position of minima in the spectra in a photon energy vs. magnetic field plot. Included in these plots will be calculated lines (fan charts) based on quasi-Ge coupled band $\vec{k}\cdot\vec{p}$ analysis with exciton correction described in Chapter IV.

A. Samples

The $In_{1-x}Ga_xAs_yP_{1-y}$ samples used in this investigation were grown by liquid-phase epitaxy on InP substrates of (100) orientation at Lincoln Laboratory.[1] The InP substrates were Fe-doped to make them semi-insulating. We started our preliminary studies in quaternary sample Q9-6 which yielded only 2-3 minima in the trans-mission spectrum. The next sample used was Q9-14A with an original

quaternary layer thickness of about 5μm. It turned out that this sample had to be etched a few times to reduce the quaternary thickness until magnetotransmission spectra with four minima were obtained. Finally, a much superior quaternary sample was grown (Q9-18) which yielded 7 to 8 minima in the magnetotransmission spectra. We made the most extensive studies on this sample and on a ternary sample $In_{0.53}Ga_{0.47}As$ (T9-50) and we shall concentrate on these two samples. Another ternary sample investigated was T9-45A, with somewhat lower electron mobility μ_e than T9-50, with no difference in position of minima in the spectra. Table III-1 summarizes some of the characteristics of the two samples studied in detail.

The net impurity concentration N_D-N_A was measured by the Hall effect, here N_D and N_A are the donor and acceptor concentrations, respectively. The quaternary sample has a slight lattice mismatch of $|\Delta a|/a \simeq 1.4 \times 10^{-3}$ where Δa is the difference between the lattice constant of the alloy and the substrate, and a is the lattice constant of the InP substrate.

B. Experimental Setup and Data Acquisition

The experimental setup for magnetoabsorption is depicted schematically in Figure III-1.

In most of the experiments, the optical setup was enclosed in a dry box flushed with dry air to suppress water vapor absorption. A hole was provided in the box directly under the magnet bore to allow the light beam to propagate unobstructed to the sampe and back

to the detection side of the optical setup.

B. 1. The Light Box

This included holders for various light sources. One
was for the tungsten lamp which constituted the light source for our
experiments. The current through this lamp was set at 9 Amperes
using a regulated power supply. Another lampholder was for spectral
lamps for the calibration of the grating monochromator. We used the
following lamps:

$$Hg(1.1A); K, Cs, Ne(1.5A).$$

The light from the lamp was focused on the entrance slit of the
grating monochromator by means of a spherical mirror.

B. 2. Chopper

A 510 Hz, 50% duty-cycle chopper was used to chop the
light before entering the monochromator. A square pulse generated
by the chopper was used as a reference signal to the PAR 5101 lock-in
amplifier.

B. 3. Grating Monochromator

In most of the experiments the grating monochromator used
was a Perkin-Elmer model 99G double-pass grating monochromator. We
used Bausch and Lomb gratings with the following specifications,
variously: one ruled with 640 lines/mm (blazed for $1.4\mu m$), two ruled
with 600 lines/mm (one blazed for $1.6\mu m$ and another for $1.0\mu m$).

The calibration of the monochromator was performed using the spectral
lamps mentioned above. The spectral lines and their wavelengths and
energies were identified using the extensive compilation of spectral
lines reported in Lincoln Laboratory Report 84G-0012 (1960)[2]
for those spectral lamps. It was found out that our calibration was
reproducible within 0.1 meV for calibrations done at various times.
Also different magnetoabsorption spectra taken on different dates
for the same magnet current yielded minima reproducible within
1 meV or less. In the spectral range between 1-1.4 eV with slit
width of 0.8 mm using a 600 lines/mm grating resolution of the double
pass was 2.5 meV. It was further noted that the resolution scaled linearly
with the slit width as large as 1.2 mm and as small as 0.2 mm.
Spectra at various slit widths in the above range were taken for the
same field values for comparison and to get optimal spectra.

B.4. Filters and Polarizers

Filters were used to cutoff higher energy light passing
through the monochromator via second or higher order reflection
from the grating. Polaroid linear polarizers were used for the
Voight configuration where $\vec{k}$, the wave vector of the incident light
propagating through the sample is perpendicular to the applied
magnetic field $\vec{H}$. In this configuration, we chose $\vec{E}||\vec{H}$ or $\vec{E} \perp \vec{H}$;
here $\vec{E}$ is the oscillatory electric field of the incident light.

For the Faraday configuration ($\vec{k}||\vec{H}$), circular polarizers
appropriate to the wavelength range of interest were used. For a

given circular polarizer (made out of a linear polarizer and a quarter-wave plate) the sense of circular polarization of light with respect to the magnetic field could be reversed by reversing the direction of the applied magnetic field. The polarizer could also serve as the filter.

B. 5. Directing and Focusing Mirrors

The diverging light emerging out of the monachromator exit slit was folded (by a flat mirror) onto a large long focal length spherical mirror to focus it onto the sample. A 45° adjustable mirror was used to direct this converging light upwards through the bore of the magnet towards the sample. In the Voigt configuration experiments a 4" bore magnet was used. This allowed for a pair of near 45° mirrors on each side of the sample, outside the dewar. The first mirror folded the converging light and allowed it to travel horizontally ($\vec{k} \perp \vec{H}$) through a ZnSe window on the tail of the dewar. The mirrors were arranged to focus the light on the sample. The sample was held vertically in a sample holder attached to the liquid-He cooled cold finger. The light transmitted through the alloy would transmit through the InP substrate unaltered (we used photon energies less than the energy gap of InP which is 1.42 eV). This light then would exit from a second ZnSe window (horizontally) and then would be folded downwards by the 45° mirror in the bore of the magnet. For the Faraday configuration measurements, we used a 2" bore magnet and a different sample holder. The dewar was equipped with a bottom window (sapphire and quartz windows could be used).

The sample holder held two near 45° mirrors to direct the light back down after it has passed through the horizontally held sample (see Figure III-2). The samples in both cases were held in the center of the magnet.

B. 6. Collecting Optics and Detector

The diverging light emerging out of the sample and directed down the bore of the magnet was then redirected by means of a second 45° mirror onto another spherical mirror and finally by means of another flat mirror was directed towards the room temperature PbS detector. This light was actually focused by means of a small radius concave mirror onto a very narrow and sharp image right onto the PbS element. The PbS element was biased at 90 volts and the oscilatory photocurrent produced by the chopped light was preamplified.

B. 7. Signal Detection and Data Acquisition

The preamplified chopped signal from the detector was then put into a PAR 5101 lock-in amplifier which was referenced with the square pulse from the chopper. The output of the lock-in was both taken to a chart reorder and to channel B of an analog-to digital converter. In each experimental run the magnetic field was held constant and the wavelength of the light emerging out of the monochromator exit slit was swept. This was done by rotating the monochromator drum automatically at a desired speed (1 or 2 minute per revolution). The shaft of a rotary helipot potentiometer was coupled to this drum. The two fixed ends of the potentiometer were connected to a regulated dc voltage source. The angle of the

grating, or equivalently the drum reading, was thus monitored by
reading the variable voltage across the variable resistor. The
drum reading voltage was then put into the channel A of the A/D
converter. The outputs of channel A and B were then punched on
paper tape as pairs representing the transmitted signal vs. drum
position voltage. These were then taken to the PDP-11/20 computer
to process the spectra. The voltage reading on channel A was
calibrated in terms of wavelength and photon energy using various
spectral lamps described before and reproducibility was excellent
(≤ 0.1 meV).

C. $T(H)/T(0)$ vs. Photon Energy Spectra

The spectra seen on the next few pages were obtained from
the data punched on the paper tape using the program Rubin System
One (RS1) under DOS-BATCH. The transmitted signal, $T(H)$, taken at
the fixed external magnetic field value H, was divided by the
zero-field transmitted signal, $T(0)$, point by point. The ratio
$T(H)/T(0)$ vs. drum voltage was then converted to the "$T(H)/T(0)$ vs.
Photon Energy" spectrum. For this purpose we used our calibration
tables (wavelength and photon energy vs. drum voltage) discussed
in Section B. 3. In several cases use was made of the smoothing
subroutines provided in the RS1 program. Absolute caution was
taken to use smoothing very carefully so as not to shift the position
of the minima by more than 0.2-0.3 meV. The smoothing helped make
a few of the oscillations at higher energies more vivid and this was

always double checked from spectra taken at the same H value at different times and at different slit widths, to eliminate spurious minima.

Figures III-3 through III-9 show some of the spectra for the various fields and polarization, for the two samples Q9-18 and T9-50.

D. Point Plots and Fan Charts

The minima appearing in the "T(H)/T(0) vs. Photon Energy" spectra were then tabulated against the H-values for each polarization configuration for each sample as described in Chapter IV. The photon energies of these minima were plotted vs. H. These point plots, and the associated fan charts which are the result of the quasi-Ge coupled band analysis with exciton corrections, will be explained in Chapter IV.

TABLE III-1   Some characteristics of the two expitaxial $In_{1-x}Ga_xAs_yP_{1-y}$ samples, grown on InP
substrates, which were used for the interband magneto-optical measurements
reported in this thesis.

Sample	x	y	$\frac{\Delta a}{a}$	$N_D\text{-}N_A$ (cm^{-3})	$\mu_e(77K)$ $(cm^2V^{-1}s^{-1})$	Epilayer Dimensions		Orientation		E_g^* (eV)
						Thickness (μm)	Edges (mm x mm)	Thickness	Edges	
Q9-18	0.25	0.52	1.4×10^{-3}	2.7×10^{15}	11,000	1.8	5.5x8	along [100]	along [100] directions	1.065
T9-50	0.47	1.0	$\lesssim 0.6 \times 10^{-3}$**	1.4×10^{16}	24,000	4.4	3x8	along [100]	along [110] directions	0.813

*Obtained from our interband magnetoabsorption experiments near liquid-He temperature.

**This is the limit of resolution of the x-ray apparatus.

FIGURE III-1 Schematic diagram of the experimental setup for the magnetotransmission experiments. In this Figure the sample is setup for the Voigt configuration where the wave vector of light $\vec{k}$ through the sample is normal to the direction of applied magnetic field $\vec{H}$. The sample geometry for Faraday configuration where $\vec{k}||\vec{H}$ is shown in Figure III-2.

Bitter Solenoid

$\vec{H}$

Sample

$\vec{k}$

Light Box

Chopper

Filter

Polarizer

Monochromator

PbS Detector

Reference

Lock-In Amplifier

Signal

Output

A/D

A/D

Drum Voltage

Transmitted Signal

Paper Punch, Computer, Plotter

chart Recorder
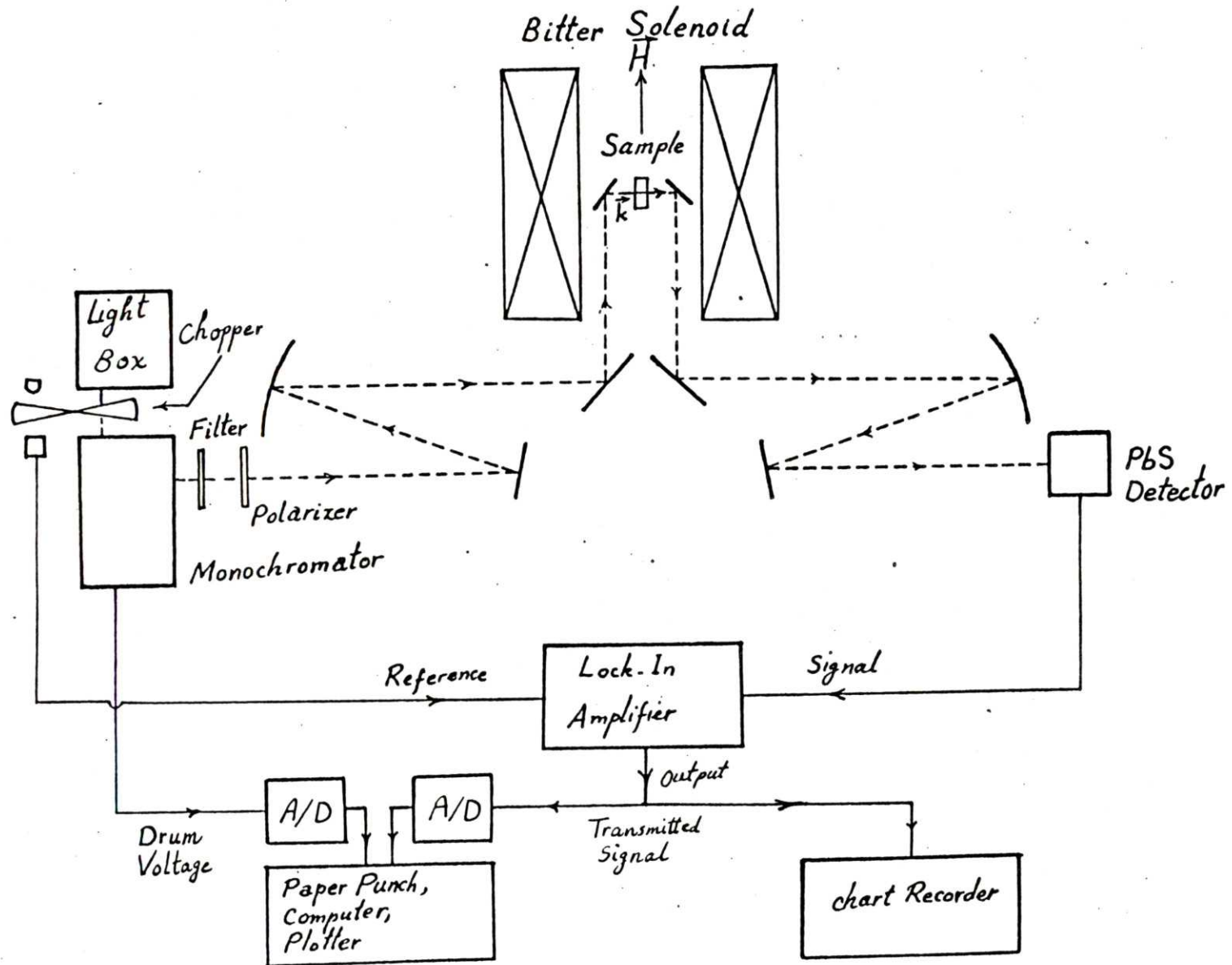
FIGURE III-2 The sample geometry for the Faraday configuration where
the light propagation vector $\vec{k}$ through the sample is parallel
to the direction of applied magnetic field, $\vec{H}$. In this
Figure S represents the sampe and M represents two flat
mirrors, at nearly 45° with respect to $\vec{H}$.
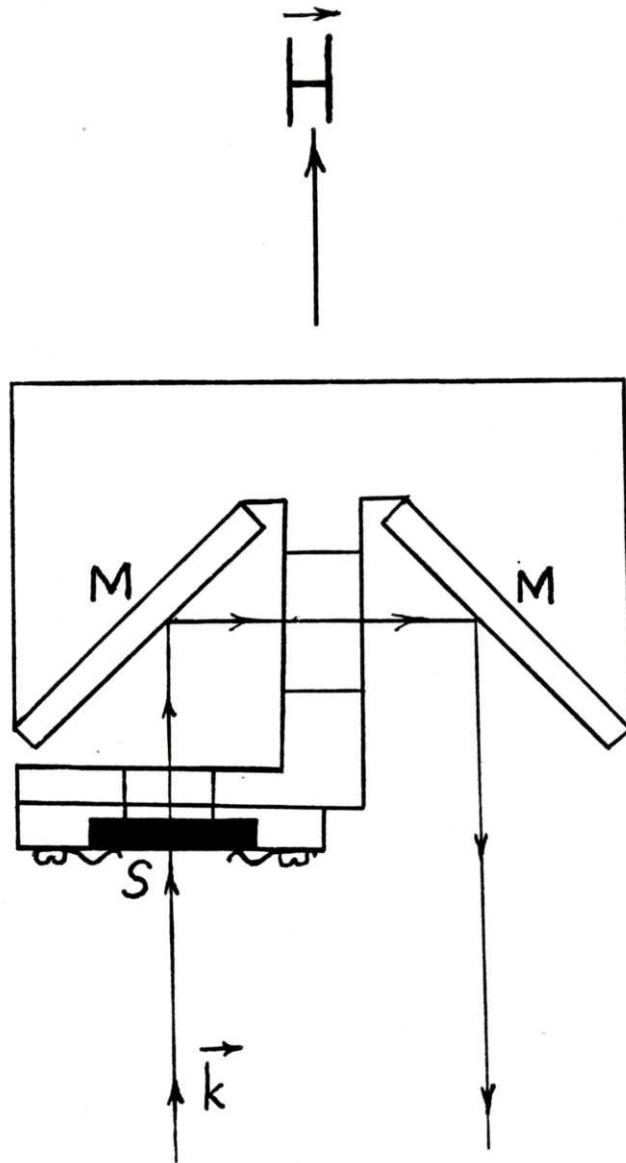
FIGURE III-3   Voigt configuration $\vec{E}||\vec{H}$ interband magnetotransmission
spectrum for Q9-18, taken at near liquid-He temperature,
at H=130.5 kOe. Bars at the bottom of the figure indicate
the calculated positions and their heights are proportional
to the square of matrix elements for transition from
light (+) and heavy (-) hole magnetic subbands to the
conduction magnetic subbands (see Chapter IV).

To represent relative intensities, the light-hole bars
should be shortened by a factor of $(m_+/m_-)^{1/2}\approx 2.4$ to approx-
imately account for the difference in the density of states.

$In_{0.75} Ga_{0.25} As_{0.52} P_{0.48}$

$\vec{E} \parallel \vec{H} \parallel [100]$

$H = 130.5$ kG

△ (a^+) Ladder □ (b^+) Ladder ▲ (a^-) Ladder ■ (b^-) Ladder

I (H) / I (0)

PHOTON ENERGY (eV)
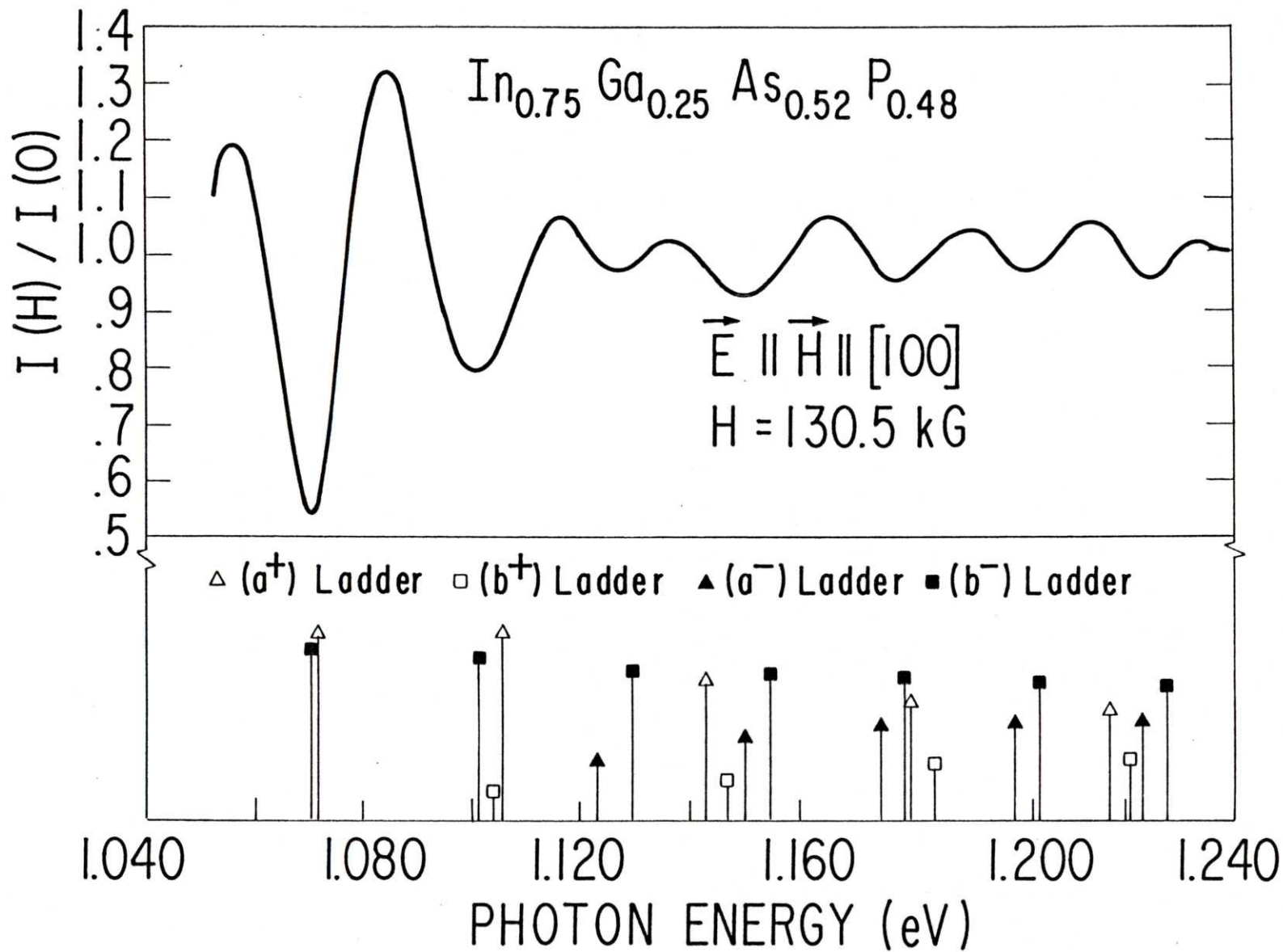
FIGURE III-4 Faraday configuration magnetotransmission spectrum
for right circularly polarized light (RCP) taken at
143.9 kOe in the quaternary sample Q9-18 in contact with
a liquid-He cold finger.
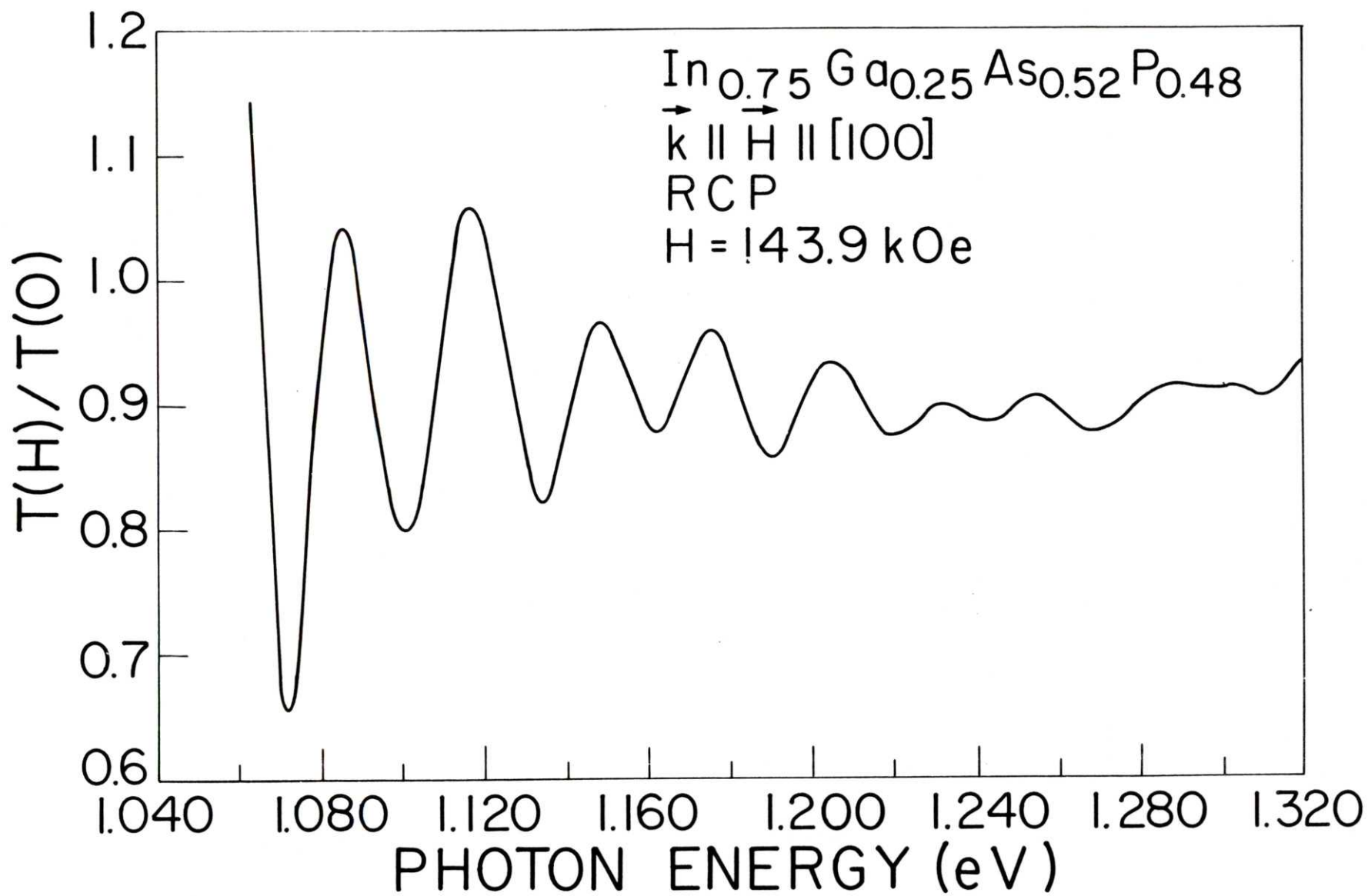
FIGURE III-5 Faraday configuration magnetotransmission spectrum
for left circularly polarized light (LCP) taken at
143.9 kOe in the quaternary sample Q9-18 in contact with
a liquid-He cold finger.
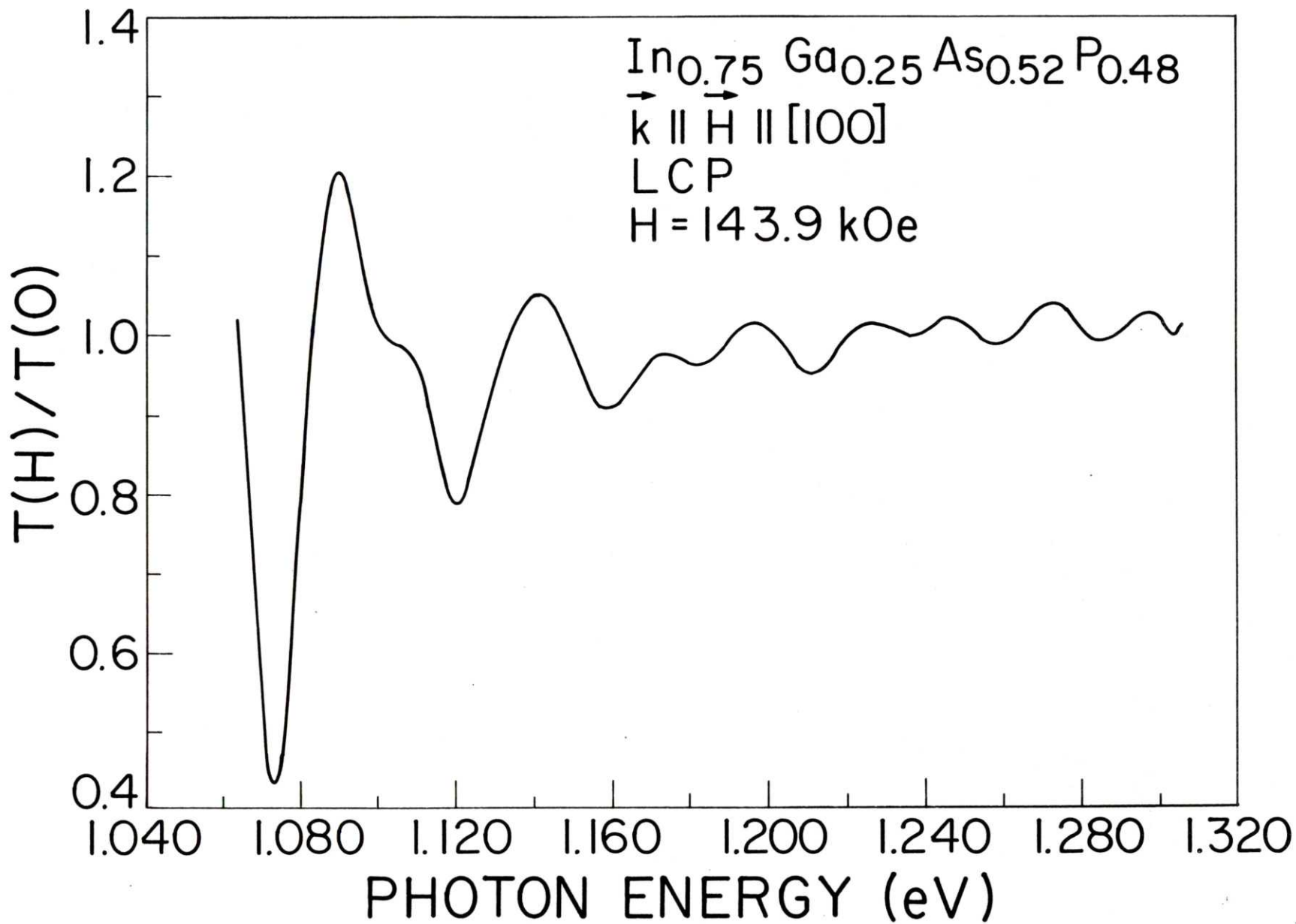
FIGURE III-6 Faraday configuration $\vec{k}||\vec{H}$ magnetotransmission spectra
for left and right circularly polarized light (LCP and RCP)
taken at 137.2 kOe for in the sample T9-50 in contact with
a liquid He cold finger.
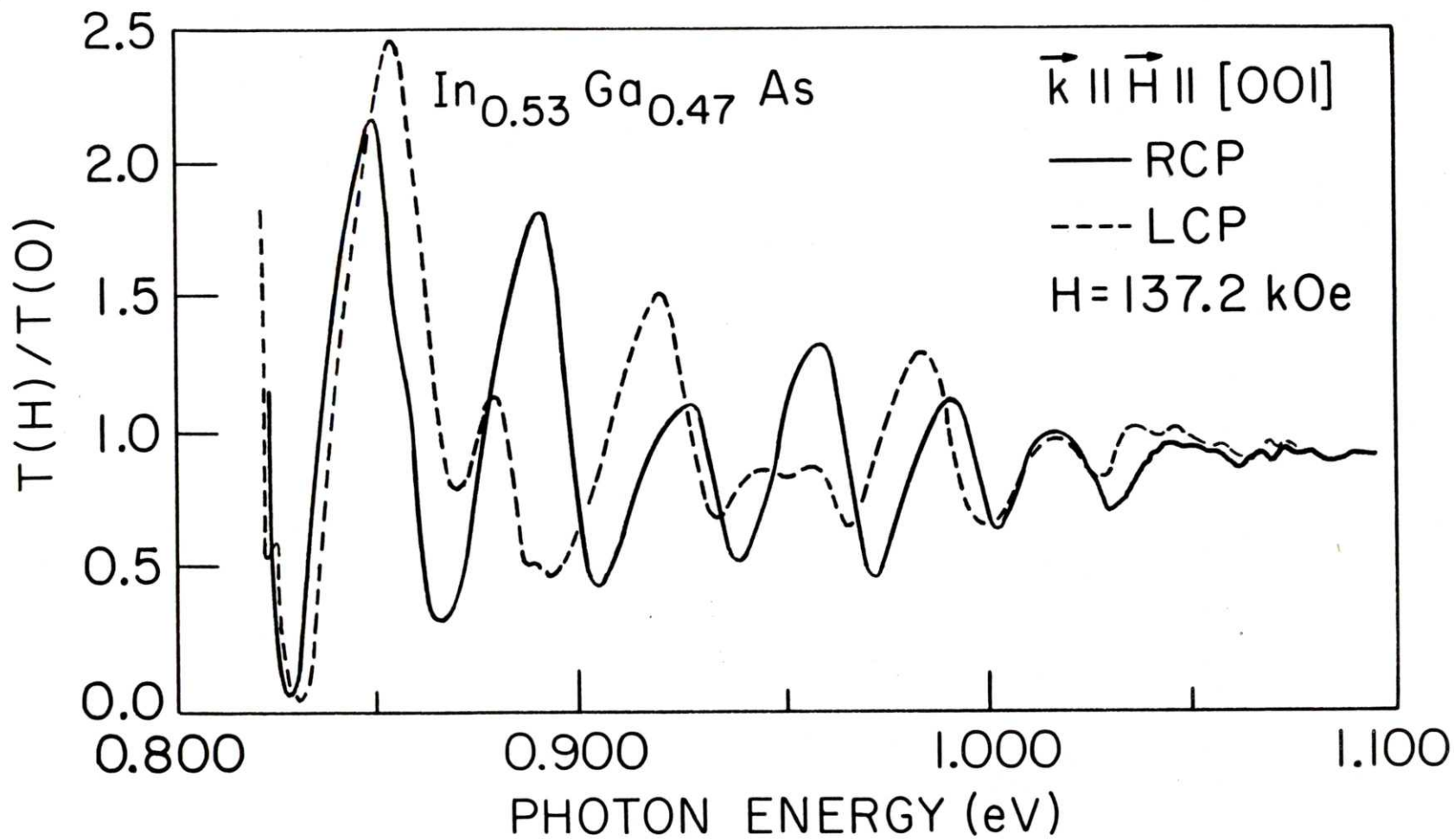
FIGURE III-7 Faraday configuration ($\vec{k}||\vec{H}$) magnetotransmission
spectra for left and right circularly polarized light
(LCP and RCP), for the sample T9-50 in contact with a
liquid-He cold finger, with H=137.2 kOe. The intensity
bars bemeath each spectrum indicate calculated energy
positions, and their heights are proportional to the
square of matrix elements for optical transitions from
light (+) and heavy (-) hole to conduction electron
Landau levels. Light hole intensity bars are reduced by
a factor of $(m_-/m_+)^{1/2}$ to reflect the difference between
light and heavy hole densities of state approximately.
(See Chapter IV.)
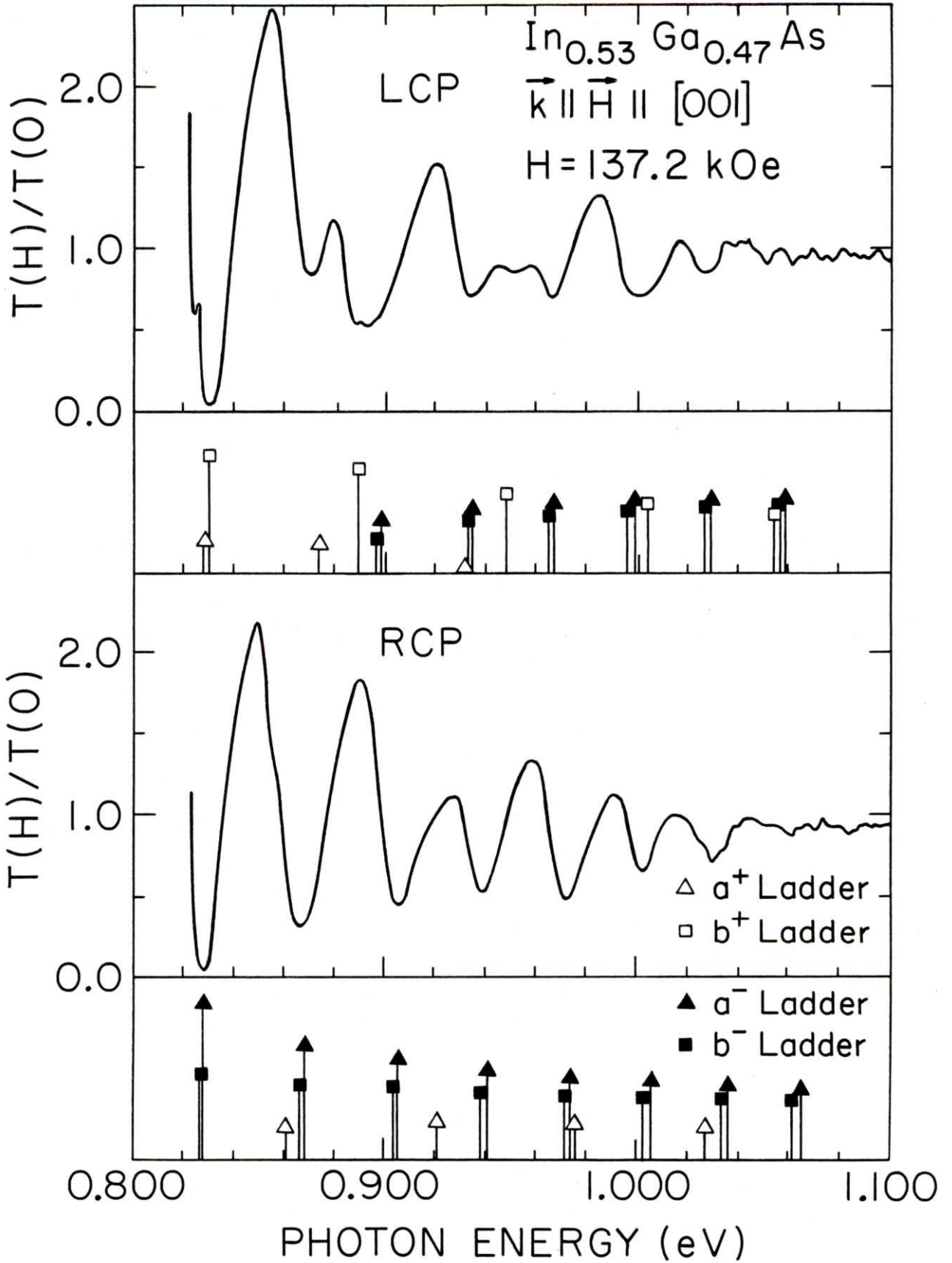
FIGURE III-8 Magnetotransmission spectrum in the Voigt configuration
for light polarized with $\vec{E}||\vec{H}$ taken at H=126.9 kOe in the
sample T9-50 in contact with a liquid He cold finger. For
a description of the bars under the spectrum see Figure III-7
caption.
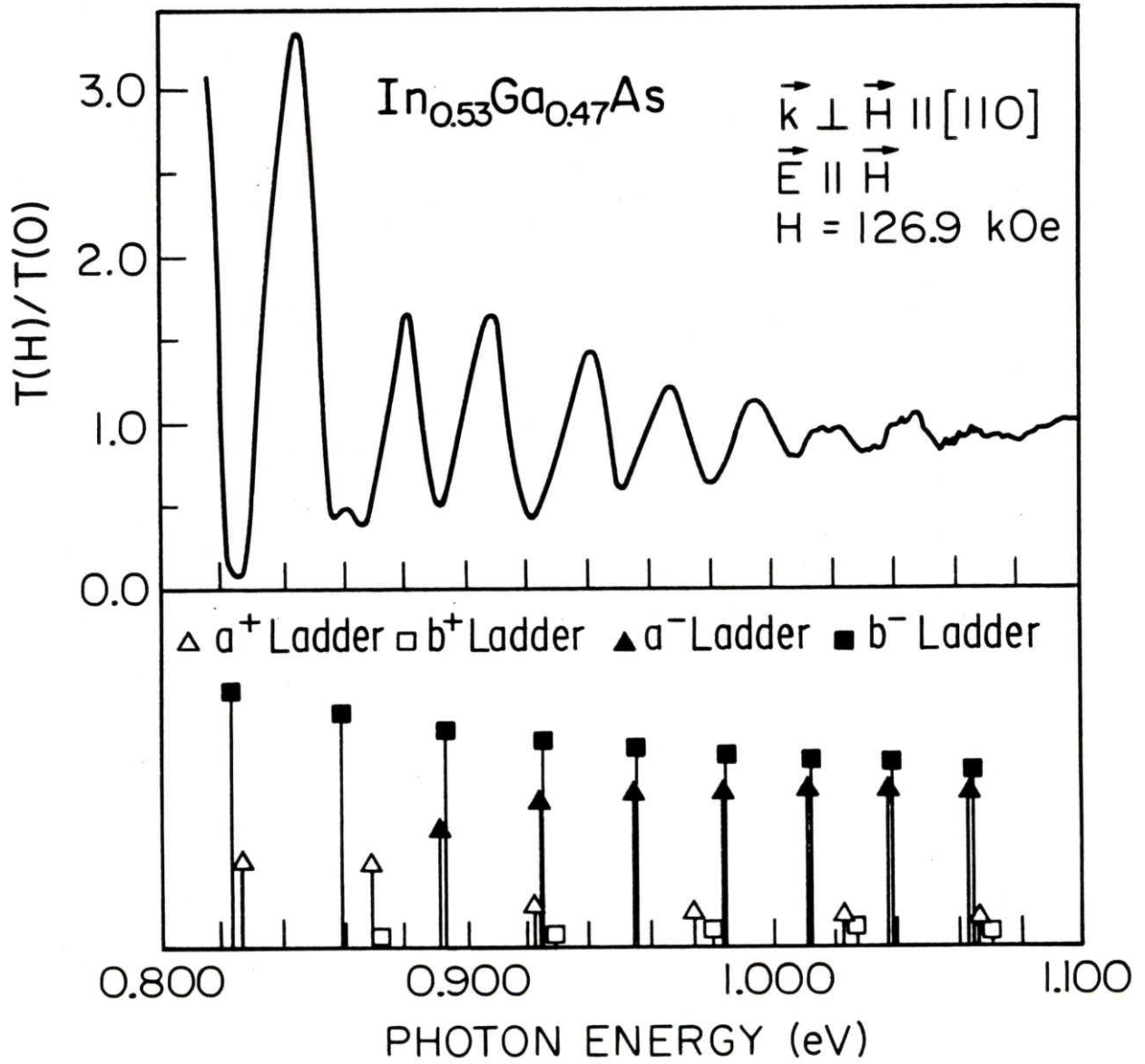
FIGURE III-9 Magnetotransmission spectrum in the Voigt configuration
for light polarized with $\vec{E} \perp \vec{H}$ taken for the sample T9-50
in contact with a liquid-He cooled cold finger at
H=130.7 kOe.
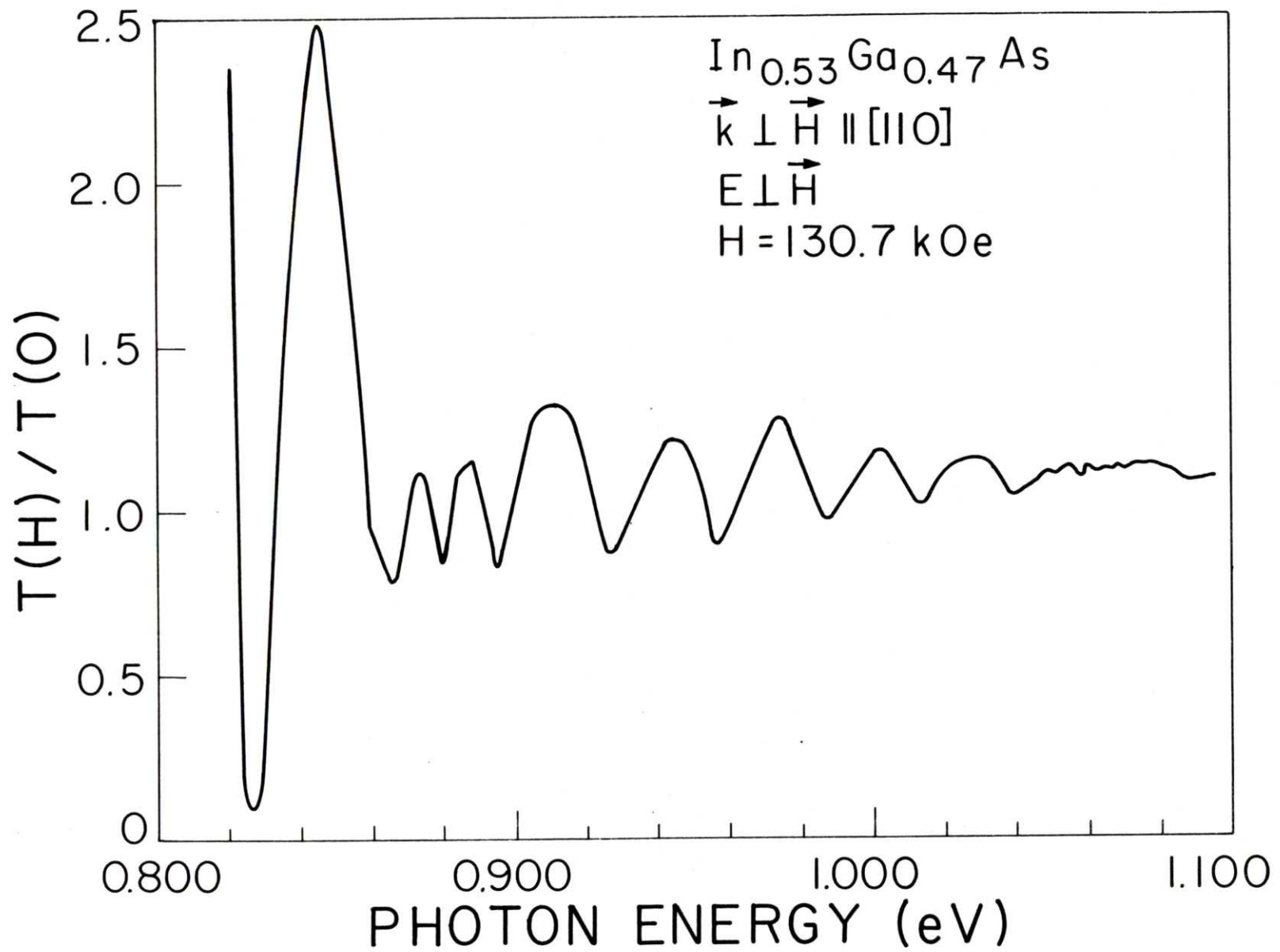
-REFERENCES

1. S. H. Groves and M. C. Plonko, in Proceedings of the 7th International Symposium on Gallium Arsenide and Related Compounds, St. Louis Conference, September 1978, (Institute of Physics Conference Series, No. 45, Ch. 1, pp.71-77, London, 1979); ibid, to be published in J.Crystal Growth.

2. Solomon Zwerdling and John P. Theriault, "Calibration of Prism Spectrometers in the Ultraviolet, Visible and Near Infrared Regions". M.I.T. Lincoln Laboratory Report 84 G-0012, July 27, 1960.

CHAPTER IV

ANALYSIS AND RESULTS

The quasi-Ge coupled band theory reviewed in Chapter II has been used to determine the $\vec{k} \cdot \vec{p}$ band parameters from our interband magnetoabsorption spectra in the ternary and the quaternary samples which was presented in Chapter III.

In this chapter we give the steps involved in applying this model to our experimental spectra. Next, we present the band parameters which we have obtained for our samples together with the fan charts calculated from the quasi-Ge model. At the end of this chapter a discussion of the results will be presented.

A. Analysis of the Spectra in Terms of the Quasi-Ge Model

A. 1. An Outline

In this section we present an outline of the steps involved in the analysis of the magnetoabsorption spectra, "T(H)/T(0) vs. Photon Energy" in the context of the quasi-Ge model reviewed in Chapter II. These are the steps involved:

Step I -- Examination of the T(H)/T(0) Spectra

The minima are assumed to eminate from the interband optical transitions from the valence band magnetic sub-bands to the conduction band magnetic sub-bands (Landau levels). The details will be given in Section A. 2.

Step II -- Identification of the Minima

Attempts are made to identify each minimum with one or more such transition mentioned above, if at all possible.

Step IIa -- Experimental Identification: Point Plots

For a given minimum in the spectrum the experiment gives us the following information (a) the photon energy E, (b) the magnetic field value H, (c) the spherical coordinate angles (θ, ϕ) made by H with respect to the cubic axes of the crystal, and (d) the polarization state of light, i.e. (σ_R, σ_L in the Faraday configuration, $\vec{E} || \vec{H}$, $\vec{E} \perp \vec{H}$ in the Voigt configuration), and (e) relative strength and width of the minimum (some minima are stronger, some weaker, some are too close to be distinguishable, and some even appear as inflection points or shoulders). At this step, for each H-orientation (c) and light polarization configuration (d) we make a separate plot of E(meV) vs. H(kOe) for all of the minima in the spectra, with the same (c) and (d) conditions. We refer to these as point plots.

Step IIb -- Assignment of Transition Labels to the Minima

Now given these five attributes (a)-(e) for a minimum, we should in general be able to use the quasi-Ge model (with the correct set of band parameters) to gain the following missing information about that minimum: which interband magneto-optical transition (transitions) are responsible (or most likely responsible) for this minimum? If the correct set of band parameters is used one is able to answer the above with the following quantities or attributes: (f) the initial state in

the valence band, i.e. whether it is a^-, b^-, a^+ or b^+, (g) the Landau quantum number of the initial state "n". Now with this specification, the final state in the conduction band (h) is automatically specified subject to the selection rule for the magneto-optical transition in the specific polarization state(d). By conduction band specification (h) we mean whether the final state is $a^c(n')$ or $b^c(n')$ and what value n' has. Finally, a correct set of quasi-Ge parameters ought to give at least a qualitatively good agreement between the calculated and the observed strengths of transitions.

To carry out Step IIb one therefore needs a set of initial parameters, which are reasonably close to the actual values, to start the analysis. Therefore, before Step IIb can be taken we need to go to Step III.

Step III -- Initial set of Band Parameters for the Start of the Analysis: Values for the Quasi-Ge Model

This is an important step; the initial set of values for the quasi-Ge band parameters, i.e., E_g, E_p, Δ, γ_1, γ_2 γ_3, κ, F, q, and N_1, has to be selected judiciously and has to be as much based on physical consideration as possible.

Step IV -- Exciton Corrections

The observed experimental values for the energy of the minima are affected (in fact reduced) by the excitonic binding energies (see Section A.3. for details). Therefore, if we are to apply the quasi-Ge model to calculate energies for the interband

magneto-optical transitions (in order to make contact with the experimentally observed values of the energies), we have to substract an appropriate amount (depending upon n' and H) according to the prescriptions of Section A.3. This can be done right after the transition energy for a particular transition and H value is calculated in the computer program.

Step V -- Relative Intensities of Transitions: To Determine Which Allowed Transitions are too Weak to be Included in the Analysis

Suppose one has the correct band parameters for the given sample. For a given polarization condition (d) there are a vast number of allowed interband magneto-optical transitions from the valence $\{a^-(n), b^-(n), a^+(n), b^+(n)\}$ magnetic sub-bands to the conduction $\{a^c(n'), b^c(n')\}$ magnetic sub-bands. It turns out that a good number of these transitions are too weak relative to the rest and hence experimentally not observable. Therefore, it is desirable (and in fact necessary) to exclude these transitions (although allowed) from the analysis. This does not mean that all of the weak transitions are eliminated. In fact, the relative strengths of the minima vary from one minimum to another in a given spectrum (usually diminishes as E is increased) and from one polarization to another (see Figures III-3 through III-9). There are some weak transitions which are still observable. However, it turns out that transitions from the a^+ light-hole series occur mainly for RCP while those originating from b^+ light-hole series occur mainly for LCP.

Step VI -- Fan Charts Using Initial Band Parameters

Having decided, on the basis of Step V, which of the allowed transitions ought to be included in the analysis, we are then ready to generate fam charts (see Figures in this chapter). A fan chart is a family of lines generated from claculated transitions energies as a function of H using a set of band parameters. Each line represents a particular transition from the set $\{a^-(n), \; b^-(n), \; a^+(n), \; b^+(n)\}$ to the set $\{a^c(n), \; b^c(n)\}$ allowed by the selection rule for optical transitions in the particular polarization configuration, (d) and H-orientation (c). If the initial parameters are chosen judiciously (i.e., are chosen close to the correct values) then in general each calculated line, with a few exceptions, will pass reasonably close by (in some cases very close by) a family of points in the "point plot" (the family representating a particular minimum as it evolves with increasing H). For some of the minima more than one calculated line will pass close by, indicating that those minima correspond to a set of close lying transitions. It turns out that it is generally possible to choose a reasonable initial set of band parameters to make correct identification of the minima (points on the point plot). The identification completes Step IIb.

Step VII -- Data Files

With the above initial identification of the points on the point plots, we now can generate data files for a given sample and a given H orientation. Each point on the data file includes five numbers: $\{IP, IT_1, IT_2, H, E\}$ where IP is the polarization state of

light, IT is the label for the identification of transition (see
Step VI), where up to two transitions can be accommodated, H is
the magnetic field value and E, the transition energy given by the
experimental spectra. In this manner, we include all or most of the
points on the "point plot". These data files are then stored to be
used in a minimization routine.

Step VIII -- Minimization Routine: Search for Optimum Band Parameters

The data files constructed according to Step VI, are now
used as inputs for a minimization routine. The minimization routine
asks for input of the data files, the direction of H with respect to
cubic axes of the crystal, and a set of values for the quasi-Ge
band parameters (E_g, E_p, Δ, γ_1, γ_2, γ_3, κ, F, q, N_1). It also asks
for identification of those parameters we may wish to vary; it also
provides for constraint equations that we may wish to impose on
these parameters, for instant to fix m_c or m_-. For each point in the
data file (see Step VII) the program then calculates the transition
energy in the quasi-Ge model and compares this with the given
experimental energy. The program thus calculates the deviation of
these two energies for each point and determines the root mean square
deviation:

$$\Delta = \{\frac{1}{N} \sum_{i=1}^{N} [E_i(H) - E_i]^2\}^{1/2} \tag{4-1}$$

where $E_i(H)$ is the calculated transition energy of the data point i
and E_i is the stored energy value of this data point, and N is the
number of such points.

The correct band parameters are expected to be obtained by
an iterative method described by Reine[1,2] and incorporated by
Weiler[3,4] in the computer program. In each iteration a new set of band
parameters are calculated based upon the old ones, so as to minimize
Δ. Details will be given in Section A.4.

This minimization routine is used until a set of band
parameters are found which minimize Δ, subject to certain constraints
on the band parameters which are based upon physical consideration.
Otherwise, one cannot even hope for convergence. This is very important
and makes the task in Step III very crucial. We will discuss these
points (initial band parameters, necessary constraints, and the
performance of the minimization routine) later on in this Chapter in
some detail.

Step IX -- Checking Band Parameters Obtained in "Step VIII"

The set of band parameters which minmize the rms deviation
mentioned in Step VIII are presumably those which most closely
represent the true band structure of the semiconductor. This has
to be tested; some of the relevant questions are:

1) How well do these parameters represent the bands from
   physical point of view and how well do they predict
   other measurements, by other methods, of these parameters
   directly or indirectly?

2) How well do these parameters explain the magneto-optical data, i.e., how closely do the new fan charts represent the data points on the point plots, and how do the newly calculated relative intensities compare with the $T(H)/T(0)$ spectra?

3) Do these new parameters give the same initial identifications deduced in Steps VI and IIb?

4) What range of values can these parameters accept and still give good fits with the experimental data, while remaining physically meaningful?

5) What can be learned from interband magneto-optical measurements on these samples?

A. 2. Details Involved in Step 1

The starting point for the analysis of the magneto-absorption data is the examination of the "$T(H)/T(0)$ vs. Photon Energy" spectra where $T(H)$ is the signal from the infrared radiation transmitted through the sample in the presence of magnetic field and $T(0)$ is that for H=o. The observed minima in these spectra are assumed to be due to interband optical transitions from the valence to the conduction band magnetic band magnetic sub-bands ILandau levels). More explicitly, these transitions are from the Landau levels of the Γ_8^V valence bands $|a^-(n)>$, $|b^-(n)>$, $|a^+(n)>$, and $|b^+(n)>$, to the magnetic sub-band (Landau levels) of Γ_6^C conduction band, i.e. $|a^C(n')>$, and $|b^C(n')>$ (see Ch.II). This is a very

important assumption upon which the whole analysis hinges. The justification for this comes from (i) the fact that all of the minima occur at energies higher than the band gap of the material, (ii) the shape of the spectra for a given polarization geometry remains essentially the same as one examines the spectra for different H values and the positions of minima shift towards higher photon energy and their distances increase with increasing H, and (iii) the assumption stated above have worked very well in explaining magneto-absorption and magnetoreflection spectra of InAs, GaAs, InP and many other semiconductors. (See for example review articles by Lax and Mavroides[5] and Aggarwal.[6]) It is also possible to have transitions from the spin-orbit split-off (Γ_7^v) band Landau levels to the conduction band (Γ_6^c) Landau levels such as observed by Groves and coworkers in Ge[7] and III-V compounds,[3] by Reine[1,2] and coworkers [7,10] in GaSb and GaAs, and by Aggarwal,[11] in Ge, among others. However, these observations were possible only in modulated magnetoreflectance and not magnetoabsorption. In our case the magneto-optical transitions from the split-off to the conduction band would be expected to occur in the tail region of the spectra where the fundamental edge absorption is high and signal to noise ratio is too low to observe such transitions by the magnetoabsorption method.

One final note concerning the spectra. Because of the linewidths involved and the richness of the structure, some close lying transitions would appear as one and there could be relatively small pulling and pushing of peaks. Also, some weaker transitions

(usually light hole transitions) are seen as inflection points or are buried in the wings of a strong transition, as mentioned earlier. This means that there is inherent approximation as far as the energy positions of transitions are concerned. Hence, good quality crystals with good homogeneity and high mobility and low temperatures are a necessary condition for obtaining finely resolved spectra. Modulation techniques (e.g. the magnetoelectroreflectance experiments of Refs. 7 and 8 which were performed at room temperature) will further enhance the fine resolution of the spectra.[1,2,6]

A. 3.   Exciton Corrections

It is known that in many semiconductors, such as InP[12] and GaAs[13,14] which are among the constituents of the quaternary system under consideration, the electron-hole pair, which is created by the optical excitation, can bind together to create "free excitons" in much the same way as an electron-positron pair can bind together to form a bound positronium "atom". In case of semiconductors this e-h binding lowers the transition energy by a small amount (typically a few meV). This energy E_B is the so-called binding energy, ($E_B > 0$). The problem of exciton in a magnetic field is an interesting, but complicated problem.[14-21] In the case of our experiments, we are not concerned with the fine structure of excitations, since our linewidths are too large for that. Thus we include the effect of excitonic binding energy using a simpler method used by Vrehen.[14] According to this method, the transition energies

calculated in the quasi-Ge model are reduced by substracting the approximate binding energy $\Delta E(n,H)$. Here n refers to the Landau quantum number of the final state (conduction band) and H is the magnetic field value. In the case of n=0, Vrehen uses

$$\Delta E(0,H) = E_B(\gamma) \cdot R \qquad (4-2)$$

and for higher n's

$$\Delta E(n,H) = E_B\left(\frac{\gamma}{2n+1}\right) \cdot R \qquad (4-3)$$

where γ is the reduced magnetic field, R is an effective Rydberg energy, and $E_B(\gamma)$ is the binding energy (defined >0) of a hydrogen-like atom in a magnetic field (reduced field) in units of R. Here

$$R \equiv R_0(\mu/m)/\kappa_e^2 \qquad (4-4)$$

and

$$\gamma \equiv \mu_B H(m/\mu)/R \qquad (4-5)$$

where κ_e is the static dielectric constant, R_0 is the atomic Rydberg constant μ_B the Bohr magneton, m the free electron mass, and

$$\mu^{-1} = m_c^{-1} + m_\pm^{-1} \qquad (4-6)$$

is the reduced mass for transition from light (+) and heavy (-) holes to the conduction band.

We have included the effect of nonparabolicty in an
approximate manner by using a field-dependent effective mass

$$\mu(n,H) \simeq \mu[1+4(2n+1)\mu_B H(m/\mu)/E_g]^{1/2} \qquad (4\text{-}7)$$

(it turns out that this results in a very small correction of
≤ 1 meV for the highest n and H).

For $E_B(\gamma)$ we have used unpublished numerical results of
Larsen based on his paper.[19]   See Table IV-1 for $E_B(\gamma)$ vs. γ. These
values of E_B are for the 1S ground state, and are in agreement with
those obtained by Praddaude.[20] The high γ values are also in very
good agreement with Altarelli and Lipari (for $\gamma>5$)[17] and Johnson and
Dickey[21] who find $E_B(\gamma) \simeq 1.6\gamma^{1/3}$ for large γ.

The method of Vrehen, namely using Eq.(4-3) for n>0, agrees
well with Table V of Ref. 17 which gives the binding energies for
$\gamma \geq 5$ for n=0, 1, and 2, and ℓ=0 series of hydrogenic exciton.

A. 4. <u>Minimization Routine</u>

We have used for our minimization routine, the method
described by Reine[1] and adopted by Weiler.[3] This approach is an
iterative one based on a generalized method of least squares.

Let $\vec{x} = (x_1, \ldots, x_j, \ldots, x_M)$ be the set of M band parameter
used in the quasi-Ge model analysis (e.g., $x_1=E_g$, $x_2=E_p$, $x_3=\gamma_1$, etc.).
Furthermore, suppose there is a set of values for these parameters,

say $\vec{x}^0 = (x_1{}^0, x_2{}^0, \ldots x_M{}^0)$, which represents the Γ_6^c, Γ_8^v, and Γ_7^v bands of the semiconductor under study most closely. Let $E(H_i; \vec{x}^0)$ be the calculated transition energy corresponding to the ith point in the data file (Steps II and VII) with the magnetic field H_i. Then these energies most closely represent the experimental transition energies. Now suppose we start out with an approximate set of band parameters $\vec{x}$ to start our analysis, then the corresponding calculated transition energies will be $E(H_i; x)$; and the rms deviation would be

$$\Delta(\vec{x}) = \{\frac{1}{N} \sum_{i=1}^{N} [E(H_i; \vec{x}) - E(H_i; \vec{x}^0)]^2\}^{1/2} \tag{4-8}$$

Let $D(x) = N[\Delta(x)]^2$. Values of $\vec{x}$ which minimize $D(\vec{x})$ will also minimize $\Delta(x)$. The derivatives of $D(\vec{x})$ with respect to the band parameters x_m are

$$\frac{\partial D(\vec{x})}{\partial x_m} = \frac{2}{N}\{\sum_{i=1}^{N} F_m(H_i; \vec{x}) [E(H_i; \vec{x}) - E(H_i; \vec{x}^0)]\} \tag{4-9}$$

where

$$F_m(H_i; \vec{x}) \equiv \frac{\partial E(H_i; \vec{x})}{\partial x_m} \qquad m = 1, \ldots, M \tag{4-10}$$

Now according to the mean value theorem of calculus, there exists a number λ, $0 \leq \lambda \leq 1$, such that

$$E(H_i; \vec{x}) - E(H_i; \vec{x}^0) = \sum_{n=1}^{M} F_n(H_i; \vec{x}^c)(\vec{x}_n - \vec{x}_n^0) \tag{4-11}$$

where $\quad \vec{x}^c = \lambda\vec{x} + (1-\lambda)\vec{x}^0$

(Note that λ and therefore $\vec{x}^C$ is not necessarily unique unless $\vec{x}$ is chosen close enought to $\vec{x}^O$. This makes the choice of initial approximate values $\vec{x}$ crucial.) Equation (4-9) becomes:

$$\frac{N}{2} \frac{\partial D(\vec{x})}{\partial x_m} = \sum_{i=1}^{N} F_m(H_i; x) [E(H_i; x) - E(H_i; x^O)]$$

$$= \sum_{i=1}^{N} F_m(H_i; \vec{x}) \sum_{n=1}^{M} F_n(H_i; \vec{x}^C)(x_n - x_n^O) \qquad (4\text{-}12)$$

This gives

$$\sum_{n=1}^{M} A_{mn}^C \, \xi_n = B_m \qquad\qquad m = 1, \ldots, M \qquad (4\text{-}13)$$

where

$$\xi_n \equiv x_n - x_n^O \qquad\qquad (4\text{-}13a)$$

$$B_m \equiv \sum_{i=1}^{N} F_m(H_i; \vec{x})[E(H_i; \vec{x}) - E(H_i; \vec{x}^O)] \qquad (4\text{-}13b)$$

$$A_{mn}^C \equiv \sum F_m(H_i; \vec{x}) \, F_n(H_i; \vec{x}^C) \qquad\qquad (4\text{-}13c)$$

The term B_m is determined by the guess $\vec{x}$ and the experimental points $E(H_i; \vec{x})$, therefore, it can be regarded as the external forcing term in the linear Eq.(4-13). The error ξ_n are the unknowns since x_n^O are unknown. The matrix A_{mn}^C is also unknown since $\vec{x}^C$ is unknown. However, Eq.(4-13) lends itself to an iterative solution (convergence not guaranteed, unless $\vec{x}$ is "close enough" to $\vec{x}^O$):

(1) Chose $\vec{x}$, i.e. a set of values for the band parameters, close to the unknown true values $\vec{x}^O$.

(2) Calculate $E(H_i; \vec{x})$ and $F(H_i; \vec{x})$, using quasi-Ge model. For F see Appendix B of Ref. 3.

(3) For $E(H_i; \vec{x}^O)$ use the experimental transition energies, since $E(H_i; \vec{x}^O)$ values are supposed to give the best estimates for the latter.

(4) Calculate $\Delta(\vec{x})$, the rms derivation using Eq.(4-8).

(5) Use (1) and (2) to calculate B_m.

(6) Approximate $F_n(H_i; \vec{x}^C)$ by $F_n(H_i; \vec{x})$.

(7) Calculate A_{mn}^c using (2) and (5).

(8) Solve Eq.(4-13) to obtain approximate errors ξ_n.

(9) Replace $\vec{x}$ by $\vec{x}-\vec{\xi}$. These are new guesses for the band parameters.

(10) Use the new $\vec{x}$'s and go to (2) and repeat steps (2) through (9) until $\Delta(\vec{x})$ shows convergence to a stationary value.

This procedure is the essence of the minimization routine. It can accommodate constraint equations among x_m's by the method of Lagrange multipliers. If the process is convergent then after each step, $\vec{x}$ (and therefore $\vec{x}^C$) gets closer to $\vec{x}$ and B_m gets smaller and step (6) becomes more and more justifiable, i.e. A_{mn}^c gets progressively closer to A_{mn} and $(\partial D/\partial x_m)$ gets progressively smaller. We should note that step (3) is inherently an approximation which the analysis cannot do anything about, because of experimental uncertainties.

The details of the computer program which incorporates this minimization technique within the contect of the quasi-Ge model are given in Ref. 3 (see especially Appendix B and C, thereof). In step (2) above, the calculated $E(H_i; \vec{x})$ which we have used includes the exciton binding energy corrections which we described in Section A.3. However, in calculating the derivatives $F_m(H_i; \vec{x})$ the exciton corrections are ignored in $E(H_i; \vec{x})$ since these derivatives are not nearly as sensitive to these corrections as $E(H_i; \vec{x})$ is.

B. Determination of the Band Parameters

As it was mentioned in Section A, to obtain the band parameters in the quasi-Ge model, we need to start with a set of band parameter values which are reasonably close to the "true" values. (Section A.1, Step III.) These initial parameters are then used in computer programs to generate fan charts, identify transitions, estimate intensities of the transitions, generate data files, and then use the minimization routine to improve the fit. This is like a boot-strap operation. The questions that we shall address in this Section are: (1) what parameters can we determine directly from the spectra (or point plots) right at the onset without the full use of the complicated computer analysis? (2) Which transition can we identify right at the outset? (3) Which of the quasi-Ge parameters are too small to affect our analysis (and therefore not really determined by our experiments)? (4) What other physical parameters involving the quasi-Ge parameters has been measured and can be used in our analysis?

B. 1. Prelinimary Analysis

(1) From the spectra and point plots we can get E_g
directly. This is done by extrapolating each family of points in a
point-plot (corresponding to the same minimum at different magnetic
field values) to H=0. In each of the different polarization cases,
we obtain nearly the same value. The energy thus obtained is
actually $E_g - E_B$, i.e., reduced by exciton binding energy at zero field.
This binding energy E_B is just R, the effective Rydberg for exciton
(see Section A.4.). R is typically 3-5 meV for materials such as
InP and GaAs and is expected to have the same typical value for our
InGaAs and InGaAsP samples. We obtain directly

$$E_g - E_B \simeq \begin{cases} 0.810 \text{ meV for T9-50} \\ 1.063 \text{ meV for Q9-18} \end{cases}$$

(2) The selection rules for RCP and LCP are different in
the following manner. For LCP: $a^\pm(n) \rightarrow a^C(n+1)$ and $b^\pm(n) \rightarrow b^C(n+1)$
whereas for RCP: $a^\pm(n) \rightarrow a^C(n-1)$ and $b^\pm(n) \rightarrow b^C(n-1)$. It is important
to recall that for the heavy hole (-) series $n \geq 1$ and for the light
hole (+) series $n \geq -1$.

In view of these facts the two lowest energy heavy hole
transition for the LCP case are $a^-(1) \rightarrow a^C(2)$ and $b^-(1) \rightarrow b^C(2)$. The
corresponding transition energies in most semiconductors and certainly
in the binary semiconductors InP, InAs, GaAs are higher than those for
the four lowest light hole transitions, namely $a^+(-1)$ $a^C(0)$, $b^+(-1)$ $b^C(0)$,

$a^+(0)$ $a^C(1)$, and $b^+(0)$ $b^C(1)$. First, we note that the energies corresponding to $a^+(-1)$, $b^+(-1)$, $a^-(1)$, and $b^-(1)$ lie close to each other and indeed, we can observe this directly from our data. Secondly, the Landau level spacings of the condution bands are larger than those of the light hole band (and more so compared to those of the heavy hole band). This is because $m_c < m_+ << m_-$. Thirdly, the g-factor in these materials under study is expected to be small compared to m/m_c (since these are not small gap materials). The above can be checked from the formulas in Chapter II using approximate band parameters.

Hence for the LCP, the first six lowest transitions are expected to be

1, 2) $a^+(-1) \rightarrow a^C(0)$ and $b^+(-1) \rightarrow b^C(0)$

3, 4) $a^+(0) \rightarrow a^C(1)$ and $b^+(-1) \rightarrow b^C(1)$

5, 6) $a^-(1) \rightarrow a^C(2)$ and $b^-(1) \rightarrow b^C(2)$

For the RCP transitions on the other hand the first two lowest transitions have to be $a^-(1)$ $a^C(0)$ and $b^-(1)$ $b^C(0)$. The next higher transitions are $a^-(2)$ $a^C(1)$, $b^-(2)$ $b^C(2)$, $a^+(1)$ $a^C(0)$ and $b^+(1)$ $b^C(0)$.

1, 2) $a^-(1) \rightarrow a^C(0)$ and $b^-(-1) \rightarrow b^C(0)$

For Voigt configuration with $\vec{E} || \vec{H}$ the lowest two transitions have to be $b^-(1)$ $a^C(0)$ and $a^+(-1)$ $b^C(0)$.

The spectra for the ternary sample T9-50 clearly shows that

the first two transitions are very close to each other compared to their energy spacing with the next higher transitions. In fact, these two lowest transitions are expected to be $a^+(-1)$ $a^C(0)$ and $b^+(-1)$ $b^C(0)$. Smallness of the energy spacing suggests that $g_c + g_+$ is a small quantity (g_+ is the g-factor of the light hole). In addition, note the energy difference $E[a^+(-1) \rightarrow a^C(0)] - E[a^+(-1) \rightarrow b^C(0)] = \mu_B H_{g_C} = E[b^-(1) \rightarrow a^C(0)] - E[b^-(1) \rightarrow b^C(0)]$. Comparing the lowest transitions in the Voigt configuration with the lowest transition in the RCP and with the two close lying transitions in the LCP case, we see that indeed $g_c \mu_B H$ is much smaller than $\hbar \omega_c = (\frac{m}{m_c})(2\mu_B H)$ as we pointed out earlier.

In summary, upon direct examination of our spectra, we can assert that the g factors for the conduction and light hole as well as the heavy hole are much smaller than m/m_c.

(3) The $\vec{E} || \vec{H}$ Voigt configuration spectra and the RCP spectra show much less structure than the LCP spectra as seen in Figures III-3 through III-9. This suggests that light hole transitions are strongest in the LCP polarization. Therefore, for our preliminary analysis we can assume that the minima which appear in the RCP and the Voigt $\vec{E} || \vec{H}$ spectra are mainly due to heavy-hole to conduction band transitions. We can then use these spectra to obtain an initial estimate for $(1/\mu_-) \equiv (1/m_c) + (1/m_-)$ following a method similar to those used in Refs. 1, 2, and 17 and described in Appendix C. According to this for each polarization configuration and each H-orientation we can plot $\varepsilon(n)$ vs. $2n\mu_B H$. Here $\varepsilon(n) \equiv (1/2\mu_B H)[E(n) - E(n-1)]$ is the spacing between two adjacent transitions for a given H, in units of

$2\mu_B H$, n being the conduction band Landau quantum number of the higher transition. According to the description in Appendix C a straight line drawn through these points (with a given light polarization and H-orientation) by the method of least squares fit intersects the $(2n\mu_B H)=0$ axis at a value equal to $(1/\mu_-)\equiv(1/m_c)+(1/m_-)$. The slope of this line also gives the measure of nonparabolicity of the conduction band as explained in Appendix C. When this preliminary analysis was performed for the sampe T9-50 we obtained somewhat different values for $(1/\mu_-)$ for the [110] and [001] orientations indicating that the anisotropy factor $\gamma_3-\gamma_2 \neq 0$. We obtained $(1/\mu_-)_{[110]}\sim 25$, and $(1/\mu_-)_{[100]}\sim 26$ for T9-50 and $(1/\mu_-)\sim 19$ for Q9-18 as preliminary values.

B. 2. Band Parameters for Q9-18

In this section we present analysis and results for the Voigt $\vec{E}||\vec{H}$ magnetoabsorption spectra of the quaternary sample Q9-18 ($In_{0.75}GA_{0.25}As_{0.52}P_{0.48}$), which was presented earlier.[26]

1. As seen from Table IV-2 the heavy-hole mass m_{hh} shows only a small variation between the binary compounds. We have used $m_{hh}=0.45m$ ($m_{hh}=m_-[100]$ the heavy hole-mass along the [100] direction). However, varying m_{hh} between 0.04 m and 0.05 m would change electron and light hole masses by less than 3%.

2. The value of $E_g=1.066$ eV was determined from extrapolating the experimental data (1.063 eV) and corrected for the exciton binding energy at H=0, $E_B \approx 3$ meV. From absorption measurements made on a similar

alloy, we expect the room temperature energy gap to be about 1.00 eV.

3. Δ=0.25 eV was chosen from a linear interpolation using values in Table IV-1, however, varying between 0.2 and 0.3 eV changes the deduced electron effective mass by less than 0.5% and the light-hole mass by less than 3%. Very recently, measurement of Δ for a number of quaternaries were performed by Herman, Lampel and Pearsall.[24] Interpolating their values for y=0.34 and y=0.61 we would get Δ=0.23 eV for our quaternary sample.

4. The anisotropy factor γ_3-γ_2 was taken to be 0.7. This is predicted by Lawaetz[25] for the binary compounds. However, choosing γ_3-γ_2=0 changes the deduced electron and the light hole mass by less than 0.15%.

5. The Kane parameter D_k, which is expected to be very small is taken to be zero for the binary semiconductors in the literature. We follow suite: this gives

$$\kappa = \gamma_3 + \frac{2}{3}\gamma_2 - \frac{1}{3}\gamma_1 - \frac{2}{3}$$

6. q, and N_1 are expected to be very small (see Appendix B). These are set to be zero. In fact our fits, and our band parameters are very insensitive to q as large as ~0.5 and N_1 as large as ~-0.1.

7. F is taken to be zero in this analysis. In other words, E_p was determined by assuming that the curvature of the Γ_6 conduction band at $\vec{k}$=0 comes entirely from the interaction with the Γ_8 and Γ_7

valence bands. E_p is expected to increase by 20% when the interaction with the Γ_8 and Γ_7 conduction bands due to admixing of the states by the antisymmetric potential is taken into account (i.e., F≠0).

8. Exciton corrections were taken into account following the discussion presented earlier. We obtained the following band parameters: E_g = 1.066 eV, Δ = 0.25 eV, E_p = 17.6 eV, m_c = 0.0608 m, $m_{hh} \equiv m_-[100]$ = 0.45m, $m_{\ell h}$ = 0.078m, γ_1 = 2.06, γ_2 = -0.35, γ_3 = 0.35, and κ = -1.234.

These values for κ and γ_3 give q=0.02 (see Appendix B) which indeed is small and has no influence on the fit, justifying q≈0 assumption. Also from Appendix B, we see that $-0.05 \lesssim N_1 < 0$. The values of N_1 in this range were seen not to influence the fit, only the reduced g_c by less than 0.2.

For various values of m_{hh}, the values obtained for $(1/\mu_-)$ and $(1/\mu_+)$ fall within a very narrow range. This is a very strong advantage of interband magnetoabsorption. Since m_{hh} turns out to be much larger than m_c these reduced masses are not very sensitive to m_{hh}, and these experiments can determine m_c within a narrow range. The values obtained from the above parameters are

$$\frac{m}{\mu_+} \equiv m\left(\frac{1}{m_c} + \frac{1}{m_+}\right) = 29.31$$

and

$$\frac{m}{\mu_-} \equiv m\left(\frac{1}{m_c} + \frac{1}{m_-}\right) = 18.65$$

We reported the above results in Refs. 26 and 27. (Figures III-3 and IV-1).

In a second attempt, we relaxed the restriction E_g=1066 meV and used the minimization routine with the previously mentioned restrictions, this time, however, letting E_g vary as well. A slight improvement (DRMS = 2.06 meV per point as compared to the earlier value of 2.23 meV) was achieved with E_g=1064.28 meV, E_p=17.985 meV, γ_1=2.254, γ_2=-0.251, γ_3=0.449, =1.136 giving m_c=0.0594m and m_+=0.0738m with $\frac{m}{\mu_+}$=30.37 and $\frac{m}{\mu_-}$=19.05, an increase of 3.5% and 2.5% respectively. This value for (m_c/m) is 2.2% lower than the one we reported, well within experimental errors.

The recent measurement of m_c=0.0603m of Nicholas, et al[28] for a sample with y=0.53 using cyclotron resonance is in excellent agreement with our result. This indicates the usefulness of interband magneto-optical measurements even though there are 10 band parameters involved and not all are known and even though some cannot be measured or deduced precisely. Reference 28, which uses intraband methods such as cyclotron resonance, magnetophonon effect, and Shubnikov de-Haas effect represents results of the most comprehensive intraband measurements of m_c for the whole range of y and suggest very strongly a linear dependence of m_c upon y in $In_{1-x}Ga_xAs_yP_{1-y}$ samples lattice matched to InP. For a review of the reports on m_c dependence on y as evolved in time see Chapter I and references therein. Table IV-7 summarizes the results for m_c/m given in Ref.28.

B.3 Band Parameters for Q9-18: Including Faraday Configuration Measurements

In order to make our study of the sample Q9-18 more complete it was decided also to make Faraday configuration interband magnetoabsorption measurements. Figures III-4 and III-5 give such spectra for RCP and LCP configurations with $\vec{H}||[100]$ for H=143.9 kOe

The quasi-Ge analysis was carried out this time by including the date from the Voigt $\vec{E}||\vec{H}$ and the Faraday RCP and LCP spectra. Using the band parameters obtained for the Voigt data, we again obtained good fits, showing that these band parameters are consistant with the additional data taken on the Faraday configuration.

Having many more data points, we decided to run over minimization procedure again to see if new values for the parameters could be found which could improve the fits. This time with minimization routine we made the following constraints:

1) As before we assumed m_{hh}=0.45m, however, values of m_{hh}=0.5 were also used which brought about very little change in the deduced band parameters, as was also the case before.

2) Δ has been measured to be ~0.25eV by Nishino, et al[29] in a sample with similar composition using electroreflectance at 77K. From measurements of Ref. 24, Δ is expected to be ~0.23±0.01eV. We used Δ=0.24 eV(as well as 0.25 and 0.23eV). This variation in Δ introduces a very small (<1%) uncertainty in the results.

3) Again $D_K=0$ was used, which gives κ in terms of the γ's.

4) q and N_1 were related to the other parameters (see Appendix B). The range of values for q is close to zero and its effect on the band parameters is extremely small. N_1 ranges between 0 and -0.07 and only affects the value of g_c by at most -0.2.

5) In each minimization trial a fixed value of F was chosen. These values were F=0, -0.5, -1, -1.5, -2, -2.5, -3, -3.5. N_1 was related to F as in Appendix B.

6) In one series of runs $\gamma_3-\gamma_2=0.7$ was fixed. In another series of runs no restriction was imposed on $\gamma_3-\gamma_2$. Another series of runs can be suggested which choses a different fixed value for $\gamma_3-\gamma_2$. We chose 0.7 since this seems to be the value most representative of the binaries.

7) In summary, in each minimization attempt, Δ, F, m_{hh}, N_1 were fixed, and E_g, E_p, γ_1, γ_2, γ_3, κ, and q were allowed to vary subject to the following constraints:

$$(1) \quad -\frac{1}{4}\gamma_1+\frac{1}{2}\gamma_2+\frac{3}{4}\gamma_3-\frac{3}{4}\kappa=\frac{1}{2} \qquad (4.14)$$

$$(2) \quad \gamma_1-\frac{5}{4}\gamma_2-\frac{3}{4}\gamma_3 \cong \frac{m}{m_{hh}} \qquad (4\text{-}15)$$

$$(3) \quad -(0.011)\gamma_3+(0.011)\kappa+q=-0.0055 \qquad (4\text{-}16)$$

$$(4) \quad \gamma_3-\gamma_2=0.7 \qquad (4\text{-}17)$$

Where Eq.(4-17) was relaxed in one series of runs. For Eq.(4.16) see Eqs.(B-21) and (b-25). For Eq.(4-15) we note that $m_{hh}=m_-[100]$ and according to Eq.(2-38) $\frac{m}{m_-} \tilde{=} \gamma_1 -\frac{1}{2}(\gamma'+3\gamma")$ where γ' and $\gamma"$ are given by Eqs.(2.23). For [100] direction $\theta = \frac{\pi}{2}$ and $\phi = \frac{\pi}{4}$ giving $f(\theta,\phi)=1$ and hence $\gamma'=\gamma_2$ and $3\gamma"=\frac{3}{2}\gamma_2 + \frac{3}{2}\gamma_3$, resulting in Eq.(4-15).

Table IV-3 shows results obtained for Q9-18 using the minimization routine with exciton corrections using the Voigt $\vec{E}||\vec{H}$, RCP and LCP pectra all with $\vec{H}||[100]$. In the minimization routine the following parameters were fixedL $\Delta=0.24$ eV, $\gamma_3-\gamma_2=0.7$, $q=N_1-0$. $m_{hh}\equiv m_-[1002=0.45m$. F was also fixed and results were obtained for various values of F. Plots were made using parameters for F=0 and for F=-2.381. The latter corresponds to $E_p=23.1$ which is obtained from the linear interpolation between the binaries InAs, GaAs, InP with E_p taken from Ref.30 which uses measured values of g_c and m_c to deduce E_p (see Appendix B and Table B-1). Plots corresponding to F=-2.381 are presented in Figures IV-2 and IV-3. Those generated with F=0 (first row of Table IV-3) turn out to be virtually identical to those corresponding to F=-2.381 for all three polarizations (Voigt E H. RCP and LCP). In other words whether we choose to ignore the effect of the higher bands on the curvature at the bottom of the conduction band (F=0) or include the effect (with E_p assumed to have the linear interpolation value) other parameters will adjust to give nearby identical fits. In Table IV-3 we have also calculated the value of α which is a measure of the nonparabolicity of the conduction band (see Appendix C) using the

band parameters for each fit. The variation of α for F=0 to F=-3.5 is from 0.94 tp 0.846, a 12.5% decrease. From F-0 to F=2.381 (E_p=23.1) α decreases by 0.049 or 5.1%. For H=150kOe on n=7 the difference between the energies of transition to $a^c(n)$ is calculated to be ~3 meV using Eq.(C-18). Numerical calculations using the quasi-Ge Hamiltonians show an even better agreement to within ~0.5 meV. This shows that the nonparabolicity of the conduction band is not large enough to narrow down the range of E_p in these materials, in contrast with the small gap materials such as InSb. Thus interband magneto-optical measurements involving Γ_8^V and Γ_6^C bands alone cannot determine E_p precisely in the quaternaries and this suggest the usefulness of P measurements involving $\Gamma_7^V \rightarrow \Gamma_6^C$ transitions, or direct measurement of g_c to obtain E_p (see Ref.30 and Appendix B). Another feature apparent from Table IV-3 is the fact that m_c, m_+ (or μ_+, μ_-), γ_1^L, γ_3^L and κ^L vary very slightly although E_p varies from 17.91 to 25.38. Varying $m_{hh} \equiv m_-[100]$ between from 0.45m to 0.4m or to 0.5m changes μ_- and μ_+ by less than 0.1%. As a result m_c and m_+ are determined to within ±1.5%. In the case of Q9-18 measurements were done with $\vec{H}||[100]$, so the anisotropy factor $\gamma_3-\gamma_2$=0.7 is used from comparison with T9-50 and the binaries InAs, GaAs and InP. It turns out that when the restriction on $\gamma_3-\gamma_2$ is removed the value obtained from the minimization routine is $\gamma_3-\gamma_2$=0.35± 0.05; nevertheless the values obtained for m_c and m_+ were the same within 0.1% or better for $\gamma_3-\gamma_2$=0.7 or 0.35.

Table IV-3 shows that the only precise measurement of g_c can norrow down E_p. Figures IV-1 through IV-3 show experimental points

corresponding to the T(H)/T(0) minima the lines are transition energies as a function of H calculated using the quasi-Ge Hamiltonians with exciton corrections. Solid lines represent heavy hole to conduction band transitions and dashed lines, light hole to conduction band. The transitions are identified in Tables IV-4 and IV-5.

In summary for $In_{0.25}Ga_{0.75}As_{0.52}P_{0.48}$ (Q9-18) we have obtained

E_g=1065±1 meV (m/μ_+) = 29.5±0.5, (m/μ_-) = 18.8±0.5.

m_c/m = 0.0602±0.001, m_+/m = 0.078±0.001,

γ_1^L = 7.5±0.2, γ_3^L = 3.1±0.1, κ^L=1.5±0.1. Assuming

$m_{hh}\equiv m_-[100]$ = 0.45±0.05, Δ = 0.24±0.01 eV and F = 0 to -3.5. We assumed $\gamma_3-\gamma_2$=0.7 although the values given above remain rather insensitive to changes equal to as much as 0.35 in $\gamma_3-\gamma_2$. For F = 0 to -3.5: $E_p \cong$ 17.5 to 25.8 eV, and $g_c \cong$ -0.05 to -1.5 Preliminary measurements of g_c[32] suggests that E_p is close to the linear interpolated value of 23.1 eV. (See also Table IV-6).

The value for $\bar{\beta}$ which we have calculated from our band parameter (Table IV-3) lies very close to the linear interpolation between those values for InP and $In_{0.53}Ga_{0.47}As$ (ternary). The value of $\bar{\beta}$ for the ternary has been measured by Hermann et al[24] who use optical pumping measurements and agrees very well with that calculated from our band parameters for the Ternary. (See also Table IV-6). Here

$$\bar{\beta} \equiv \frac{1}{3} \frac{3(m/\mu_+) + (m/\mu_-)}{(m/\mu_+) - (m/\mu_-)}$$

The conduction effective mass values for y=0 to y=1 reported in Ref.28 and obtained from cyclotron resonance and magnetophonon reson- ance are seen to lie on a straight line (see Table V-7). This is in excellent agreement with our results for both the quaternary Q9-18 (x=0.25, y=0.52) and the ternary T9-50 (x=0.47, y=1). The above discussion indicates that (1) interband magneto-optical measure- ments, and (2) the interband measurements such as cyclotron and magneto phonon resonance and (3) optical pumping measurements (including electron spin resonance) are complementary methods for measuring band parameters of semiconductors. It is interesting to note that they all fall in the category of magneto-optics.

B. 4. Band Parameters for T9-50

Analysis of the data for T9-50 follows exactly the same line as presented for Q9-18. Qualitatively, many of the assertions about Q9-18 hold for T9-50. Tables similar to Table IV-3 were generated and the following results were obtained:

1) In what follows the minimization routine was run each time with the parameters Δ, q, N_1, were kept fixed. E_g, E_p, γ_1, γ_2, γ_3, and κ were free to vary subject to $D_K=0$ and m_-=fixed. We obtained the following results

   (a) $\underline{\Delta=0.35 \text{ eV vs. } \Delta=0.36 \text{ eV}}$: Optimization in each gave

same DRMS. The following changes were observed:

m_c by $\lesssim$ 0.1%, μ_- by $\lesssim$ 0.2%, g_c by $\lesssim$ 0.5%.

μ_+ by $\lesssim$ 0.1% and E_g, E_p and $(\gamma_3-\gamma_2)$ by $\lesssim$ 0.005%.

(b) $\underline{N_1=0 \text{ vs. } N_1=-0.03}$: In the case g_c changed by 0.12 and $(\gamma_3-\gamma_2)$ by 0.2%. The other parameters changed by less than 0.005%.

(c) $\underline{q=0 \text{ vs. } q=0.03}$: In this case $(\gamma_3=\gamma_2)$ changed by $\lesssim$0.4% m_+ and μ_+ changed $\lesssim$ 0.05% and the other parameters by less than 0.001%.

Therefore, we note that whether we set $q=N_1=0$, or we use their estimated values (Appendix B), no difference is made in the fits, and we might as well set them equal to zero.

2) In what follows we run the minimization routine with $m_-=0.5 \, m$, $\Delta= 0.35$ eV, $q = N_1=D_K=0$. We then run the optimization routine with F=0, -0.5, -1, -1.5, -2, -2.2, -2.4, -2.5, -3, -3.5. We observed that DRMS varies from 2.687 meV for F=0 to 2.676 for F=-2 through F=-2.5 and to 2.683 for F=-3.5. Hardly a decisive minimum to narrowly determine F. Considering light hole transitions only we still did not get a decisive minimum for DRMS to determine F narrowly.

(a) The value of E_p varies from 21.0687 eV to 27.0441 eV. The interpolated value of E_p=25.35 eV corresponding to F=2.46 give DRMS=2.687 meV. We see that our measurements cannot precisely measure E_p. However, with N_1=0, the value of g_c changes from -3.2 to -4.67. If as in Appendix B we use

the estimated value of N_1=0.014F-0.02 the range of g_c would be -3.3 to -4.95. Therefore, a measurement of g_c with good precision can determine E_p. (Refer to Table IV-**8**.)

(b) The value of E_g varies between 812.77 and 813.29 meV; also for m_/m between 0.4 and 0.6 and a given F, optimal values of E_g varies by about 0.5 meV. Therefore, interband magnetoabsorption experiments yield E_g=813±0.5 meV.

(c) Again for F=0 to -3.5 the minimization routine yielded 0.8035 γ_3-γ_2 0.751 for m_{hh}=0.5m. In fact for m_{hh}/m between 0.4 and 0.5, optimal values for γ_3-γ_2 lie between 0.74 and 0.83. As mentioned before interband magnetoabsorption experiments determine γ_3-γ_2 narrowly provided spectra are taken with $\vec{H}$ along different crystal axes. In the case of T9-50, we had taken spectra with $\vec{H}||$[100] and with $\vec{H}||$[110].

(d) The values for μ_+/m and μ_-/m are again narrowly determined by interband magnetoabsorption measurements. Again, with m_{hh}/m=0.5, as F was varied between 0 and -3.5, μ_+/m changed from 0.02293 to 0.02318, a change of 0.3%. This gave 43.14≤m/μ_+≤43.60 similarly 0.03848 μ_-/m≤0.03799 giving 25.92≤m/μ_+≤26.32. For different values of m_/m between 0.4 and 0.6 these values change by about ±0.2% It is also found that fits with values differing by ±1% to ±2% of these values although strictly not optimal in the

mathematical sense, still give fits quite as good. This means that

$$(m/\mu_+) = 43.4\pm1.0$$

$$(m/\mu_-) = 26.1\pm0.5$$

(e) For $m_{hh}/m=0.5$ and F from 0 to -3.5 the values for m_c/m changes from 0.04112 to 0.04181, i.e., by 2% whereas the value for m_+/m changes from 0.05186 to 0.05201, a mere 0.2%. For different values of m_{hh}/m between 0.4 and 0.6 and a given F, m_c changes by 3%, and m_+, by 2%. Therefore our experiments give $m_c/m = 0.0415$ $(1\pm5\%) = 0.0415\pm$ Q0015 and $m_{\ell h}/m = 0.0515\pm0.0015$.

(f) $\beta \simeq 3\pm0.05$ in excellent agreement with Ref. 24.

(g) $\gamma_1^L \simeq 10.6\pm0.2$, $\gamma_2^L \simeq 4.0\pm0.1$, $\gamma_3^L = 4.8\pm0.1$, $\kappa^L = 3.3\pm0.1$.

TABLE IV-1 Binding energy E_B of the 1S state of a hydrogen-like atom
(in units of the effective Rydberg R) vs. the reduced
magnetic field γ, (see Text).

γ	E_B	γ	E_B	γ	E_B
0.0	1.000	1.5	1.869	23.4	4.629
0.025	1.025	1.6	1.906	25.0	4.733
0.05	1.049	1.7	1.941	30.0	5.031
0.075	1.072	1.8	1.975	34.95	5.293
0.1	1.095	2.0	2.041	40.0	5.535
0.15	1.139	2.2	2.103	45.0	5.754
0.2	1.181	2.4	2.162	50.0	5.957
0.25	1.220	2.5	2.191	55.0	6.146
0.3	1.258	2.6	2.218	62.91	6.422
0.4	1.329	2.8	2.272	69.9	6.645
0.5	1.394	3.0	2.323	83.88	7.048
0.6	1.454	3.5	2.444	97.0	7.384
0.7	1.511	5.0	2.750	100.0	7.519
0.8	1.564	7.5	3.152		
0.9	1.613	8.388	3.273		
1.0	1.661	10.0	3.474		
1.1	1.707	12.58	3.755		
1.2	1.749	15.0	3.985		
1.3	1.791	17.48	4.198		
1.4	1.831	20.0	4.392		

TABLE IV-2   Band parameters for binary semiconductors determined from interband magneto-optical measurements used to estimate band parameters for $In_{1-x}Ga_xAs_yP_{1-y}$.

	InAs[a]	GaAs[a]	InP[b]
E_g(eV)	0.41	1.52	1.42
Δ(eV)	0.38	0.34	0.11
E_p(eV)[c]	20	22	17
m_c/m_o	0.024	0.067	0.079
m_{hh}/m_o	0.4	0.45$\pm$0.07	0.45$\pm$0.05
$m_{\ell h}/m_o$	0.026	0.082	0.12
$\gamma_3 - \gamma_2$	0.7[d]	0.7	0.7[d]

[a]From values quoted in Ref.6.

[b]Ref.23.

[c]These values for E_p are not deduced from direct measurements of g_c and m_c. Therefore these were not used in our actual calculations, instead, we used E_p values given in Ref.30 (see Table B-1).

[d]Ref.25.

Table IV-3

Band parameters obtained for the sample Q9-18 using the minimization routine with exciton corrections using data from the Voigt $\vec{E} \parallel \vec{H}$, RCP, and LCP spectra, all with $\vec{H} \parallel [100]$. In the minimization routine, the following parameters were fixed: $\Delta = 0.24$ eV, $\gamma_3 - \gamma_2 = 0.7$, $q = N_1 = 0$, $m_{hh} \equiv m_-[100] = 0.45$ m, and F.

F	DRMS (meV)	E_g (meV)	E_p (eV) / g_c †	γ_1 / γ_3	γ_1^L / γ_3^L, κ^L	m_c/m / m_+/m	μ_+/m / m/μ_+	μ_-/m / m/μ_-	$\bar{\beta}$	α / $(m/m_c)^2\alpha$
0	3.459	1064.29	17.9055 / -0.064† / -0.20 †	1.9485 / 0.2964	7.5565 / 3.1004 / 1.5152	0.05955 / 0.07757	0.03369 / 29.68	0.05259 / 19.015	3.377	0.964 / 271.86
-1.0	3.457	1064.35	20.1497 / -0.32 / -0.51	1.2343 / -0.0607	7.5448 / 3.0945 / 1.5093	0.05963 / 0.07771	0.03374 / 29.64	0.05265 / 18.99	3.379	0.959 / 269.78
-2.0	3.458	1064.55	22.3021 / -0.57 / -0.82	0.5489 / -0.4034	7.5262 / 3.0853 / 1.5001	0.06001 / 0.07787	0.03389 / 29.51	0.05295 / 18.86	3.371	0.931 / 258.61
-2.381*	3.459	1064.66	23.0996 / -0.66 / -0.93	0.2956 / -0.5301	7.5278 / 3.0860 / 1.5008	0.06023 / 0.07792	0.03397 / 29.44	0.05312 / 18.825	3.365	0.915 / 252.12
-3.0	3.468	1064.89	24.3700 / -0.81 / -1.11	-0.1064 / -0.7311	7.5219 / 3.0831 / 1.4979	0.06067 / 0.07799	0.03413 / 29.30	0.05346 / 18.71	3.354	0.880 / 239.19
-3.5	3.479	1065.10	25.3764 / -0.93 / -1.25	-0.4225 / -0.8891	7.5193 / 3.0818 / 1.4966	0.06111 / 0.7803	0.03427 / 29.18	0.05381 / 18.58	3.338	0.846 / 226.59

*Parameters used in Figs. IV-4 and IV-5. Value of E_p corresponds to the linear interpolation (see Table B-1).

†The lower value for $|g_c|$ corresponds to $N_1 = 0$, the higher value corresponds to $N_1 = 0.14$ F - 0.034 as in Table B-2. α is a measure of the nonparabolicity of the conduction band given by Eq. (C-18) in Appendix C.

$$\bar{\beta} = \frac{1}{3} \frac{3(m/\mu_+) + (m/\mu_-)}{(m/\mu_+) - (m/\mu_-)}$$

TABLE IV-4   Identification of Interband Transition Lines in the Voigt Configuration (i.e. $\vec{k} \perp \vec{H}$) for $\vec{E} || \vec{H}$.

Label	Transition	Label	Transition	Label	Transition
1	$b^-(1)a^c(0)$	11	$b^+(2)a^c(1)$	21	$b^+(4)a^c(3)$
2	$a^+(-1)b^c(0)$	12	$a^-(3)b^c(4)$	22	$a^-(6)b^c(7)$
3	$b^-(2)a^c(1)$	13	$b^-(5)a^c(4)$	23	$b^-(8)a^c(7)$
4	$a^+(0)b^c(1)$	14	$a^+(2)b^c(3)$	24	$a^-(7)b^c(8)$
5	$b^+(1)a^c(0)$	15	$b^+(3)a^c(2)$	25	$b^-(9)a^c(8)$
6	$a^-(1)b^c(2)$	16	$a^-(4)b^c(5)$	26	$a^+(4)b^c(5)$
7	$b^-(3)a^c(2)$	17	$b^-(6)a^c(5)$	27	$b^+(5)a^c(4)$
8	$a^+(1)b^c(2)$	18	$a^-(5)b^c(6)$	28	$a^-(8)b^c(9)$
9	$a^-(2)b^c(3)$	19	$b^-(7)a^c(6)$	29	$b^-(10)a^c(9)$
10	$b^-(4)a^c(3)$	20	$a^+(3)b^c(4)$		

TABLE IV-5 Identification of Interband Transitions in the Faraday
Configuration (i.e. $\vec{k} || \vec{H}$)

	RCP	LCP
1.	$a^-(1)a^C(0)$	$a^+(-1)a^C(0)$
2.	$b^-(1)b^C(0)$	$b^+(-1)b^C(0)$
3.	$a^+(1)a^C(0)$	$a^+(0)a^C(1)$
4.	$a^-(2)a^C(1)$, $b^-(2)b^C(1)$	$b^+(0)b^C(1)$
5.	$a^-(3)a^C(2)$, $b^-(3)b^C(2)$	$a^+(1)a^C(2)$
6.	$a^+(2)a^C(1)$	$a^-(2)a^C(3)$, $b^-(2)b^C(3)$
7.	$a^-(4)a^C(3)$, $b^-(4)b^C(3)$	$b^+(1)b^C(2)$
8.	$a^-(5)a^C(4)$, $b^-(5)b^C(4)$	$a^-(3)a^C(4)$, $b^-(3)b^C(4)$
9.	$a^+(3)a^C(2)$	$a^-(4)a^C(5)$, $b^-(4)b^C(5)$
10.	$a^-(6)a^C(5)$, $b^-(6)b^C(5)$	$b^+(2)b^C(3)$
11.	$a^-(7)a^C(6)$, $b^-(7)b^C(6)$	$a^-(5)a^C(6)$, $b^-(5)b^C(6)$
12.	$a^+(4)a^C(3)$	$a^-(6)a^C(7)$, $b^-(6)b^C(7)$
13.	$a^-(8)a^C(7)$, $b^-(8)b^C(7)$	$b^+(3)b^C(4)$
14.	$a^-(9)a^C(8)$, $b^-(9)b^C(8)$	$a^-(7)a^C(8)$, $b^-(7)b^C(8)$
15.	$a^+(5)a^C(4)$	$a^-(8)a^C(9)$, $b^-(8)b^C(9)$
16.	$a^-(10)a^C(9)$, $b^-(10)b^C(9)$	$b^+(4)b^C(5)$
17.	$a^-(11)a^C(10)$, $b^-(11)b^C(10)$	$a^-(9)a^C(10)$, $b^-(9)b^C(10)$
18.	$a^+(6)a^C(5)$	$a^-(10)a^C(11)$, $b^-(10)b^C(11)$
19.	$a^-(12)a^C(11)$, $b^-(12)b^C(11)$	$b^+(5)b^C(6)$
20.	$a^-(13)a^C(12)$, $b^-(13)b^C(12)$	$a^-(11)a^C(12)$, $b^-(11)b^C(12)$

Table IV-6

Optical Pumping Measurements in $In_{1-x}Ga_xAs_yP_{1-y}$ Epitaxial Samples (After Ref. 24)*

x	y	E_g (eV)	$E_g + \Delta$ (eV)	Δ(eV)	$\bar{\beta}$	m_c/m	m_+/m	$g_c{}^a$
0	0	1.423 ± 0.0005^b	1.531 ± 0.0025^b	0.108^b	4.1 ± 0.5^c	0.079^b	0.12 ± 0.01^b	+1.24
0.16	0.34	1.19 ± 0.01	$1.37\pm0.005^\dagger$	0.18	$4.2\pm0.4^\dagger$	0.066^d	0.109 0.9a	+0.50
0.26^a	0.60^a	1.035^a		0.25^a			0.072^a	-1.25
0.30	0.61	1.035 ± 0.01	1.29 ± 0.01	0.255	3.4 ± 0.4	0.052^d	0.072 ± 0.01	
0.39	0.84	0.875 ± 0.01	1.18 ± 0.01	0.305		0.046^d	0.061 ± 0.007	-3.0
0.47	1	0.80 ± 0.1 0.810	$1.15\pm0.01*$	0.35 0.340	$3.0\pm0.2^\dagger$	0.041^d	0.051 ± 0.005	$-4.2\pm25\%$

*Values in this table are obtained by Hermann, Lampel, and Pearsall[24] and at T = 1.7K, unless otherwise indicated.

†These results were the same at 1.7 K and 77 K.

^{a}T.P. Pearsall, Private Communication.

^{b}From Ref. 23.

^{c}Calculated from Ref. 23.

^{d}From Ref. 33.

TABLE IV-7   Conduction band effective mass obtained by cyclotron resonance and magnetophonon resonance for $In_{1-x}Ga_xAs_yP_{1-y}$. (After Ref.28).

| Alloy composition | | Cyclotron[†] resonance | Magnetophonon[†] resonance | |
| | | | InP mode | InGaAs mode |
x	y	m^*_{HF}/m	m^*_{HF}/m	m^*_{HF}/m
0.11	0.23	0.0693	0.071*	...
0.15	0.33	0.0666	...	...
0.25	0.53	0.0603	...	...
0.25	0.54	...	0.0602	0.0587
0.26	0.58	...	0.0585	0.0565
0.26	0.59	...	0.0583	0.0565
0.30	0.64	0.055	...	...
0.38	0.84	0.0468	0.0478	0.0468
0.41	0.91	...	...	0.0441
0.47	1.0	0.041*	...	0.043*

[†] $m^*_{HF} \equiv$ High frequency or true "bare" mass

* From Ref.33

Table IV-8

Band Parameter for T9-50, with $\Delta = 0.35$ eV, $q = 0$, $N_1 = 0$, $m_-[100]=0.5m$ kept fixed[*]

	Run	F	DRMS (meV)	$\gamma_3 - \gamma_2$	E_g (meV)	E_p (eV) / g_c	m_c/m	m_+/m	μ_+/m / m/μ_+	μ_-/m / m/μ_-	γ_1^L / γ_3^L
1	22.6	0	2.687	0.8034	812.77	21.0687 / -3.202	0.04112	0.05186	0.02293 / 43.60	0.03799 / 26.32	10.6406 / 4.8188
2	22.7	-0.5	2.683	0.7969	812.77	21.9711 / -3.425	0.04112	0.05190	0.02294	0.03799	
3	22.8	-1.0	2.680	0.7907	812.80	22.856 / -3.643	0.04115	0.05194	0.02296	0.03802	
4	22.9	-1.5	2.678	0.7844	812.85	23.7244 / -3.856	0.04122	0.05197	0.02299	0.03808	
5	22.10	-2.0	2.676	0.7783	812.93	24.5765 / -4.066	0.04132	0.05199	0.02302	0.03817	
6	22.10	-2.2	2.676	0.7758	812.97	24.9131 / -4.148	0.04137	0.05200	0.02304	0.03821	
7	22.12	-2.4	2.676	0.7734	813.01	25.2472 / -4.23	0.04143	0.05200	0.02306 / 43.365	0.03826 / 26.13	
8	22.13	-2.5	2.676	0.772	813.03	25.4134 / -4.271	0.04146	0.0520	0.02307 / 43.35	0.03828 / 26.12	10.615 / 4.7868
9	22.14	-3.0	2.678	0.7657	813.15	26.2355 / -4.472	0.04162	0.05201	0.02312	0.03842	
10	22.15	-3.5	2.683	0.7591	813.29	27.0441 / -4.67	0.04181	0.05201	0.02318 / 43.14	0.03858 / 25.92	

[*]This Table is the result of minimization routine with exciton corrections using the data for T9-50 taken in the following configurations: Faraday, RCP and LCP with $\vec{H}||[100]$, Voigt $\vec{E}||\vec{H}$ and $\vec{E}_\perp\vec{H}$ with $H||[110]$.

FIGURE IV-1 Point plot and fan chart (photon energy vs. magnetic
field) for the magnetoabsorption spectra obtained in the
Voigt configuration ($\vec{k} \perp \vec{H}$) with $\vec{E} || \vec{H}$ for the sample Q9-18.
Transmission minima at various magnetic fields are shown
by the dots. Curves are calculated transition energies
based on the quasi-Ge analysis with exciton corrections.
Solid lines represent the heavy hole to conduction band
transitions, dashed lines represent the light hole to
conduction band transitions. The transitions are numbered
according to Table IV-4 in the order of increasing
energies as follows: 1,2,3,5,4,6,7,8,11,9,10,12,13,14,15,16,17,
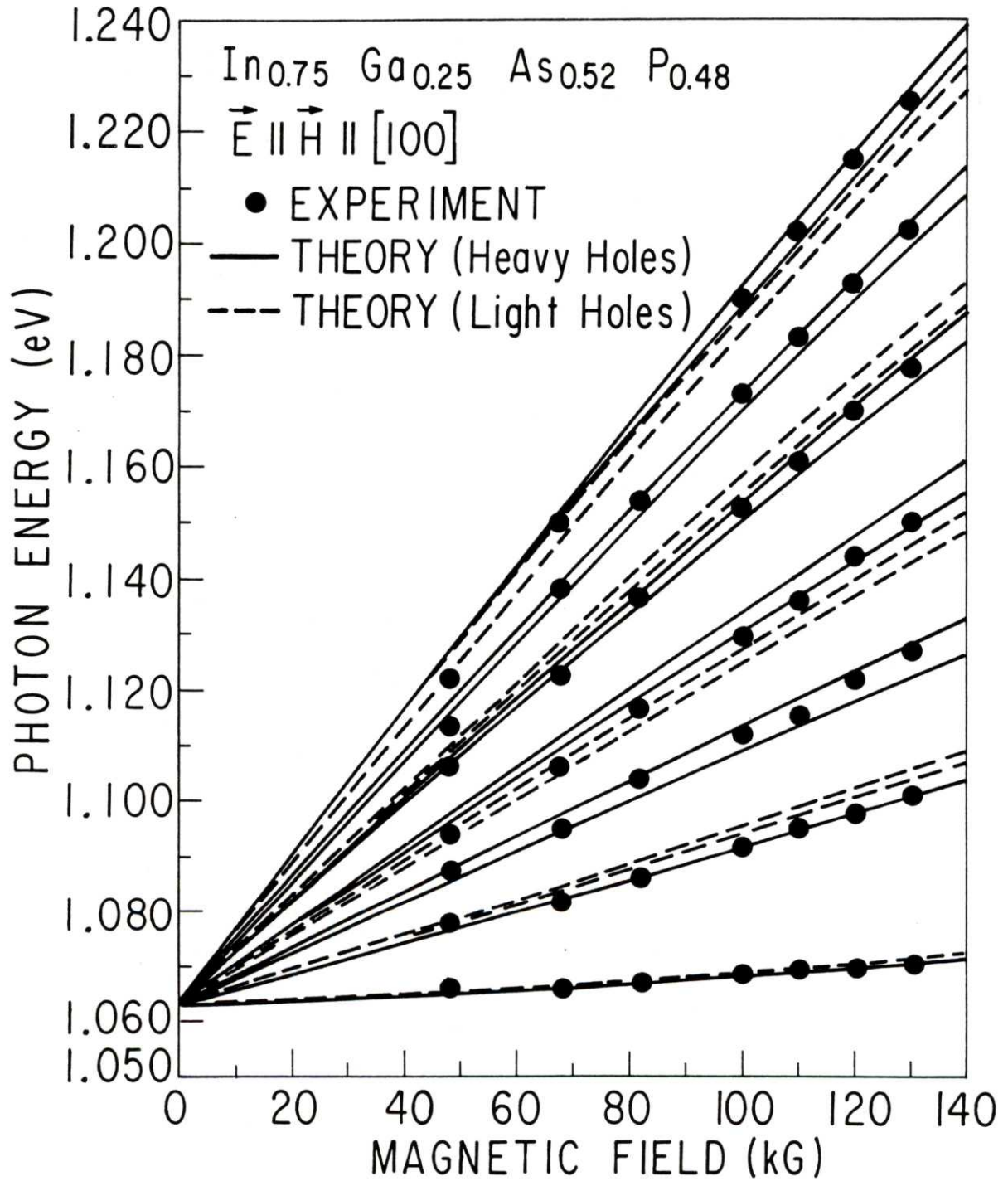20,21,18,19.

FIGURE IV-2   Point plot and fan chart (photon energy vs. magnetic field)
for the interband transitions in the Faraday configuration
($\vec{k} || \vec{H}$) with RCP polarized light for Q9-18. Dots represent
experimental data (minima in transmission spectra). Lines
represent calculated transition energies based on the
quasi-Ge analysis with exciton corrections and are numbered
according to Table IV-5. The solid lines represent the heavy
hole to conduction band transitions. The dashed lines
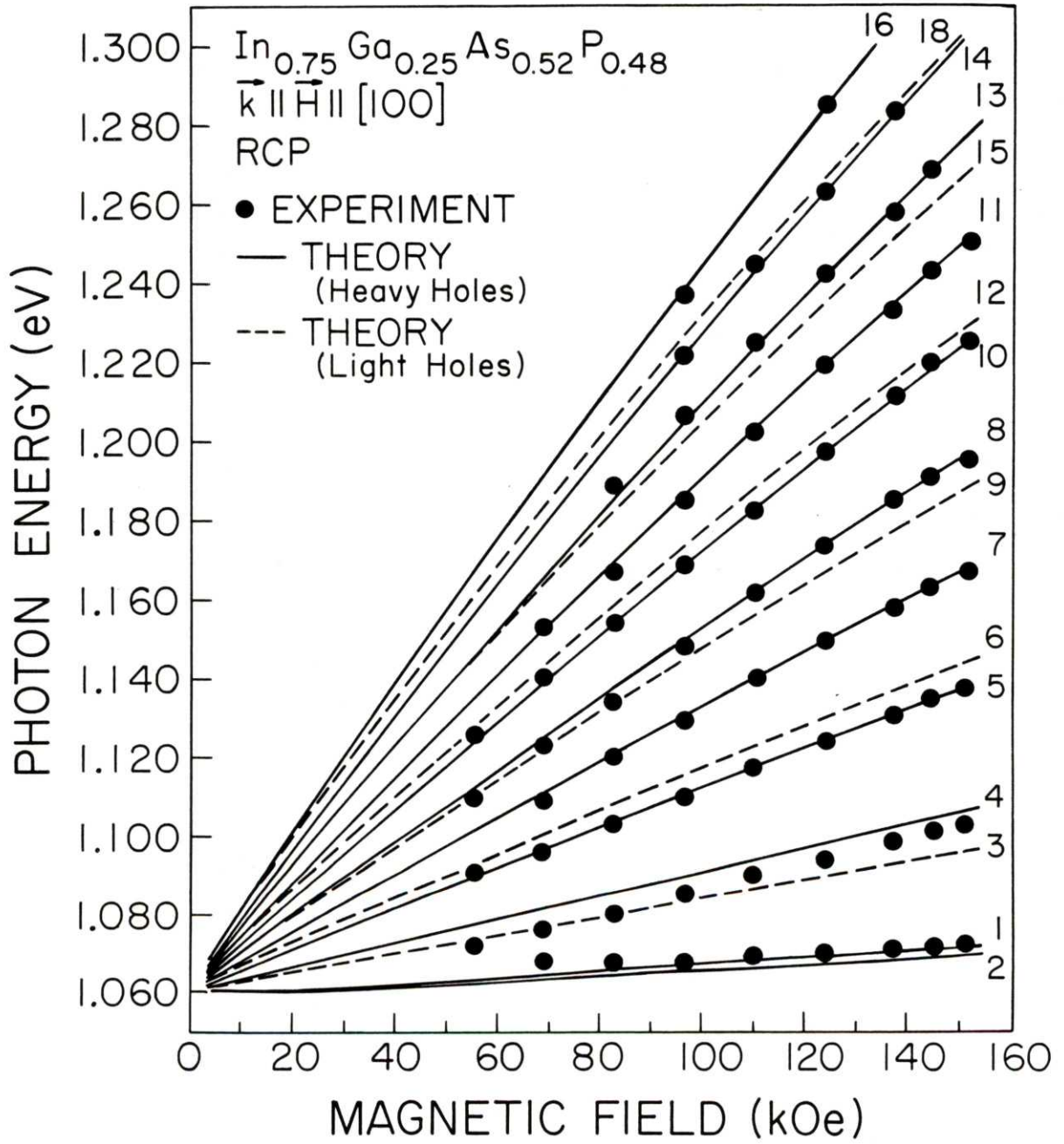represent transition from the light hole to the conduction
band.

$In_{0.75} Ga_{0.25} As_{0.52} P_{0.48}$
$\vec{k} \parallel \vec{H} \parallel [100]$
RCP

● EXPERIMENT
— THEORY (Heavy Holes)
--- THEORY (Light Holes)

FIGURE IV-3   Point plot and fan chart (photon energy vs. magnetic field) for the interband transitions in the Faraday configuration ($\vec{k}\|\vec{H}$) with LCP polarized light for Q9-18.   The calculated transition lines are labeled according to Table IV-5. The unnumbered line corresponds to the two close-lying transitions $a^-(1)a^c(2)$ and $b^-(1)b^c(2)$.
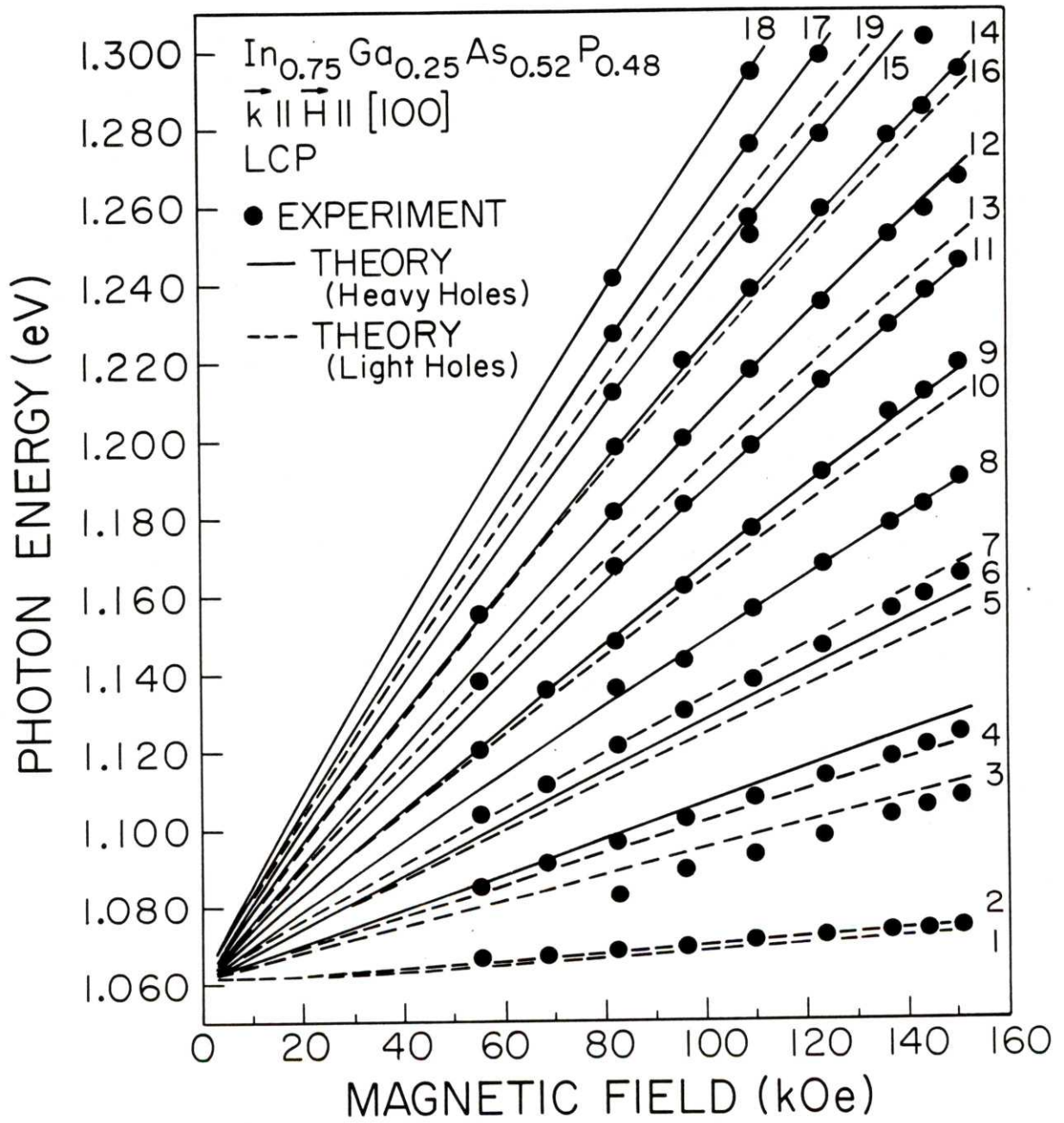
FIGURE IV-4 Point plot and fan chart (photon energy vs. magnetic
field) for the interband transitions in the Voigt configura-
tion ($\vec{k} \perp \vec{H}$) with $\vec{E} || \vec{H}$ for the sample T9-50. Transitions
are numbered according to Table IV-4.
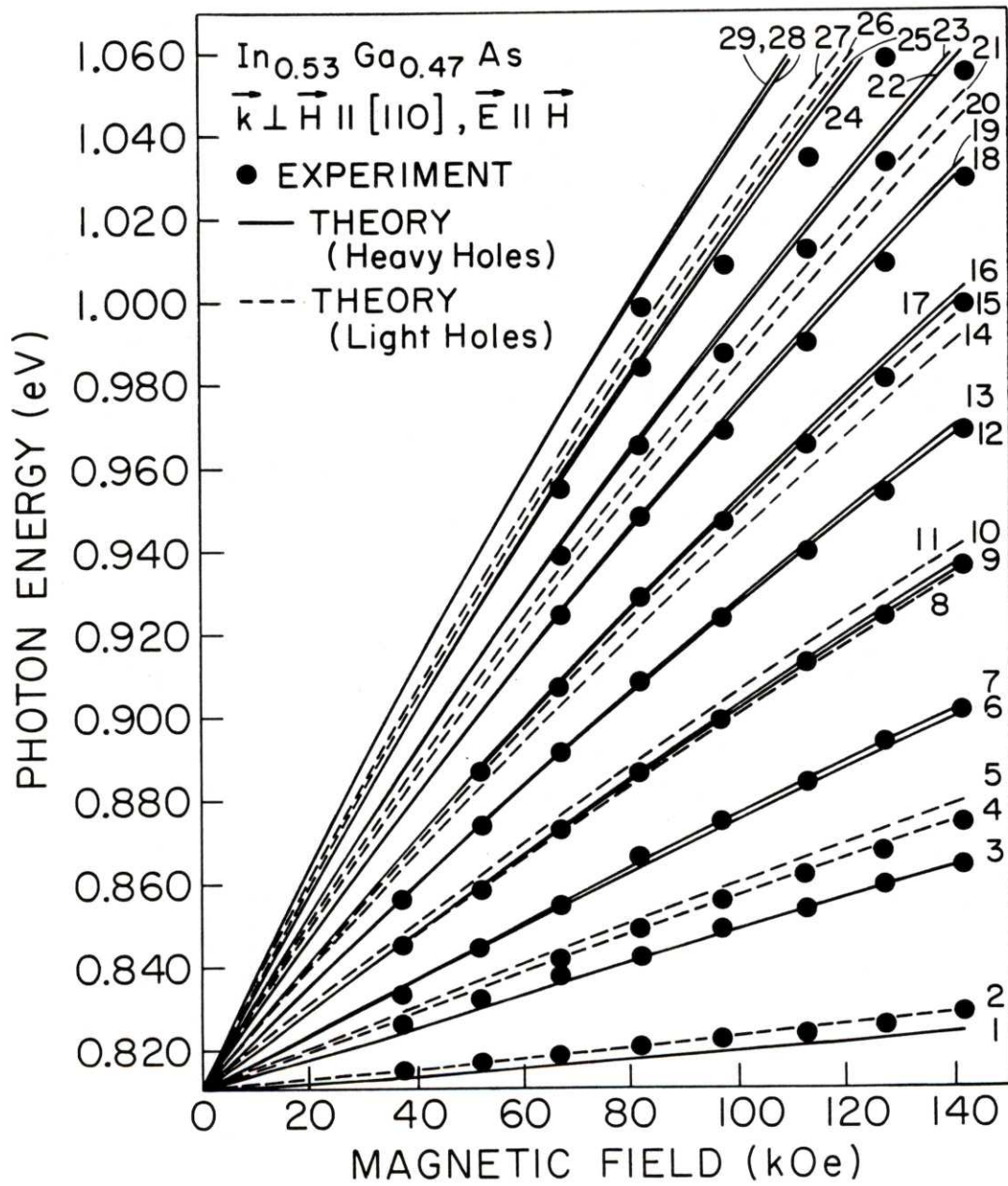
FIGURE IV-5 Point plot and fan chart (photon energy vs. magnetic
field) for the interband transitions in the Faraday
configuration ($\vec{k}||\vec{H}$) with RCP polarized light for T9-50.
The transitions are numbered according to Table IV-5.

FIGURE IV-6 Point plot and fan chart (photon energy vs. magnetic field) for the interband transitions in the Faraday configuration ($\vec{k}||\vec{H}$) with LCP polarized light for the sample T9-50. The calculated transtion lines are labeled according to Table IV-5. The unnumbered line corresponds to the two close-lying transitions $a^-(1)a^C(2)$ and $b^-(1)b^C(2)$.
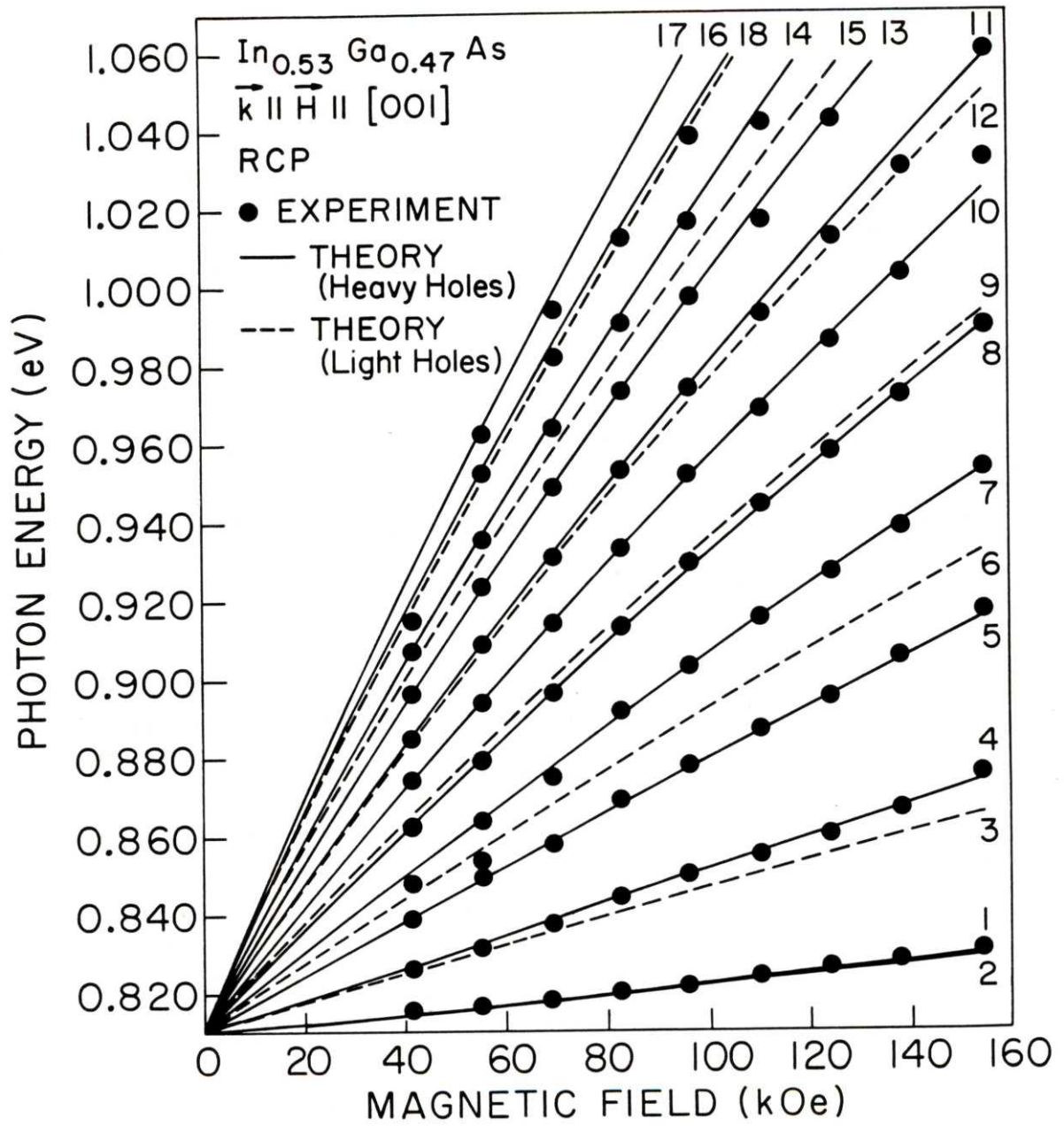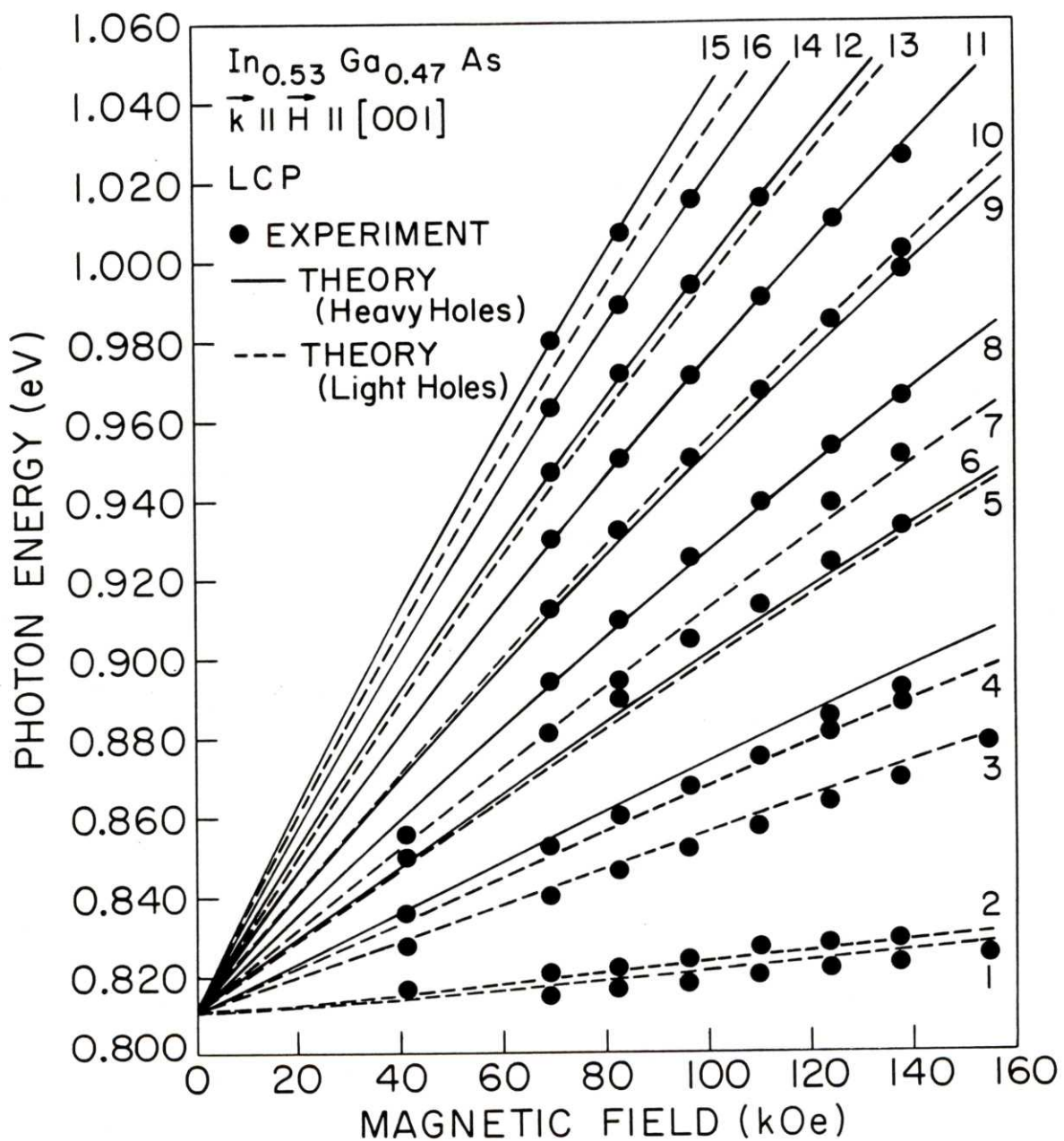
REFERENCES

1. M. Reine, Ph.D. Thesis, Massachusetts Institute of Technology, 1970.

2. M. Reine, R. L. Aggarwal, and B. Lax, Phys. Rev. B5, 3033 (1972).

3. M. H. Weiler, Ph.D. Thesis, Massachusetts Institute of Technology, 1977.

4. M. H. Weiler, R. L. Aggarwal, and B. Lax, Phys. Rev. B17, 3269 (1978); this paper is based on Ref. 3.

5. B. Lax and J. G. Mavroides, "Interband Magnetooptical Effects" in Semiconductors and Semimetals, (R. K. Willardson and A. C. Beer, eds.) Vol. 3, p. 321 (Academic Press, New York, 1967).

6. R. L. Aggarwal, "Modulation Interband Magnetooptics" in Semiconductors and Semimetals, (R. K. Willardson and A. C. Beer, eds.), Vol. 9, p. 151 (Academic Press, New York, 1972).

7. S. H. Grove, C. R. Pidgeon, and J. Feinleib, Phys. Rev. Letters, 17, 643 (1966).

8. C. R. Pidgeon, S. H. Groves, and J. Feinlieb, Solid State Commun. 5, 677 (1967).

9. M. Reine, R. L. Aggarwal, B. Lax, and C. M. Wolfe, Phys. Rev. B2, 458, (1970).

10. M. Reine, R. L. Aggarwal, and B. Lax, Phys. Rev. B5, 3033, (1972).

11. R. L. Aggarwal, Phys. Rev. B2, 446 (1970).

12. D. Bimberg, K. Hess, N. O. Lipari, J. J. Fischbach and M. Altarelli, Physica 89B, 139 (1977).

13. Ibid, in "Proc. 13th Int. Conf. on Physics of Semic". Rome (1976). F. G. Fumi, editor, p.142.

14. Q. H. F. Vrehen, J. Phys. Chem. Solids 29, 129 (1968).

15. R. J. Elliott and R. Loudon, J. Phys. Chem. Solids 8, 383 (1959); J. Phys. Chem. Solids 15, 196 (1960). This was the pioneering work on the theoretical aspects of excitons in high magnetic field.

16. M. Altarelli and N. O.Lipari, Phys. Rev. B7, 3798 (1973); (E) 8, 4046 (1973).

17. Ibid, Phys. Rev. B9, 1733 (1974). Also see references cited in this paper.

18. Ibid, Bull. Am. Phys. Soc. 24, 275 (1979); Ibid, in "Proceedings of Oji International Seminar on the Application of High Magnetic Fields in Semiconductors and Magnetic Materials", Hakone, Japan, 10-13, Sept. 1980.

19. D. M. Larsen, J. Phys. Chem. Solids 15, 196 (1960).

20. H. Praddaude, Phys. Rev. A6, 1321 (1972).

21. E. J. Johnson and D. H. Dickey, Phys. Rev. B1, 2676 (1970).

22. E. O. Kane, J. Phys. Chem. Solids 1, 249 (1957).

23. P. Rochon and E. Fortin, Phys. Rev. B12, 5803 (1975).

24. C. Hermann, G. Lampel, and T. P. Pearsall, in "Proceedings of the 15th International Conference on the Physics of Semiconductors", Kyoto, Japan, 1-5 September 1980.

25. P. Lawaetz, Phys. Rev. B4, 3460 (1971).

26. K. Alavi, R. L. Aggarwal, and S. H. Groves, in "Proceedings of the International Conference on Solids and Plasmas in High Magnetic Field", Cambridge, Massachusetts, 18-20 September 1978, edited by R. L. Aggarwal, et al (North-Holland Publishing Co., Amsterdam 1979) p.136; also published in J. Magn. Magn. Mater. 11, 136 (1979).

27. K. Alavi, R. L. Aggarwal, and S. H. Groves, Bull. Am. Phys. Soc. 24, 336 (1979).

28. R. J. Nicholas, S. J. Sessions, and J. C. Portal, Appl. Phys. Lett. 37, 178 (1980).

29. T. Nishino, Y. Yamazoe, and Y. Hamakawa, Appl. Phys. Lett. 33, 861 (1978).

30. C. Hermann and C. Weisbuch, Phys. Rev. B15, 823 (1977).

31. Ibid, Phys. Rev. B15, 816 (1977).

32. T. P. Pearsall, Private Communications.

33. R. J. Nicholas, J. C. Portal, C. Houlbert, P. Perrier, and T. P. Pearsall, Appl. Phys. Lett. 34, 492 (1979)

CHAPTER V

CONCLUSION

A. Summary

This work represents an account of the first interband magneto-optical investigations in members of the $In_{1-x}Ga_xAs_yP_{1-y}$ semiconducting alloy family which are important materials both technologically and from the point of view of the III-V semiconductor physics. In this thesis we have included our results of interband magneto-absorption for two samples:

$$In_{0.75}Ga_{0.25}As_{0.52}P_{0.48} \text{ (Q9-18), and } In_{0.53}Ga_{0.47}As \text{ (T9-50),}$$
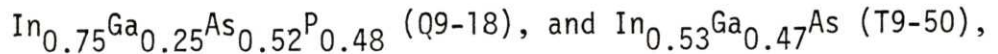
both grown by liquid phase epitaxy on InP substrates of (100) orientation at M.I.T. Lincoln Laboratory. The experiments were carried out at M.I.T. Francis Bitter National Magnet Laboratory using high field Bitter magnets. Magnetoabsorption spectra were obtained, at near liquid helium temperatures, for several field values up to 155 kOe sweeping the wavelength of monochromatic infrared light, in both the Voigt configuration ($\vec{k} \perp \vec{H}$) with $\vec{E} || \vec{H}$ and $\vec{E} \perp \vec{H}$ polarization, as well as in the Faraday configuration ($\vec{k} || \vec{H}$) with right and left circular polarization. The structure in the spectra was attributed to optical transitions from the heavy and light hole magnetic sub-bands to the conduction sub-bands and the transition energies obtained from the experimental spectra were used to form the basis of electronic

band analysis in the context of the quasi-Ge coupled band formalism. This analysis involves explicitly the conduction band, the heavy hole, the light hole, and the spin-orbit split-off valence bands of the fundamental edge, and treats the other bands as perturbations whose effect appears as adjustable coefficients in the quasi-Ge 8x8 $\vec{k}\cdot\vec{p}$ Hamiltonian. This analysis was attempted to identify and fit the experimental data to the interband magneto-optical transitions. In the analysis we included an approximate exciton correction, which is small. This analysis was carried out to determine band parameters, which would best fit the interband measurements carried out in this work, consistant with physical considerations. A range of acceptable values for the band parameters was thus obtained. The quasi-Ge band parameters are E_g, E_p, γ_1, γ_2, γ_3, κ, F, q and N_1, defined earlier. Our analysis shows that N_1, which is a small correction to the conduction band g-factor due to higher bands, does not affect our results. That is to say reasonable range of values for N_1 leave our fits and our band parameters unchanged. A similar conclusion was reached regarding q. This means that these parameters could be set equal to zero. It was found that even for a relatively wide range of heavy hole mass m_- values, and a wide range of F (the higher bands' contribution to the conduction band mass m), our best fits to the data would yield a very narrow range of values for the energy gap E_g, and the reduced effective masses μ_+ and μ_- for the light (+) and heavy (-) hole to conduction band transitions. Similarly, a narrow range of values was obtained for

γ_3-γ_2 when measurements were made with the magnetic field along more than one crystal axis. Since $m_- >> m_c$ the value of μ_- is rather insensitive to m_-. Therefore, our magnetoabsorption measurements have been able to determine m_c within a narrow range. Hence, combining the result for μ_+ and m_c, the light hole mass m_+ is also determined within a narrow range.

Our values for m_c, are in excellent agreement with intra-band measurements using cyclotron and magnetophonon resonance techniques. Furthermore, our results for μ_+, μ_- and m_+ are in excellent agreement with those obtained from optical pumping measurements recently reported.

The value of m_c cannot precisely determine the interband transition energy E_p. This is because of higher band contributions to the curvature of the Γ_6 conduction band. This contribution can be as high as 20% compared to the contribution of the Γ_7 and Γ_8 valence bands. In fact our data accepts a rather wide range of F (between 0 and -3) resulting in an uncertainty in E_p. Values of E_p corresponding to F=0 as well as those corresponding to the value obtained from linear interpolation among the binary constituents InAs, GaAs, and InP give good fits. The value of E_p can be narrowly determined provided the conduction band g-factor g_c is measured within a narrow range and E_g and Δ are known, since N_1, representing the higher bands' contribution to g_c, is quite small. Recent prelim-inary measurements of g_c by optical pumping methods gives values for E_p close to the interpolated values.

The linear dependence of m_c upon y, which is strongly
suggested by cyclotron and magnetophonon as well as our magnetoabsorp-
tion measurements, seems to suggest that the E_p values as a function of
alloy composition y should show a small bowing downwards away from
linearity. This point needs to be investigated further, and
accurate g_c measurements will be useful in this regard.

Finally, if the exciton corrections are ignored the
parameters deduced from the analysis would be affected by about 2%
or less.

In summary, interband magnetooptical studies offer a
relatively simple, and effective method for obtaining accurate
measurements of a number of band parameters. These measurements do
not require high concentration of conduction electrons and therefore
give band parameters for $\vec{k}=0$. This is in contrast with some intra-
band methods, such as Shubnikov-de Haas which require high electron
concentration which then necessitates complicated corrections to the
measured data.

B. Suggestions for Future Studies

In what follows, we give some suggestions for further
experimental studies in the InGaAsP semiconducting alloy family.

1) Electroreflectance measurement of transitions from
Γ_7 as well as Γ_8 bands to the Γ_6 bands of the fundamental gap using

room temperature magnetoelectroreflectance or Schottky-Barrier

magnetoelectroreflectance at low temperature.

2) Above studies using Stress-modulated magnetroreflection.

3) Cyclotron resonance measurement of hole masses.

4) Accurate measurement of E_p by measuring g_c accurately using optical pumping methods which is already being carried out by others.

5) Interband magneto-optical studies in other members of this alloy family.

6) Study of the effect of lattice mismatch on the band parameters.

APPENDIX A

ELECTROREFLECTANCE OF InGaAsP/InP EPITAXIAL ALLOYS

Electroreflectance (ER) is a very sensitive technique for measuring the fundamental energy gap E_0, and the corresponding spin-orbit split-off band energy $E_0+\Delta_0$, as well as higher energy critical points such as E_1, $E_1+\Delta_1$, E_0', $E_0'+\Delta_0'$, even at room temperature.[1-3] Recently the ER technique has been successfully applied to a member of the InGaAsP family to measure E_0 and $E_0+\Delta_0$ at low temperature using Schottky barriers.[4] More recently, the electrolyte electroreflectance technique has been used to measure E_0, $E_0+\Delta_0$, and higher energy critical points.[5,6] In this report we present results of electroreflectance measurements in four different samples of InGaAsP and one sample of InP using the electrolyte technique.[1,2] The characteristics of the samples used in this study are summarized in Table A-1. The samples LPE - 91, LPE - 92, and LPE - 93 were provided by Dr. Zong-Long Liau of M.I.T. Lincoln Laboratory. These epitaxial samples were grown from the same melt composition at different growth temperatures (640.2°C, 628.6°C, and 630.85°C respectively), to give various lattice mismatches as in Table A-1.

The electroreflectance method as shown in the present study is sufficiently sensitive to detect slight variations in the energy gap E_0 of the samples.

The samples were immersed in a sample cell containing a
dilute electrolyte with a quartz window at the bottom making a
small angle with the surface of the samples to separate out the
unwanted reflection from the window. One electrode was soldered
to the back of the sample. The edges and the back of the sample
were covered with black wax for electric insulation from the
electrolyte. A piece of platinum wire with one end immersed in
the electrolyte made up the second electrode. A modulating voltage
with square wave form at 85 Hz was applied between the two electrodes
with or without the dc bias. With the resistivity of the electro-
lyte negligibly low this voltage drop occurs almost entirely in
the narrow semiconductor-electrolyte interface, thus creating a
high electric field on the surface of the semiconductor, normal
to this surface. In addition to the external voltage, there is a
built-in internal voltage at this interface of order of a few
volts. The electrolyte used in case of the first three samples
in Table A-1 was a 0.002 molar solution of KOH in deionized H_2O.
for the other two samples a very dilute solution of HF in deionized
H_2O (1-2 drop in 0.5 litre of H_2O) was used. The optical setup is
essentially similar to that described in Chapter III except for the
following: (1) A single pass monochromator was used, (2) for the
InP and Q9-77B sample we used a Bausch and Lomb grating with 640
lines/mm blazed for 1.4 μm (blaze angle $\theta_B = 26° 45'$) and for the
LPE-91 through LPE-93 samples the grating had 300 lines/mm blazed
for 1.0 μm ($\theta_B = 8°38'$), (3) no dry air was used, and (4) the

incident light was not chopped. Light from the tungsten lamp was passed through the grating monochromator and filters, and was focused on the sample going through the quartz bottom window and the electrolyte. The light reflected from the sample was then focused on a room temperature PbS detector. Due to electric field modulation, the reflected signal had a modulated component, ΔR. The modulated signal from the PbS dector, ΔR, was detected by a lock-in amplifier locked to a reference signal synchronous with modulated voltage applied to the sample. The wavelength λ was swept and ΔR vs. λ was stored on paper tape for computer analysis. For each sweep the conventional reflection spectrum, R vs. λ, was also obtained with a chopper and lock-in amplifier. $\Delta R/R$ spectra were calculated numerically, and plotted vs. photon energy. Figures A-1 through A-3 show some of the electroreflectance spectra obtained in this study.

The intensities and energies of the observed peaks in the ER spectra are summarized in Table A-2. The values for E_0 and $E_0+\Delta_0$ are calculated from our tabulated data using the three parameter method of Aspnes and Rowe,[7] although we realize that this method applies only to the low field regime for centrosymmetric crystals, or for certain polarizations and crystal surfaces (see Refs. 3, and 8-11) in case of zinc-blend type crystals. As is apparent from our spectra, one can see the onset of Franz-Keldysh oscillations which appear in the high-field regime.[3] The appearance of Franz-Keldysh oscillations as well as the large

magnitude of $\Delta R/R$ even for peak-to-peak voltage, V_{pp}, of only 0.08 V is remarkable and shows that these quaternary samples possess relatively high electron mobility, compared to those in Refs. 5 and 16. Another feature of the spectra is the following. As shown for example for sample LPE-91 in Table A-2, the positions of A and B peaks remain constant within 1 meV and that of A' and B' peaks within 5 meV, when V_{pp} are varied from 0.08 to 2.0 volts. However, the intensity of the peaks do not scale linearly with V_{pp}. Here A and B refer to the largest peaks (corresponding to E_0) with A having the lower energy, $E_A < E_B$. Similarly A' and B' refer to the $E_0 + \Delta_0$ edge with $E_{A'} < E_{B'}$, do not scale linearly with V_{p-p}. The spectra, however, seem to shift with the applied dc voltage. The piezoreflectance contribution which could be present in our case (see Refs. 8-11) is estimated to introduce only a small correction to the spectra. This point, however, needs to be investigated in the future using the polarization dependence of this contribution. One point of uncertainty is the effect of the built-in potential on shifting the values of E_0 and $E_0 + \Delta_0$, which could depend on the electrolyte used. However, this dependence on the dc voltage is expected to be small. For instance, from lines 7-9 in Table A-2, it is apparent that a change of 1.16 V in the dc bias shifts the A and B peaks only 10 meV, and the E_0 value calculated by the three parameter method of Aspnes and Rowe[7] shows only a 4 meV shift and $E_0 + \Delta_0$, a 19 meV shift. This point needs further investigation. Finally, the

small variation in the lattice mismatch induces remarkable changes
in the spectra, in terms of peak positions and line widths, as
seen in Figure A-3. The new small peaks between the two largest
peaks in the LPE - 92 spectra may be due to the strains induced
by the relatively large lattice mismatch.

In conclusion, we have shown our first results of electro-
lyte electroreflectance of some members of the InGaAsP family with
some of the samples purposely lattice mismatched to the InP sub-
strates. Spectra show quantitative as well as qualitative differ-
ences. We believe electroreflectance offers a very sensitive
tool in observing such changes. We suggest that further investi-
gations especially with polarized light and as a function of dc
bias could facilitate further understanding of the spectra. Finally,
it is noted that the spin-orbit split-off edge is observable with
the aid of electroreflectance method even at room temperature.
Therefore, magneto-optical measurement of the spin-orbit split-
off to conduction band transitions in the quaternary alloys should
be possible, using electrolyte method at room temperature, as
reported for Ge, GaSb, InSb, and InAs.[13,14]

TABLE A-1   Characteristics of the expitaxial $In_{1-x}Ga_xAs_yP_{1-y}$ samples grown on InP substrates used in the present electroreflectance studies.

Sample	x	y	$\Delta a/a$*	E_o(eV)
InP**	0	0	-	1.34 §
Q9-77B	0.23	0.52	$\leq 6 \times 10^{-4}$	1.0 §§
LPE-91	(0.17)+	(0.4)+	-0.143%	1.08
LPE-92	(0.17)	(0.4)	+0.205%	"
LPE-93	(0.17)	(0.4)	0.13%	"

* Lattice constant mismatch of epitaxial layers relative to InP substrates.

**Bulk sample.

§ Reference 1 of this Appendix.

§§Estimated from Reference 15 of this Appendix.

+ Values in parenthesis are those given in Table 1, line 1 of Reference 12 for quaternary grown from the same melt composition at a different temperature resulting in $\frac{\Delta a}{a} \leq 0.03$. This melt composition consisted of the following atom fraction percentages: In(95.77%), Ga(0.35%), As(3.54%) and P(0.34%).

TABLE A-2   Summary of the electroreflectance measurements.   External V is measured from the platinum electrode to the sample electrode.

Line Figure	Sample	$\frac{\Delta a}{a}$ %	electrolyte	External dc	V(volts) pp	E_A(eV) $10^6(\Delta R/R)$	E_B(eV) $10^6(\Delta R/R)$	E_0(eV)*	$E_A{}'$(eV) $10^6(\Delta R/R)$	$E_B{}'$(eV) $10^6(\Delta R/R)$	$E_0+\Delta_0$(eV)*	Δ_0(eV)*
1 A-1	InP	--	KCℓ/H₂0	-2.2	3.0	1.337 -44814	1.356 24492	1.342	1.439 6196	1.471 180	1.442	0.100
2 A-2	Q9-77B	--	KCℓ/H₂0	1.0	2.0	0.978 -13412	0.999 10285	0.986	1.235 -166	1.269 579	1.264	0.278
3	LPE-91-0.143		KCℓ/H₂0	0.0	0.08	1.096 -2598	1.115 1285	1.101	1.305 -145	1.343 37	1.310	0.209
4 A-3	LPE-91-0.143		KCℓ/H₂0	0.0	0.4	1.096 -9675	1.115 4733	1.101	1.309 -544	1.348 44	1.310	0.209
5	LPE-91-0.143		KCℓ/H₂0	0.0	2.0	1.094 -17934	1.114 9623	1.100	1.309 -955.5	1.340 47.5	1.310	0.210
6 A-3	LPE-92	0.203	HF/H₂0	0.0	0.4	1.037 -9043	1.081 11548	1.063	1.269 -676	1.314 983	1.296	0.233
7	LPE-93	0.13	HF/H₂0	0.0	0.4	1.059 -31337	1.096 9971	1.065	1.286 -2475	1.334 1468	1.302	0.237
8	LPE-93	0.13	HF/H₂0	0.56	0.4	1.063 -28477	1.090 6821	1.066	1.230 342	1.291 -2350	1.290	0.224
9	LPE-93	0.13	HF/H₂0	0.6	0.4	1.054 -23976	1.098 7997	1.062	1.284 -1468	1.332 1209	1.305	0.243
10 A-3	LPE-93	0.13	HF/H₂0	0.0	0.4	1.054 -25116	1.098 10183	1.064	1.282 -1863	1.329 1559	1.303	0.239

*Based on the three-point method of Reference 7.

FIGURE A-1 Electrolyte electroreflectance spectrum of the InP
bulk sample from (100) surface. In this and all of
the other measurements the external applied voltage
was measured as the voltage drop from the platinum
electrode to the sample electrode measured externally.
The two larger peaks A and B($E_A < E_B$) correspond to the
fundamental edge, and the A' and B'($E_{A'} < E_{B'}$) peaks, to
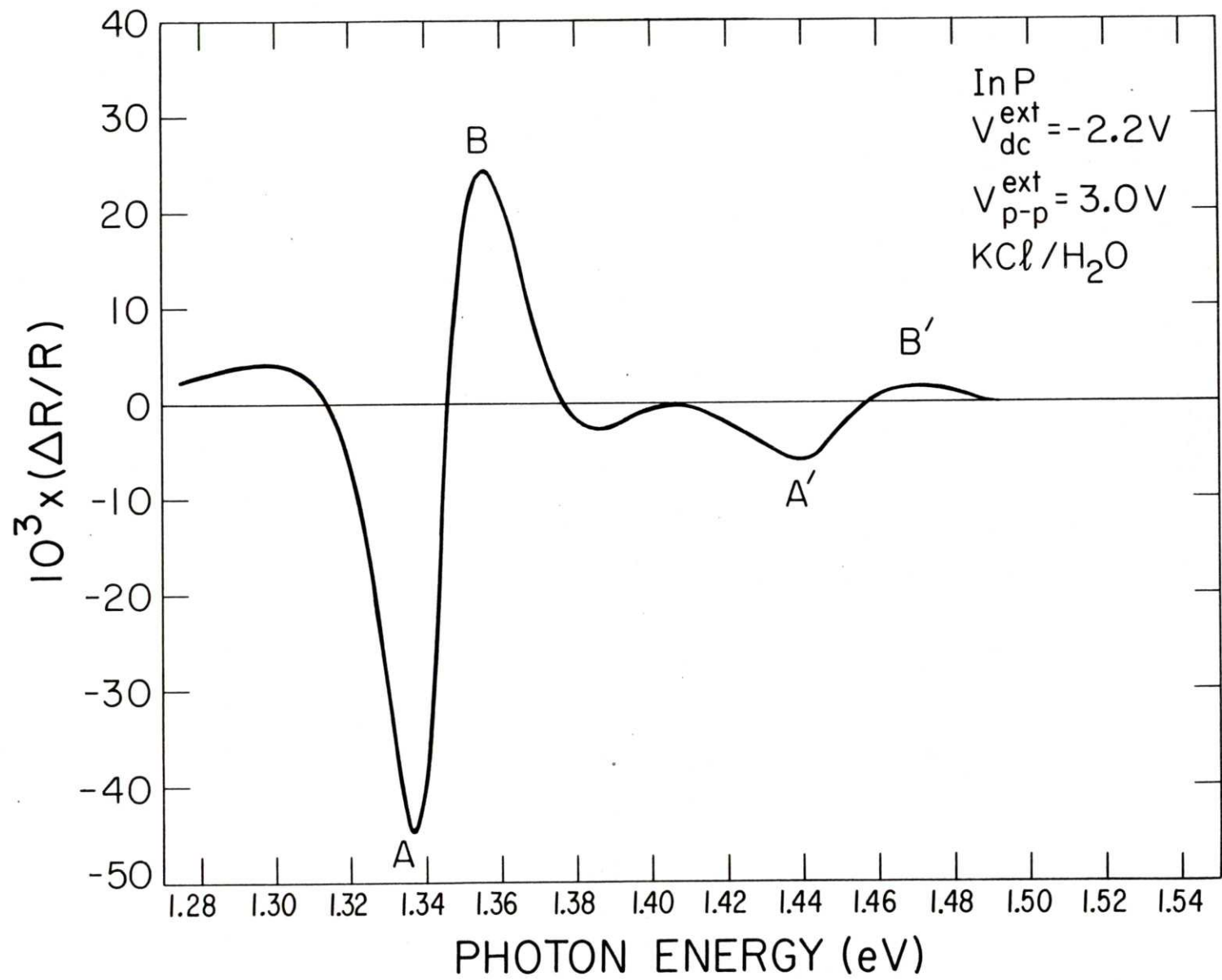the corresponding spin-orbit split-off edge.

FIGURE A-2 Electrolyte electroreflectance of spectrum of the
          quaternary sample Q9-77B from (100) surface. Note the
          onset of Franz-Keldysh oscillations.
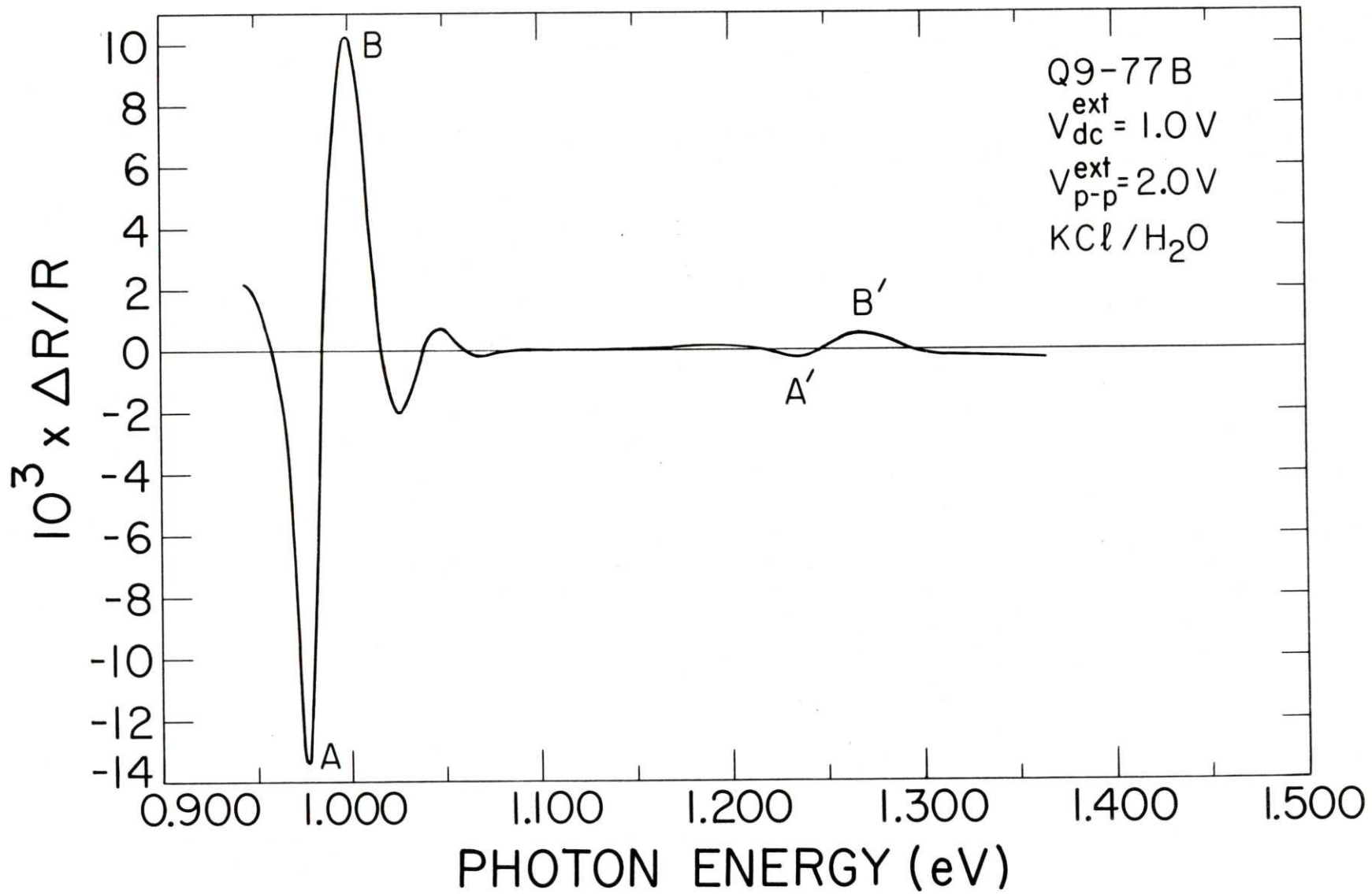
FIGURE A-3 Electrolyte electroreflectance spectrum of the three
            quaternary samples LPE-91, LPE-92, and LPE-93. Note the
            qualitative differences as well as the change in peak
            positions and linewidths among the three samples. The
            two small peaks between the two large ones in the LPE-92
            spectrum may be caused by the strains due to the relatively
            large lattice mismatch with the substrate.
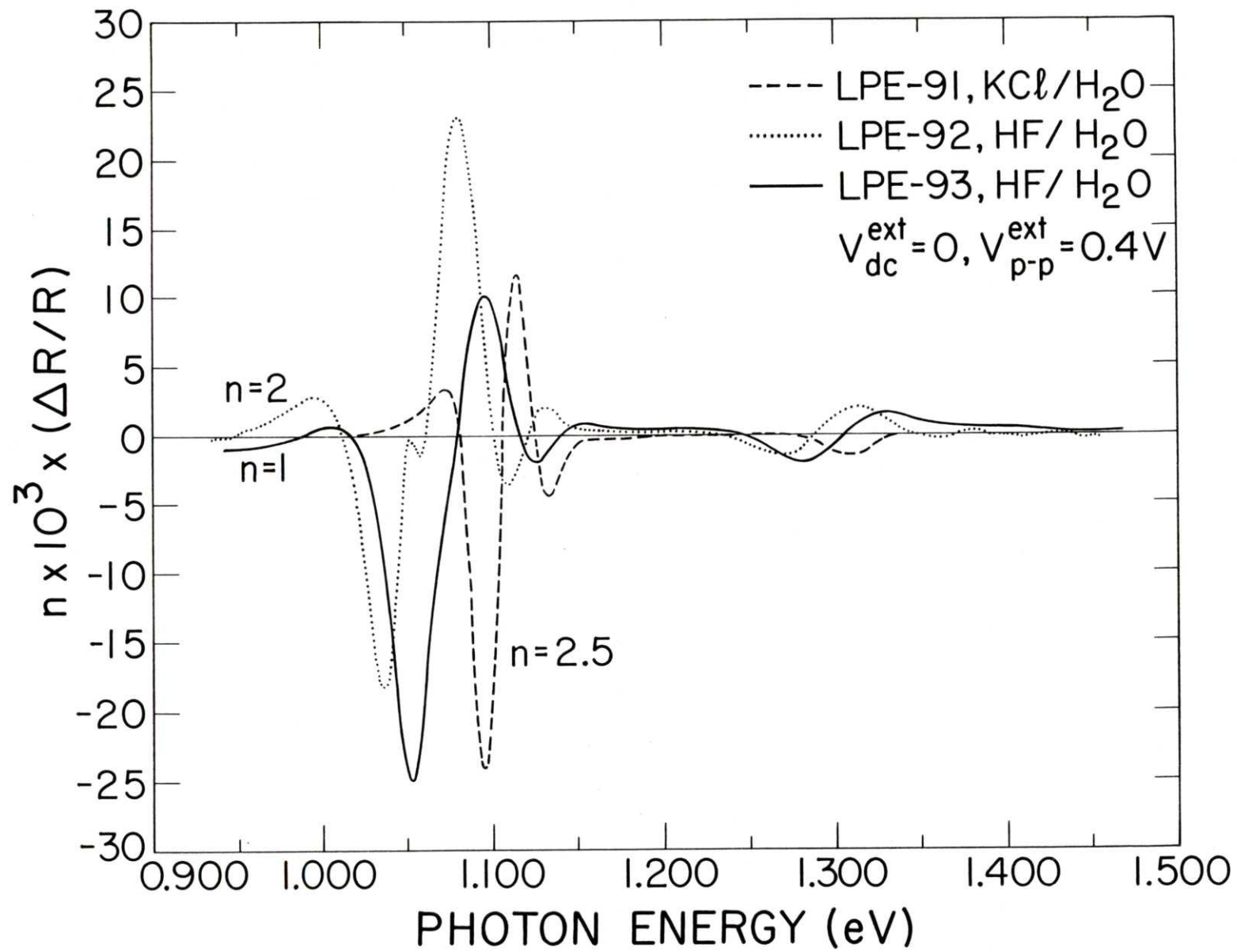
REFERENCES

1. M. Cardona, K. L. Shaklee, and F. H. Pollak, Phys. Rev. 154, 696 (1967).

2. M. Cardona, Modulation Spectroscopy, (Academic Press, N.Y. 1969) and References therein.

3. D. E. Aspnes, Surface Science, 37, 418 (1973).

4. T. Nishino, Y. Yamazoe, and Y. Hamakawa, Appl. Phys. Lett. 33, 861 (1978).

5. E. H. Perea, E. E. Mendez, and C. G. Fonstad, Appl. Phys. Lett. 36, 978 (1980).

6. P. M. Laufer, F. H. Pollak, R. E. Nahory, and M. A. Pollack; Bull. Am. Phys. Soc. 25, 441 (1980); also private communications.

7. D. E. Aspnes and J. E. Rowe, Phys. Rev. Lett. 27, 18 (1971).

8. E. Mohler, Phys. Status Solidi 29, K55 (1968); ibid, 38, 81 (1970).

9. D. E. Aspnes and A. A. Studna, Phys. Rev. B7, 4605 (1973).

10. D. S. Kyser and V. Rehn, Solid State Commun. 8, 1437 (1970).

11. S. Tachi, A. Moritani, M. Koshinaka, and J. Naka, Japan J. Appl. Phys. 19, 533 (1980).

12. M. Feng, T. H. Windhorn, M. M. Tashima, and G. E. Stillman, Appl. Phys. Lett. 32, 758 (1978).

13. S. H. Groves, C. R. Pidgeon, and J. Feinleib, Appl. Phys. Lett. 17, 643 (1966).

14. C. R. Pidgeon, S. H. Groves, and J. Feinleib, Solid State Commun. 5, 677 (1967).

15. J. J. Hsieh, J. of Electron. Materials 7, 31 (1978).

APPENDIX B

THE $\vec{k} \cdot \vec{p}$ PARAMETERS AND ESTIMATIONS

The $\vec{k} \cdot \vec{p}$ parameters of Table II-2 will be given here in terms of sums over intermediate states when applicable. Some of these parameters are related to those introduced by Kane[1] who used the single group representations of T_d instead of the double group representation used by Weiler.[2]

    1) $P \equiv -i(h/m) <S| \, p_x \, |X>$ (Ref. 1)   (B-1)

    2)   C is allowed by the spin-orbit interaction and is defined by Dresselhaus,[3]

$$ C \equiv \frac{h^2}{2\sqrt{3} \, m^2 c^2} \sum_{\Gamma_i' = \Gamma_4', \, \Gamma_5'} \frac{<Y\uparrow|H_{so}|\Gamma_i'\uparrow><\Gamma_i'\uparrow|p_y|Z\uparrow>}{E_0 - E(\Gamma_i')} $$

Where E_0 is the valence band energy at $\vec{k}=0$. The P and C are parameters in the single group representation of T_d. In the double group representation, additional parameters P' and C' are obtained. These new parameters are expected to be very close to the unprimed ones.

    3)   The parameters γ_1, γ_2, γ_3, κ are linear combinations of the Kane parameters A_K, B_K, C_K, and D_K:

$$ \gamma_1 = -\frac{2}{3}(A_K + B_K + 2C_K + 2D_K) - 1 \qquad \text{(B-3a)} $$

$$ \gamma_2 = -\frac{1}{3}(A_K + B_K - C_K - D_K) \qquad \text{(B-3b)} $$

$$\gamma_3 = -\frac{1}{3}(A_K - \frac{1}{2}B_K + C_K - D_K) \tag{B-3c}$$

$$\kappa = -\frac{1}{3}(A_K - \frac{1}{2}B_K - C_K + D_K) - \frac{1}{3} \tag{B-3d}$$

The Kane parameters are defined in terms of matrix elements of $\vec{p}$ among the $\vec{k}=0$ states belonging to the single-group representation of T_d,

$$A_K \equiv \frac{1}{m} \sum_{\Gamma_1'} \frac{|<X|p_x|\Gamma_1'>|^2}{E_0 - E(\Gamma_1')} \ , \qquad\qquad B_K \equiv \frac{1}{m} \sum_{\Gamma_3'} \frac{|<X|p_x|\Gamma_3'>|^2}{E_0 - E(\Gamma_3')}$$

$$C_K \equiv \frac{1}{m} \sum_{\Gamma_4'} \frac{|<X|p_y|\Gamma_4'>|^2}{E_0 - E(\Gamma_4')} \ , \qquad\qquad D_K \equiv \frac{1}{m} \sum_{\Gamma_5'} \frac{|<X|p_y|\Gamma_5'>|^2}{E_0 - E(\Gamma_5')} \tag{B-4}$$

where E_0 is the $\vec{k}=0$ energy of the valence band (E_v). The other Kane parameters are

$$F = \frac{1}{m} \sum_{\Gamma_4'} \frac{<S|p_x|\Gamma_4'>}{E_0 - E(\Gamma_4')} \tag{B-5}$$

where in Eq.(B-4) E_0 is the conduction band energy at $\vec{k}=0$,(i.e., E_c).

$$G = \frac{1}{m} \sum_{\Gamma_4'} \frac{<S|p_x|\Gamma_4'><\Gamma_4'|p_x|Z>}{E_0 - E(\Gamma_4')} \tag{B-6}$$

where E_0 is an average of E_c and E_v. Actually for $E(\Gamma_4') >> E_g \equiv (E_c - E_v)$, G would be insensitive to whether one uses E_c or E_v.

4) When the spin-orbit splitting of the higher Γ_4 bands is included (i.e., $\Gamma_4' \rightarrow \Gamma_8', \Gamma_7'$) another four parameters are obtained:[2]

$$q = \frac{8}{27} \frac{i}{m} \sum_{\Gamma_8'} \frac{<\psi_{3/2}^8|p_x|\Gamma_8'><\Gamma_8'|p_y|\psi_{3/2}^8>}{E_v - E(\Gamma_8')} \qquad \text{(B-7)}$$

$$N_1 = -\frac{i}{m} \sum_{\Gamma_8'} \frac{<\psi_{1/2}^6|p_x|\Gamma_8'><\Gamma_8'|p_y|\psi_{1/2}^6>}{E_c - E(\Gamma_8')} \qquad \text{(B-8)}$$

$$N_2 = \frac{1}{m} \sum_{\Gamma_8'} \frac{<\psi_{1/2}^6|p_x|\Gamma_8'><\Gamma_8'|p_x|\psi_{-3/2}^8>}{E_0 - E(\Gamma_8')} \qquad \text{(B-9)}$$

$$N_3 = \frac{-i}{m} \sum_{\Gamma_8'} \frac{<\psi_{1/2}^6|p_x|\Gamma_8'><\psi_8'|p_y|\psi_{-3/2}^8>}{E_0 - E(\Gamma_8')} \qquad \text{(B-10)}$$

In the single group approximation N_1 can be expressed as

$$N_1 \simeq \frac{1}{3m} \sum_{\Gamma_4'} \frac{|<S|p_x|\Gamma_4'>|^2}{[E_c - E(\Gamma_4')]} \frac{\Delta_0'}{[E_c - E(\Gamma_4')]} \qquad \text{(B-11)}$$

where

$$\Delta_0' = E(\Gamma_8^c) - E(\Gamma_7^c) \qquad \text{(B-12)}$$

as shown in Figure II-1. The higher-band energies which appear throughout this Appendix are those for $\vec{k} = 0$.

Considering the leading term explicitly   Eq.(B-11) can be written as[4]

$$N_1 \simeq \frac{1}{3m} |<S|p_x|\Gamma_4'>|^2 \left(\frac{E(\Gamma_8^C) - E(\Gamma_7^C)}{[E_C-E(\Gamma_7^C)][E_C-E(\Gamma_8^C)]} \right) + C' \qquad (B-13)$$

where Γ_8^C and Γ_7^C are the next higher energy bands beyond the four-bands ehich have been considered explicitly in the 8x8 $\vec{k}\cdot\vec{p}$ analysis and

$$C' = \frac{1}{3m} \sum_{\Gamma_4''} \frac{|<S|p_x|\Gamma_4'>|\cdot\Delta_0''}{[E_C-E(\Gamma_4'')]^2} \qquad (B-14)$$

is the contribution from all other intermediate states.   We define

$$E_p' \equiv (2/m) |<S|p_x|\Gamma_4''>|^2 \equiv P'^2 \qquad (B-15)$$

Similarly for q, in the single-group approximation, one obtains

$$q \simeq \frac{4}{9m} \sum_{\Gamma_4'} \frac{|<x|p_y|\Gamma_4'>|^2 \Delta_0'}{[E_0-E(\Gamma_4')]^2} \qquad (B-16)$$

which yields

$$q \simeq -\frac{4}{9} \frac{\Delta_0'}{E(\Gamma_4^C)-E_v} C_K \qquad (B-17)$$

in agreement with the result of Hensel and Suzuki.[5] Eqs. (B-11) and (B-5) gvive

$$N_1 \simeq \frac{1}{3} \frac{\Delta_0'}{E(\Gamma_4^C) - E_c} F \qquad (B-18)$$

In Eqs. (B-17) and (B-18) for $E(\Gamma_4^C)$ we can use Γ_8^C or Γ_7^C, since $\Delta_0' \ll \Gamma_7^C \sim \Gamma_8^C$.

We take Eq.(B-17) further. From Eqs.(B-3) it is seen that

$$C_K = D_K + \frac{1}{2}(3\kappa - 3\gamma_3 + 1) \qquad (B-19)$$

the parameter D_K is estimated to be nearly zero in most of the literature which gives

$$-\frac{1}{4}\gamma_1 + \frac{1}{2}\gamma_2 + \frac{3}{4}\gamma_3 - \frac{3}{4}\kappa - \frac{1}{2} = D_K = 0 \qquad (B-20)$$

and

$$C_K = \frac{1}{2}(3\kappa - 3\gamma_3 + 1) \qquad (B-21)$$

Hence, a knowledge of the higher band energies $E(\Gamma_8^C)$ and $E(\Gamma_7^C)$ helps to reduce the number of parameters by relating q and N_1 to the rest of $\vec{k} \cdot \vec{p}$ parameters through Eqs.(B-18) and (B-21).

Estimation of N_1

Hermann and Weisbuch[4] have also considered explicitly one set of higher bands namely Γ_4^C (which in their notation is called Γ_5^C) which consist of the doubly degenerate Γ_8^C and spin orbit split-off Γ_7^C (see Figure II-2). There are two typographical errors in their paper: In Eq.(4) P^2 shoud read $-P^2$ and in Eq.(6) A multiplies everything to its right and not just the first term. Using their expressions we get

$$F = -\frac{1}{6} P'^2 \left(\frac{2}{E(\Gamma_8^C)-Eg} + \frac{1}{E(\Gamma_7^C)-Eg} \right) + \frac{1}{2} C \qquad \text{(B-22)}$$

$$N_1 = -\frac{1}{6} P'^2 \left(\frac{-1}{E(\Gamma_8^C)-Eg} + \frac{1}{E(\Gamma_7^C)-Eg} \right) + \frac{1}{2} C' \qquad \text{(B-23)}$$

where P'^2 is the interband transition energy proportional to the square of momentum matrix element, C and C' come from other higher bands not included explicitly with $C \approx -2$ or perhaps -1 and $C' \approx -0.02$. One observation is that $N_1 << F < 0$. Table B-2 summarizes some of the values useful for Eqs.(B-22) and (B-23). These equations give N_1 in terms of F:

$$N_1 = \frac{\Delta_0'}{2[E(\Gamma_7^C)-E_g] + [E(\Gamma_8^C)-E_g]} \left(F - \frac{C}{2} \right) + C' \qquad \text{(B-24)}$$

which is close enough to Eq.(B-18). Using $E_g = 0.813$ eV for the ternary and $E_g = 1.065$ eV for the quaternary and using interpolated values from

TABLE B-1   Some of the band parameters for InAs, GaAs, InP as well as values obtained from linear interpolation for the ternary and the quaternary samples (refer to Figure II-1).

	InAs[a]	GaAs[a]	$In_{0.53}Ga_{0.47}As$[b]	InP[a]	$In_{0.75}Ga_{0.25}As_{0.52}P_{0.48}$[b]
E_g(eV)	0.42	1.519	(0.937)	1.423	(1.70)
Δ(eV)	0.38	0.34	(0.36) 0.35±0.01[d]	0.108[c]	(0.24) 0.23[e]
*E_0'(eV)	4.60	4.659	(4.63)	4.79	(4.71)
**$E_0'+\Delta_0'$(eV)	4.44	4.488	(4.46)	4.72	(4.62)
Δ_0'(eV)	0.16	0.171	(0.165)	0.07	(0.12)
m_c/m	0.0230	0.0667		0.0803	
g_c (exp'tal)	-14.8	-0.44	-4.2±25%[f]	1.26	
$P^2 \equiv E_p$(eV)	22.2± 0.5	28.9± 0.9	(25.35)	20.7± 1.5	(23.1)
$P'^2 \equiv E_p'$ $\{$ C=-2 (eV)	0.2	6	(2.8)	2.1	(2.5)
C=-1	4	9	(6.4)	6	(6)
F	-1±1	-1.9± 0.5	(-1.4±0.8)	-0.9±1	(-1.2±0.9)

[a]Taken from Ref. 4, unless otherwise noted.

[b]Values in parantheses are from linear interpolations.

[c]After Ref. 6.

[d]After Ref. 7.

[e]Estimated from Ref. 7.

[f]After Ref. 9.

*$E_0' \equiv E(\Gamma_7^C)-E(\Gamma_7^V)$

**$E_0'+\Delta_0' \equiv E(\Gamma_8^C)-E(\Gamma_7^V)$

Table B-1 we get

TABLE B-2

		C=-2, C'=-0.02	C=-1, C'=0.02	Eq.(B-18)
T9-50	$N_1 \simeq$	(0.014)F - 0.034	(0.014)F - 0.027	0.014 F
Q9-18	$N_1 \simeq$	(0.011)F - 0.031	0.011 F - 0.026	0.011 F

This shows that N_1, the higher band contribution to g_c, is much smaller than F, the higher band contribution to m_c, as pointed out in Ref.4. For physically reasonable values of F, N_1 is seen to be very small (see Table B-1) so that it can be neglected in Eq.(3-18). Thus

$$g_c = 2[1 - \frac{E_p}{3} \frac{\Delta}{E_g(E_g+\Delta)}] \qquad (B-25)$$

Precise measurement of g_c, and E_g thus yields $E_p(P^2$ in the notation of Ref.4) to a good precision. This value of E_p can then be used to obtain F using Eq.(2-17), since m_c can be determined very precisely using interband magnetoabsorption or cyclotron resonance. The effect of higher bands on m_c and g_c was considered for InSb earlier by Groves, in a similar fashion.[8]

Estimate of q

Using Eqs.(B-17) and (B-21) and Table B-1 we can estimate
q:

$$q \simeq - \frac{4}{3} \frac{\Delta_0'}{2E(\Gamma_7^C) + E(\Gamma_8^C)} \ c_K \qquad\qquad (B-17)'$$

$$q \simeq \frac{1}{2}(-3\kappa + 3\gamma_3 - 1) \times \begin{cases} (0.017) & \text{for T9-50} \\[10pt] (0.011) & \text{for Q9-18} \end{cases} \qquad (B-26)$$

We can use Table B-2 and Eq.(B-26) as two constraint equations
in our minimization routine (Ch.IV). It turns out that for the values
of κ, and γ_3 obtained from our minimization routine q is very samll, just
as N_1 turns out to be. For typical values of q and N_1 the effect of
these parameters on our experimental spectra is negligible and they
can be set equal to zero.

REFERENCE

1. E. O. Kane, J. Phys. Chem. Solids $\underline{1}$, 249 (1957).

2. M. H. Weiler, Ph.D. Thesis, Massachusetts Institute of Technology, (1977).

3. G. Dresselhaus, Phys. Rev. $\underline{100}$, 580 (1955).

4. C. Hermann and C. Weisbuch, Phys. Rev. B$\underline{15}$, 823 (1977).

5. J. C. Hensel and K. Suzuki, Phys. Rev. Letts $\underline{22}$, 838 (1969).

6. P. Rochon and E. Fortin, Phys. Rev. B$\underline{12}$, 5803 (1975).

7. C. Hermann, G. Lampel, and T. P. Pearsall, in Proceedings of the 15th International Conference on the Physics of Semi-conductors, Kyoto, Japan, 1-5 September 1980.

8. S. H. Groves in M.I.T. Lincoln Laboratory Solid State Research Quarterly Report, 16 Oct. 1970 (3rd Quarter), p.33.

9. T. P. Pearsall, Private Communication.

APPENDIX C

NONPARABOLICITY OF THE CONDUCTION BAND

C. 1. Conduction Band Energies Up to H^2 (or k^4)

In Chapter II, Eq.(2-52), we presented an expression for the energy of the conduction band up to k^4, which included F, the higher bands' contribution to m_c. This can be rewritten as

$$E_c = E_g + \left(\frac{m}{m_c}\right)\frac{\hbar^2 k^2}{2m} - \left(\frac{m}{m_c} - 1 - 2F\right)\left(\frac{m}{m_c} - 1\right)\left(\frac{3+4Q+Q^2}{3+5Q+Q^2}\right)\frac{1}{E_g}\left(\frac{\hbar^2 k^2}{2m}\right)^2 \quad (C\text{-}1)$$

where

$$Q \equiv (\Delta/E_g) \qquad\qquad\qquad (C\text{-}2)$$

In a magnetic field, the average of a- and b-series energies for a given n is obtained when the following substitution is made in Eq.(C-1):

$$(\hbar^2 k^2/2m) \rightarrow (n+\tfrac{1}{2})(2\mu_B H) \qquad\qquad (C\text{-}3)$$

The result is

$$E_c(n) = E_g + (n+\tfrac{1}{2})^2 \frac{\hbar^2 k^2}{2m} - (n+\tfrac{1}{2})^2 (2\mu_B H)^2 \frac{1}{E_g} \times$$

$$x\left(\frac{m}{m_c} - 1 - 2F\right)\left(\frac{m}{m_c} - 1\right)\left(\frac{3+4Q+Q^2}{3+5Q+Q^2}\right) \qquad (C\text{-}4)$$

Note that in the derivation of Eqs. (C-3) and (C-4) the assumption is

that $\gamma_1 = -1$, $\gamma_2 = \gamma_3 = 0$, $\kappa = -\frac{1}{3}$, as in Kane's model, which ignores the effect of higher bands. To obtain expression which allow values for γ_1, γ_2, γ_3 and κ other than the above, we can follow the treatment presented in Ref. 1. According to this presentation first the determinant equations for the eigenvalue problems of Eqs.(2-13), for the quasi-Ge model have been obtained [Eq.(102), Ref.1]. The eigen-energies are then assumed to have a power series expansion in powers of $(2\mu_B H)$:

$$E_c = E_g + (2\mu_B H) \, E_1^c + (2\mu_B H)^2 \, E_2^c + \ldots \qquad (C-5)$$

One can then obtain

$$E_1^c = (n+\tfrac{1}{2})\frac{m}{m_c} \pm \frac{1}{4} \, g_c \qquad (C-6)$$

where + is for the a-series and − for the b-series. For the mean value of E_2^c for a and b series we have obtained

$$E_2^c = - (n+\tfrac{1}{2})^2 \cdot \frac{1}{E_g}(\frac{m}{m_c} - 1 - 2F)\{Q_1(\frac{m}{m_c}+\gamma_1)+Q_2(\gamma'+3\gamma'')\}$$
$$+ \, \eta+\xi \qquad (C-7)$$

where
$$\begin{cases} Q_1 \equiv \dfrac{3+4Q+2Q^2}{3+5Q+2Q^2} & (C-8) \\[2ex] Q_2 \equiv \dfrac{3+Q}{3+2Q} & (C-9) \end{cases}$$

and η and ξ are independent of n.

$$\eta = -\frac{1}{E_g}\left(\frac{m}{m_c} - 1 - 2F\right)\{\tfrac{1}{4} \quad [(1-Q_2)(\tfrac{m}{m_c} - 1 - 2F)-1]\} \times \tag{C-10}$$

$$\times (2-Q_1-Q_2)$$

$$\xi = -\frac{1}{E_g}\left(\frac{m}{m_c} - 1 - 2F\right)\{\tfrac{1}{2} Q_1\gamma_1 + \tfrac{1}{4} Q_2(2\gamma' - 3\gamma'') \tag{C-11}$$

$$-\tfrac{1}{4}(2Q_1+Q_2)\kappa \cdot -\tfrac{1}{4}\frac{1}{1+Q} \qquad \}$$

$$E_c = (n+\tfrac{1}{2})(\tfrac{m}{m_c})(2\mu_B H) - (n+\tfrac{1}{2})^2 (\tfrac{m}{m_c} - 1 - 2F) \times$$

$$\times \{Q_1(\tfrac{m}{m_c}+\gamma_1) + Q_2(\gamma'+3\gamma'')\}\frac{1}{E_g}(2\mu_B H)^2 + \eta + \xi \tag{C-13}$$

It turns out that the first term in Eq.(C-7) is much larger than η and for large n certainly much larger than both η and ξ. Therefore, in Eq.(C-7) we can ignore η and ξ for large n. Thus the nonparabolicity of the conduction band up to k^4 can be determined from Eq.(C-7) when the following substitution is made:

$$(n+\tfrac{1}{2})(2\mu_B H) \to \frac{\hbar^2 k^2}{2m} \tag{C-14}$$

We then obtain

$$E_c = (\tfrac{m}{m_c})\frac{\hbar^2 k^2}{2m} - (\tfrac{m}{m_c} - 1 - 2F)\{Q_1(\tfrac{m}{m_c}+\gamma_1) + Q_2(\gamma'+3\gamma'')\}\frac{1}{E_g}(\frac{\hbar^2 k^2}{2m})^2 \tag{C-15}$$

or

$$E_c = E_0(1-\alpha\frac{E_0}{E_g}) \tag{C-16}$$

where

$$E_0 = \frac{\hbar^2 k^2}{2m_c} \tag{C-17}$$

and

$$\alpha \equiv \left(\frac{m_c}{m}\right)^2 \left(\frac{m}{m_c} - 1 - 2F\right)' \{Q_1\left(\frac{m}{m_c} + \gamma_1\right) + Q_2(\gamma' + 3\gamma'')\} \tag{C-18}$$

In the Kane model $F=0$, $\gamma_1=-1$, $\gamma'=\gamma''=0$, and one can recover expressions given for example by Vrehen[2] who found $\alpha=0.83$ for GaAs. It is important to note that Eqs.(C-13) and (C-18) determine the nonparabolicity more accurately since Kane model is only an approximation.

C. 2.   Nonparabolicity of the Conduction Band and Interband Transitions

It is seen in the Figures of Chapter IV (expecially those for the Voigt and the RCP polarization-configurations), for a given magnetic field value, the spacing between adjacent transitions decreases as one goes higher in energy. This is a consequence of the non-parapolicity of the conduction band and can be seen from Eq.(C-13).

In the point plots for the Voigt and the RCP configurations we can assume that the minima come essentially from the heavy hole-to-conduction band transitions, and the nonparabolicity of the heavy hole band can be ignored (since it has a much heavier effective mass) consequently using Eqs.(2-23), (C-13) and (C-18) we have obtained the

following expression for the energy separation between two adjacent transitions for a given H where n is the conduction band quantum number:

$$E(n)-E(n-1) = (\frac{m}{m_c}+\frac{m}{m_-})(2\mu_B H)-[(n+\frac{1}{2})-(n-\frac{1}{2})]^2 \alpha\frac{1}{E_g}(2\mu_B H)^2(\frac{m}{m_c})^2 \quad (C-19)$$

$$\epsilon(n)\equiv\frac{E(n)-E(n-1)}{2\mu_B H} = (\frac{m}{\mu_-})-2n\alpha(\frac{m}{m_c})^2\frac{1}{E_g}(2\mu_B H) \quad (C-20)$$

where μ_+ is the reduced effective mass for the heavy (-) as light (+) hole transitions to the conduction band:

$$\frac{1}{\mu_\pm} = \frac{1}{m_c} + \frac{1}{m_\pm} \quad (C-21)$$

Equation (C-20) can be written as

$$\epsilon(n) = (\frac{m}{\mu_-})-[2\alpha(\frac{m}{m_c})^2\frac{1}{E_g}](2n\mu_B H), \quad (n\geq 1) \quad (C-22)$$

Following Vrehen[2] and Reine and coworkers[3] one can measure $\epsilon(n)$ directly from the spectra (Figures IV-, 2, 4, 5), for each configuration e.g. H||[100] or H||[110]. One can then plot $\epsilon(n)$ vs. $(2n\mu_B H)$, and fit a straight line through these points by the method of least squares. The intersection of this line with the $(2n\mu_B H) = 0$ axis would be just $(1/\mu_-)$ for that particular orientation e.g. [100] or [110]. This can also show the anisotropy of the heavy hole band. The slope of the line will also determine α, the nonparabolicity. These measurements

can be used for obtaining preliminary values for some of the parameters to be used for the analysis of spectra as pointed out in Chapter IV.

REFERENCES AND NOTES

1. R. L. Aggarwal, "Modulated Interband Magnetooptics" in
    Semiconductors and Semimetals (R. K. Willardson and A. C. Beer eds.)
    Vol.9, p.151.

    In Ref.1 the following corrections should be taken into account:
    (i)   In Eq.(78) $-i\gamma''$ should be replaced by $+i\gamma''$, consequently
    (ii) In Eq.(78) the sign of $s[6n(n+1)]^{1/2}\gamma''$ should be changed, and
    (iii) In Eq.(81), $F=-[6n(n+1)]^{1/2}\gamma''$.
    (iv) In Eq.(83) the following should be added to the right hand
          side $-s^4 A[B(L_1 L_2 - L_3^2) - F^2 L_2 - G^2 L_1 + 2FG L_3]$.
    (v)   In Eqs.(105 and (106), $(n-\frac{3}{2})$ should be replaced by $(n+\frac{1}{2})$,
    (vi) In Eq.(108) in the second line $-\frac{A+B}{E_g+\Delta}$ should be replaced by
          $-\frac{AB}{E_g+\Delta}$.

2. Q. H. F. Vrehen, J. Phys. Chem. Solids 29, 129 (1968).

3. M. Reine, Ph.D. Thesis, Massachusetts Institute of Technology (1970);
    M. Reine, R. L. Aggarwal, and B. Lax, Phys. Rev. B5, 3033 (1972).

Biographical Note

Name: Kambiz Alavi

Parents: Seyyed Mohammad Kazem Alavi
          Bibi Ozra Naji

Birth: May 22, 1950, Ahvaz, Iran
        (Officially: Sept. 1, 1949, Tehran, Iran)

High Schools: Amir-Kabir, Masjid-i-Soleiman (1961-63)
               Hadaf No. 1, Tehran (1963-1967)

University: M.I.T. Sept. 1968-present
             S.B. Physics June 1972
             Doctoral Exam completed Feb. 1975
             S.M. Physics June 1977
             Ph.D. Physics June 1981

Teaching experience: T.A., Junior Physics Lab, 1 year
                      T.A., a one year graduate course in Stat. Mech.
                      2 years

Research: R.A., National Magnet Laboratory
                      Supported by N.S.F.

Publications and Meeting Speeches:

"Third-Order Nonlinear Susceptibility of CdTe in the 10 μm Region"
K. Alavi, N. Lee, R. L. Aggarwal, and B. Lax, Bull. Am. Phys. Soc. 23,
411 (1978) March meeting, Washington, D.C.

"Oscillatory Magneto-transmission of $In_{1-x}Ga_xAs_yP_{1-y}$ Alloys"
K. Alavi, R. L. Aggarwal, and S. H. Groves, presented at the Int'l.
Conf. on Solids and Plasmas in High Magnetic fields, Cambridge, Mass.(1978).
Also published in J. Magn. Magn. Mater. 11, 136 (1979)

"Interband Magneto-Optical Studies in $In_{1-x}Ga_xAs_yP_{1-y}$ Alloys",
K. Alavi, R. L. Aggarwal, S. H. Groves, Bull. Am. Phys. Soc. 24, 336
(1979) March Meeting, Chicago, Ill.

"Interband Magnetoabsorption of $In_{0.53}Ga_{0.47}As$", K. Alavi, R. L
Aggarwal, and S. H. Groves, Phys. Rev. B21, 1311 (1980).

"Interband Magneto-optical Studies in $In_{1-x}Ga_xAs_yP_{1-y}$ Semiconducting
Alloys", K. Alavi, R. L. Aggarwal, and S. H. Groves, Bull. Am. Phys.
Soc. (1981), March Meeting, Phoenix, Arizona.

"Electrolyte Electroreflectance in $In_{1-x}Ga_xAs_yP_{1-y}$ Semiconducting
Alloys", K. Alavi, R. L. Aggarwal, S. H. Groves, and Z.-L. Liau, Bull.
Am. Phys. Soc. (1981), March Meeting, Phoenix, Arizona.